

Digital copy produced with permission of the author.

Julkaisu digitoitu tekijän luvalla.

Lappeenrannan teknillinen korkeakoulu
Lappeenranta University of Technology

Teuvo Partanen

**ON THE APPLICATION OF
BEAM ON ELASTIC FOUNDATION THEORY
TO THE ANALYSIS OF STIFFENED PLATE STRIPS**

Acta Universitatis
Lappeenrantaensis 86

ISBN 978-952-214-799-8 (PDF)

Teuvo Partanen

**ON THE APPLICATION OF
BEAM ON ELASTIC FOUNDATION THEORY
TO THE ANALYSIS OF STIFFENED PLATE STRIPS**

*Thesis for the degree of Doctor of Science
(Technology) to be presented with due
permission for public examination and
criticism in the Auditorium of the Student
Union House of Lappeenranta University of
Technology, Lappeenranta, Finland on the
8th of October 1999, at noon.*

ISBN 951-764-361-6
ISSN 1456-4491

Lappeenranta teknillinen korkeakoulu
Monistamo 1999

Errata

1) On page 8 row 3 ... about the x and y axis. shall be ... about the y and x axis.

2) On page 31

$$w_0(x, y) = \sum_n A_n \cos(\gamma_n x) , \quad \gamma_n = \frac{n\pi}{a} , \quad n = 1, 3, 5... \quad (4.2-2)$$

shall be

$$w_0(x, y) = \sum_n A_n \cos(\gamma_n x) \cos(\eta_n y) , \quad \gamma_n = \frac{n\pi}{a} , \quad n = 1, 3, 5... \quad (4.2-2)$$

3) On page 35

$$M_{x,1}(x, y) = \sum_n \frac{M_{n,1}}{\cosh(\gamma_n B/2)} \frac{\gamma_n B}{4} [((1 - \nu) \tanh(\gamma_n B/2) + \frac{2\nu}{\gamma_n B/2}) \cosh(\gamma_n y) - 2(1 - \nu) \frac{y}{B} \sinh(\gamma_n y)] \sin(n\pi/2) \cosh(\gamma_n x) . \quad (4.2-15)$$

shall be

$$M_{x,1}(x, y) = \sum_n \frac{-M_{n,1}}{\cosh(\gamma_n B/2)} \frac{\gamma_n B}{4} [((1 - \nu) \tanh(\gamma_n B/2) + \frac{2\nu}{\gamma_n B/2}) \cosh(\gamma_n y) - 2(1 - \nu) \frac{y}{B} \sinh(\gamma_n y)] \sin(n\pi/2) \cos(\gamma_n x) . \quad (4.2-15)$$

4) On page 48 last section, second row

... under constant axial pretraining... shall be ... under uniform axial pretraining...

5) On page 60 in Figure 4.6-1 k_j shall be k_ϕ .

ABSTRACT

Acta Universitatis Lappeenrantaensis 86

Teuvo Partanen

On the Application of Beam on Elastic Foundation Theory to the Analysis of Stiffened Plate Strips

Lappeenranta, 1999

ISBN 951-764-361-6

UDK 624.014.25 : 539.388.1 : 624.072/.073

ISSN 1456-4491

The main objective of this thesis is to show that plate strips subjected to transverse line loads can be analysed by using the beam on elastic foundation (BEF) approach. It is shown that the elastic behaviour of both the centre-line section of a semi-infinite plate supported along two edges, and the free edge of a cantilever plate strip can be accurately predicted by calculations based on the two parameter BEF theory. The transverse bending stiffness of the plate strip forms the foundation. The foundation modulus is shown, mathematically and physically, to be the zero order term of the fourth order differential equation governing the behaviour of BEF, whereas the torsion rigidity of the plate acts like pre-tension in the second order term.

Direct equivalence is obtained for harmonic line loading by comparing the differential equations of Levy's method (a simply-supported plate) with the BEF method. By equating the second and zero order terms of the semi-infinite BEF model for each harmonic component, two parameters are obtained for a simply-supported plate of width B : the characteristic length, $1/\lambda$, and the normalized sum, n , being the effect of axial loading and stiffening resulting from the torsion stiffness, n_{in} . This procedure gives the following result for the first mode when a uniaxial stress field was assumed ($\nu = 0$): $1/\lambda = \sqrt{2B/\pi}$ and $n_{in} = 1$.

For constant line loading, which is the superimposition of harmonic components, slightly differing foundation parameters are obtained when the maximum deflection and bending moment values of the theoretical plate, with $\nu = 0$, and BEF analysis solutions are equated: $1/\lambda = 1.47B/\pi$ and $n_{in} = 0.59$ for a simply-supported plate; and $1/\lambda = 0.99B/\pi$ and $n_{in} = 0.25$ for a fixed plate. The BEF parameters of the plate strip with a free edge are determined based solely on finite element analysis (FEA) results: $1/\lambda = 1.29B/\pi$ and $n_{in} = 0.65$, where B is the double width of the cantilever plate strip.

The stress biaxiality, $\nu > 0$, is shown not to affect the values of the BEF parameters significantly. The result of the geometric nonlinearity caused by in-plane, axial and biaxial loading is studied theoretically by comparing the differential equations of Levy's method with the BEF approach. The BEF model is generalised to take into account the elastic rotation stiffness of the longitudinal edges. Finally, formulae are presented that take into account the effect of Poisson's ratio, and geometric non-linearity, on bending behaviour resulting from axial and transverse in-plane loading. It is also shown that the BEF parameters of the semi-infinite model are valid for linear elastic analysis of a plate strip of finite length. The BEF model was verified by applying it to the analysis of bending stresses caused by misalignments in a laboratory test panel.

In summary, it can be concluded that the advantages of the BEF theory are that it is a simple tool, and that it is accurate enough for specific stress analysis of semi-infinite and finite plate bending problems.

ACKNOWLEDGEMENTS

The work described in this thesis was performed in the Laboratory of Steel Structures of the Department of Mechanical Engineering, Lappeenranta University of Technology, Finland.

Professor Erkki Niemi was the supervisor of the work, and is thanked for his continuous support, valuable discussions, and the provision of experimental facilities.

I express my gratitude to the two official pre-disputation examiners of this dissertation, Dr. Matti Hakala of VTT, Finland, and Prof. Antti Pramila of Oulu University of Technology, Finland, for their valuable corrections and comments.

I wish to express particular thanks to Prof. Heikki Martikka, Dr. Timo Nykänen, Mr. Timo Björk and Mr. Tapani Halme for their comments and their encouraging friendship throughout the work. I wish to thank the personnel of the Department of Mechanical Engineering for their help in carrying out the experimental testing and in preparing the final document.

Dr. John Ion is thanked for advice on the English text.

The Support Fund of Lappeenranta University of Technology is acknowledged for financial assistance during the work.

Most important of all, my sincerest appreciation goes to my wife, Riitta, and our children, Maria, Tuomo and Antti for their continuous support and understanding. Finally, this thesis is dedicated to the memory of my father, Arvo Partanen.

Teuvo Partanen

September 29th, 1999
Lappeenranta, Finland

TABLE OF CONTENTS

ABSTRACT	i
ACKNOWLEDGEMENTS	ii
TABLE OF CONTENTS	iii
NOMENCLATURE	vi
 1. INTRODUCTION	
1.1 Background and objectives of study	1
1.2 Goals and scope of study	4
1.3 Contents	5
 2. CLASSICAL ANALYSIS OF PLATE STRIP BASED ON LÉVY'S METHOD	
2.1 Differential equation of plate bending	7
2.2 Analysis of plate strips based on single Fourier series (Levy's method)	9
2.3 Semi-infinite plate strips under lateral edge loads	
2.3.1 Deflection functions	10
2.3.2 Internal forces	13
2.3.3 Reaction forces at the line $x = 0$	14
 3. APPLICATION OF BEF THEORY TO THE ANALYSIS OF PLATE STRIPS	
3.1 BEF foundation models	16
3.2 Finite element formulations for semi-infinite BEF	18
3.2.1 Deflection $w(x)$ and slope of deflection $\phi(x)$ functions	20
3.2.2 Internal forces in a semi-infinite beam element on elastic foundation	20
3.2.3 Stiffness matrix of a semi-infinite beam element on elastic foundation	21
3.3 Application of BEF theory to the analysis of a simply-supported plate strip	
3.3.1 BEF parameters under harmonic loading	22
3.3.2 BEF parameters under constant lateral line loading	23
3.3.3 Effect of constant edge moment loading on bending behaviour	26
 4. ON GENERALISATION OF THE BEF MODEL	
4.1 FEA verification of simply-supported semi-infinite plate strip model	27
4.2 Analysis of a fixed semi-infinite plate strip using classical plate theory,	

FE analysis and BEF theory	
4.2.1 Determination of BEF parameters of a fixed plate under lateral line loading	29
4.2.2 Constant edge moment loading	40
4.3 Application of BEF theory to the analysis of a semi-infinite plate strip with a free edge	42
4.4 Geometric non-linear effect of in-plane loading on bending behaviour	
4.4.1 Geometric non-linear BEF model	45
4.4.2 Geometric non-linearity under constant lateral line loading	49
4.5 Effect of biaxial stress state on bending behaviour	52
4.5.1 Linear analysis	52
4.5.2 Effect of geometric non-linearity caused by axial in-plane loading	53
4.5.3 Effect of geometric non-linearity caused by transverse in-plane loading	55
4.5.4 Combined effect of geometric non-linearity caused by axial and transverse in-plane loading on bending behaviour	57
4.6 The generalised BEF model	58
4.6.1 Model for plates supported elastically along longitudinal edge lines	58
4.6.2 Cantilever plate model	64
5. ANALYSIS OF PLATE STRIPS OF FINITE LENGTH BASED ON BEF THEORY	
5.1 BEF finite element formulations	
5.1.1 Literature review	66
5.1.2 Deflection function $w(x)$, $-1 < n < 1$	67
5.1.3 Internal forces in a two node beam element on an elastic foundation	70
5.1.4 Element stiffness matrix	71
5.2 Application of BEF theory to analysis of a plate strip of finite length	73
5.3 Discussion	78
6. CASE STUDY: EXPERIMENTAL VERIFICATION OF APPLICATION OF BEF THEORY TO ANALYSIS OF STIFFENED PLATE	
6.1 Introduction	79
6.2 Experimental tests	
6.2.1 Shape of the panel	79
6.2.2 Instrumentation and strain gauge measurements	81

6.3 FEA models and results	
6.3.1 FE models	82
6.3.2 Results of shell element FEA	82
6.4 Two parameter BEF models and results	85
6.4.1 Geometric linear analysis model and results	86
6.4.2 Geometric non-linear analysis results	87
6.5 Summary of results and discussion	88
6.5.1 Comparison of BEF and FE analysis with experimental measurements	89
6.5.2 Discussion of present design recommendations	91
6.5.6 New model for angular misalignment for plates of differing thickness	93
 7. DISCUSSION AND CONCLUSIONS	
7.1 Summary and conclusions	94
7.2 Future research	96
 REFERENCES	98
APPENDICES	100

NOMENCLATURE

Latin upper case letters

$A_{i,m}, B_{i,m}$	unknown deflection amplitudes i of harmonic component m , $i = 1, 2, 3, 4$
A_n, B_n	unknown deflection amplitudes n
C_n, D_n	unknown deflection amplitudes n
B	stiffener spacing; width of I-beam flange
E	modulus of elasticity
E'	$E/(1-\nu^2)$
$F_i, F_{i,m}$	nodal point load component i , $i = 1, 2, 3, 4$; harmonic component m
F_0	nodal point load
I	flexural moment of inertia of a beam or a plate of unit width
K	bending or flexural rigidity of plate of unit width
K_b	contribution of bending stress in stress concentration
K_{gnl}	factor for geometric non-linearity
K_h	factor for differing thickness
K_s	structural stress concentration
K_v	factor for transverse bending
L	length of beam; length of angular misalignment
M	bending moment of a beam; or a plate of unit width, in general
M_x, M_y	bending moments (per unit width) producing axial stresses in x and y directions
$M_{x,0}, M_m$	edge moment loading in x direction at $x = 0$ line; component m of $M_{x,0}$
$M_{x,0}$	bending moment in x direction resulting from external loading in simply-supported plate
$M_{x,1}$	bending moment in x direction resulting from edge moment $M_{y,1}$
$M_{y,1}, M_{n,1}$	unknown edge moment in y direction at $y = B/2$; component n of $M_{y,1}$
$M_{y,0}$	bending moment in y direction resulting from external loading
$M_{y,1}$	bending moment in y direction resulting from edge moment $M_{y,1}$
$M_{xy} = M_{yx}$	twisting moment per unit width
$M_{xy,1}$	twisting moment in y direction resulting from $M_{y,1}$
M_0	point couple loading
$M_{1,\infty}$	bending moment in x direction at $x = 0$ of a semi-infinite BEF strip
M_1	bending moment in x direction at $x = 0$ of a BEF strip of length L
M_2	bending moment in x direction at $x = L$ of a BEF strip of length L
N, N_m	axial load per unit width; harmonic component m ; second order, Pasternak foundation parameter
$N_{cr,x}$	critical buckling load of the two parameter foundation model BEF
$N_{cr,y}$	critical buckling load in y direction
N_{Eul}	elastic buckling load of simply-supported bar in y direction
N_w	elastic buckling load in x direction of one parameter BEF model
N_x, N_y	axial load in x and y directions

$N_{xy} = N_{yx}$	in-plane shear load
Q_x	pure shear force in x direction ($= \partial M_x / \partial x$)
Q_y	pure shear force in y direction ($= \partial M_y / \partial y$)
U_1	deflection at $x = 0$ of a semi-infinite BEF or a BEF of length L
$U_{1,\infty}$	deflection at $x = 0$ of a semi-infinite BEF
U_2	slope of deflection at $x = 0$ of a semi-infinite BEF, or a BEF of length L
$U_{2,\infty}$	slope of deflection at $x = 0$ of a semi-infinite BEF
U_3	deflection at $x = L$ of a BEF of length L
U_4	slope deflection at $x = L$ of a BEF of length L
$U_{i,m}$	nodal displacement component i of harmonic component m , $i = 1, 2, 3, 4$
$V(x)$	generalised shear force, transverse to the non-deformed x axis
V_x	edge force in x direction;
V_0, V_m	constant line loading at $x = 0$ line; harmonic component m
V_1	support reaction at $x = 0$ of a BEF of length L
$V_{1,\infty}$	support reaction of a semi-infinite BEF at $x = 0$
$X(x), Y(y)$	deflection functions in x and y directions
$X_m(x), Y_m(y)$	component m of deflection function

Latin lower case letters

a	length in x direction
b	width of cantilever plate; $B/2$ of a flange
dx, dy	differential lengths in x and y directions
e_0	eccentricity of offset misalignment
h, h_1, h_2	thickness of plate; thickness of the thinner (1) or thicker (2) plate
k, k_m	Winkler foundation modulus; harmonic component m
k_ϕ	rotation spring coefficient of line spring at longitudinal edge line
m	root of a characteristic equation; index in series expressions
$m_x, m_{x,gnl}$	normalised moment in x direction; resulting from geometric non-linearity
$m_{x,ss}, m_{x,fix}$	normalised moment in simply-supported (ss) and fixed (fix) plates
$m_{y,1}$	normalised edge reaction moment resulting from $M_{y,1}$ in y direction
$m_1(AL)$	finite length factor of moment resulting from deflection U_1
$m_{2,1}(AL)$	finite length factor of moment at $x = L$ resulting from U_1
$m_{2,2}(AL)$	finite length factor of moment at $x = L$ resulting from U_2
n	normalised second order foundation parameter in general; index in series expressions
n_m	axial load ratio N/N_α of component m
n_{lin}	foundation parameter ratio $n (= N/N_w)$ when axial load is zero
n_x	axial membrane load ratio $N/N_{\alpha,x}$
n_y	transverse membrane load ratio $N_y/N_{\alpha,y}$
p, p_z	index; pressure loading in z direction
$q(x)$	distributed load of intensity q in z direction
r	stiffness ratio

r, r_{gnl}	normalised rotation; resulting from geometric non-linearity
r_{fix}	normalised rotation in fixed plate
$r_2(\lambda L)$	finite length factor of rotation U_2
s, s_{gnl}	normalised deflection; resulting from geometric non-linearity
$s_{\text{ss}}, s_{\text{fix}}$	normalised deflection in simply-supported (ss) and fixed (fix) plates
$u_1(\lambda L)$	finite length factor of deflection U_1
$v_1(\lambda L)$	finite length factor of edge reaction at $x = 0$ resulting from U_2
w, w_m	plate/beam deflection in z direction; of component m
w_0	deflection resulting from external loading in simply-supported plate
w_1	deflection resulting from unknown edge moment $M_{y,1}$
x, y	in-plane co-ordinate axis
z	co-ordinate axis normal to the plate (in the lateral direction)
z_0	depth of angular misalignment

Greek letters

Δ	auxiliary variable; change of
α, α_m	parameter containing second order BEF expressions; harmonic component m
α_{lin}	parameter in BEF expressions when the axial load is zero
β, β_m	parameter containing second order BEF expressions; harmonic component m
β_t	parameter containing second order BEF expressions under high tension loading
ϵ	axial strain
γ_n	auxiliary variable $n\pi/a$
η, η_m	auxiliary variable $\sqrt{(N/EI)}$; auxiliary variable $m\pi/B$
λ, λ_m	characteristic of a beam on elastic foundation; harmonic component m
$1/\lambda, 1/\lambda_m$	characteristic length of BEF; harmonic component m in plate analysis
ν	Poisson's ratio (0.3 used for steel; written ν in equations)
σ	axial stress, normal stress
σ_b	bending stress
σ_m	nominal membrane stress
$\sigma_{m,cl}$	membrane stress at centre-line
σ_s	structural stress
σ_x, σ_y	axial stress in x and y directions
$\tau_{xy} = \tau_{yx}$	shear stress
φ	slope of deflection
φ_0	angle of angular misalignment; slope of deflection $\partial w_0 / \partial y$ resulting from external loading at $y = B/2$ line
φ_1	slope of deflection $\partial w / \partial y$ resulting from edge moment $M_{y,1}$ at $y = B/2$ line
ψ	auxiliary variable

Matrices and vectors

$\{A\}$, $\{A_m\}$	deflection amplitude vector; harmonic component m
$[D]$, $[D_m]$	coefficient matrix of derivation operation of $[H(x)]$: $[H'(x)] = [H(x)][D]$; harmonic component m
$[D^2]$, $[D_m^p]$	$[D][D]$; $[D^p]$ correspondingly, $p = 2, 3, 4$; harmonic component m
$[E]$, $[E_m]$	see $[G]$; harmonic component m
$\{F\}$, $\{F_m\}$	element nodal load vector; harmonic component m
$\{F_{eq}\}$	equivalent nodal load vector
$\{F_g\}$	external load vector
$[G]$, $[G_m]$	shape function coefficient matrix: $[G] = [E]^{-1}$; harmonic component m
$[H(x)]$	matrix of shape function containing x dependent terms
$[H_m(x)]$	harmonic component m of $[H(x)]$
$[I]$	unit matrix
$[N(x)]$	shape function of deflection: $[N(x)] = [H(x)][G]$
$[N_m(x)]$	harmonic component m of $[N(x)]$
$[S]$	stiffness matrix of one element, in general
$[S_g]$	global stiffness matrix
$[S_t]$	stiffness matrix under high tension loading
$\{U\}$, $\{U_m\}$	nodal point displacement vector; harmonic component m

Abbreviations

BEF	beam on elastic foundation
Eqn, Eqns	equation; equations
FE, FEA	finite element; FE analysis
Fig.	figure
fix	fixed
gnl	geometric non-linear
lin	geometric linear
ss	simply-supported
SHS	square hollow section
CH	$\cosh(\alpha L)$
SH	$\sinh(\alpha L)$
ch	$\cosh(\beta L)$; $\cosh(\beta_t L)$
sh	$\sinh(\beta L)$; $\sinh(\beta_t L)$
c	$\cos(\beta L)$; $\cos(\eta L)$
s	$\sin(\beta L)$; $\sin(\eta L)$

Subscripts

c	compression
cl	centre-line

cr	critical
def	defined
eq	equivalent
Eul	Euler
g	global
gnl	geometric nonlinear
lin	linear
m	index; membrane
max	maximum
min	minimum
mod	model
n	index
nom	nominal
t	tension
W	Winkler
w	deflection w related
x,y,z	coordinates x,y,z
0	initial; applied loading
1	unknown 1; end 1
2	end 2
∞	related to semi-infinite BEF

Superscripts

-1	inverse of a matrix
' , "	derivative, d/dx ; second derivative etc
T	transposition of a matrix

Constants and other symbols

e	base of Napierian or natural logarithms: 2.71828...
i	unit imaginary number: $i^2 = -1$
π	3.14159...
\rightarrow	lim , approaching
\times	multiplied by (when necessary)
/	divided by
\sum	sum
$<, >$	smaller than ; larger than
$\sqrt{\quad}$	square root
[]	matrix
{ }	vector

\approx	approximately equal to
\mp	plus or minus
d, ∂	derivative of a one or two dimensional function, respectively
∇^2	two dimensional Laplacian operator
- · - · -	symmetry
- - - - -	antimetry

Chapter 1

INTRODUCTION

The chapter begins with an introduction to the problems related to the design of load-carrying welded plate structures that are subjected to alternating loading. Manufacturing tolerances increase the structural stress of plate sections, illustrated in two figures. This extra stress, the plate bending stress, must be taken into account in fatigue analysis in particular. Unfortunately, a detailed stress analysis based on plate theory is tedious, or based on finite element analysis time-consuming. The objective of the study, presented in Section 2.2, was to develop original, simple calculation methods for specific plate problems. The content of the thesis is described briefly at the end of the chapter.

1.1 Background and objectives of study

The primary task of a structural engineer is to ensure that the resistance of a structure is greater than the loading it experiences. Strength analysis of structures is based on two principles: i) structures made of ductile material subjected to static loading are designed against plastic collapse; ii) structures made of brittle material, structures susceptible to a loss of stability under in-plane loading, or structures subject to fatigue loading are primarily designed according to linear elastic stress analysis.

Elastic stress analysis has traditionally been based on classical methods, and often limited to a global level analysis. For some problems, with distinct boundary conditions, closed form solutions describing deflection functions can be obtained. Nowadays, numerical finite element analysis (FEA) methods are available for the analysis of the internal force distribution at a global level, often used in conjunction with a local model to determine stress concentrations at geometric discontinuities. Further refined element models are needed to take into account all the relevant factors, this being the shortcoming that has the most significant effect on the accuracy of FE analysis results.

Stress analysis is a mathematical idealisation of natural structural behaviour. In a static strength analysis, to define the maximum plastic load capacity, some stress redistribution at the joints is normally allowed. The elastic stress analysis for fatigue assessment is complicated by the true geometrical shape of the structure, especially at the joints of welded structures. Under fatigue loading, the sum of the stresses resulting from various loading components at the critical locations of welded joints are equally damaging.

Because of fabrication tolerances and differing plate thicknesses at butt joints, the midplanes of the plates can easily be offset. During the welding process the joints distort angularly when cooling from the melting temperature. These two types of deviation from the idealised geometry are called *axial* and *angular misalignments*, illustrated in Fig.1.1-1. When subject to in-plane loading transverse to the misaligned

joint, the plate will deflect laterally, causing out-of-plane bending stresses which are superimposed on the membrane stress. The axial stress in the thickness direction, which consists of the membrane stress and the bending stress caused by misalignments, is illustrated in the figures. The equivalent loads of nominally straight structures under axial loading per unit width, N , which result from the misalignments in Fig. 1.1-1, are shown in Fig. 1.1-2.

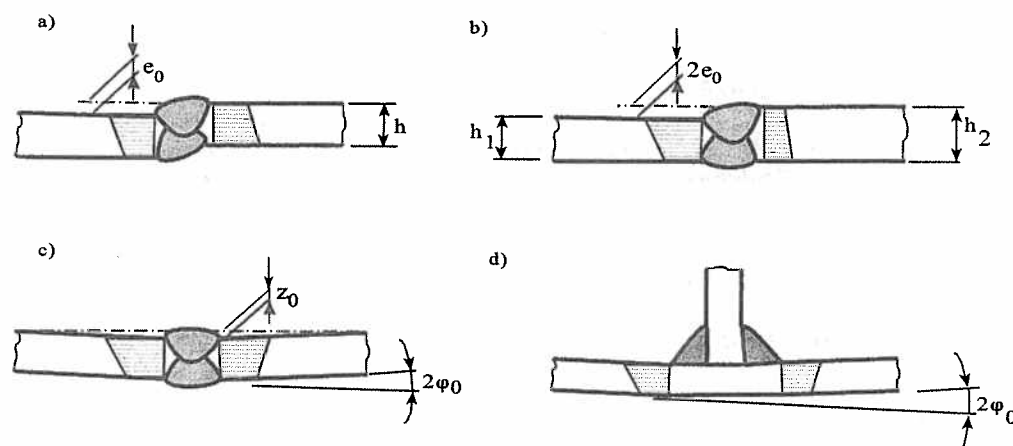


Figure 1.1-1 Welded joints containing different types of misalignment.

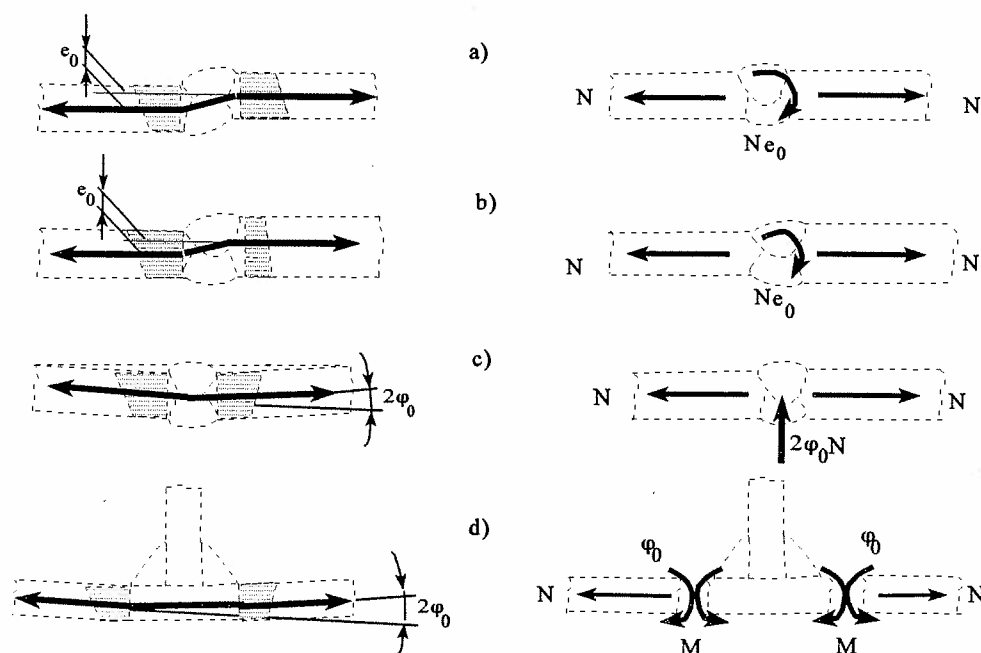


Figure 1.1-2 Equivalent lateral loading of aligned plates caused by misalignment shown by force flow and by corresponding free body models.

In Figs 1.1-2a) and b), the effect of an axial misalignment of magnitude e_0 is equivalent to a point couple, Ne_0 . As can be seen in Fig. 1.1-2a), e_0 originates from manufacturing tolerances in a joint comprising plates of equal thickness. In a joint comprising plates of differing thickness, with the lower surface aligned, Fig. 1.1-2b), e_0 is 50% of the thickness step, $h_2 - h_1$. In a butt joint containing an angular misalignment characterised by an angle, φ_0 , Fig. 1.1-2c), the axial load, N , produces a lateral load, $N\varphi_0$, for an ideally-aligned plate geometry. An angular misalignment in a butt joint can also be characterised by a depth, z_0 , shown in Fig 1.1-1c). In a fillet-welded T joint, the angular misalignment can only be characterised by the angle φ_0 . When a geometric non-linear analysis is performed, the T joint can be analysed based on the constrained rotation, φ_0 .

In static analysis of structures made of ductile materials, the induced bending stress effect of an angular misalignment is not normally taken into account when the in-plane loading is tensile. In fatigue assessment, these bending stresses may or may not be taken into account on the loading side, depending on the design approach (Hobbacher, 1996). In the traditional *nominal stress approach* the stress concentration caused by the joint geometry and the effect of misalignments are implicitly included in the fatigue strength data: these data have been determined as the nominal membrane stress of laboratory specimens containing some degree of misalignment. When the shape and stress distribution differ significantly between the laboratory test specimen and the designed structure, a certain global level concentration must be taken into account in fatigue design based on the nominal stress approach. In the modern method, referred to as the *structural, geometric, or hot-spot stress approach*, which is based on the structural stress, concentrations are included on the loading side. The structural stress, linearly distributed in the thickness direction, includes the effect of misalignments, and contains the effect of all these concentrations.

The stress analysis of shells, plates and plate sections is based on the modified local nominal stress, since the fatigue strength data have been determined based on relatively well-aligned specimens from conventional tension testing. Stress concentrations caused by excessive misalignment belong to the local nominal stress category. In general, local nominal stress concentrations are called *macrogeometric effects*. Finite element methods, and in some cases, classical stress analysis, can be applied to determine the stress state at the local nominal stress level of accuracy. Maddox (1985) presented elementary, highly simplified design equations for calculating the stress concentration resulting from misalignment. His results have subsequently been applied in design recommendations (Hobbacher, 1996).

Parametric formulae derived using either calculation method, FEA or classical, are the fast tools used for everyday fatigue design work. By using classical methods, the (macrogeometric) stress concentration factors are based on mathematically correct parametric functions of membrane stress and bending stress distributions. Theoretically correct stress functions are complicated in the analysis of internal statically-indeterminate structures, such as continuous plate sections. Numerical

analysis is often needed to provide a solution. The application of the resulting theoretically correct stress concentration functions in everyday design work is laborious. Simplified but accurate analysis formulae are needed.

Sometimes a rigorous solution for one problem can be applied to an other with minor modifications. As an example, the one parameter beam on elastic foundation (BEF) solution, originally developed by Winkler (1867), is directly applicable to the axisymmetric analysis of discontinuity stresses in cylindrical shells. The membrane stiffness in the circumferential direction resisting expansion, or compression in the radial direction under pressure loading, forms the foundation stiffness of the BEF model. The accuracy is normally sufficient for the analysis of discontinuity stresses in spherical and conical shells. FEA using shell or solid elements is a rapid method of testing the applicability and accuracy of simplified calculation models for more complicated problems.

The one parameter BEF method has been applied to determine the hot spot (structural) stress gradient in a number of details in stiffened plate structures by interpreting FEA results (Partanen, Tarjauori, and Niemi, 1992) and (Partanen, 1992).

1.2 Goals and scope of study

The study considers the application of geometric non-linear two parameter BEF theory to the stress analysis (at the local nominal stress level of accuracy) of longitudinally-stiffened plate strips subjected to external line loads. Plate strips are plates infinite or semi-infinite in one (longitudinal) direction. The line loads are of constant value and transverse to the longitudinal support line, being either lateral, Fig. 1.2-1, or edge moment, such as that shown in Fig. 1.1-2a) and b). Fig. 1.2-1a) shows a simply-supported plate of width B loaded with a transverse line load in the lateral z direction. This corresponds to an equivalent loading caused by an angular misalignment, Fig. 1.1-2c), when loaded in-plane in the longitudinal direction, x . The following are to be shown: i) that the bending stiffness resisting the lateral deflection under uniform pressure loading (the inverse of the deflection normalised by the load) forms the foundation (k); and ii) the effect of the torsional stiffness of the plate forms the second parameter (N) of the BEF model, shown in Fig. 1.2-1d). The BEF solutions are applicable to a unit width strip, dy , in *three* cases:

- the centre-line section, $y = 0$, of a simply-supported plate, Fig. 1.2-1a)
- the centre-line section, $y = 0$, of a plate fixed at the two longitudinal edge lines $y = \pm B/2$, Fig. 1.2-1b)
- the free-edge line $y = b = B/2$ of a cantilever plate, Fig. 1.2-1c).

It will be shown that if the two parameters of the BEF analysis model are determined based on the equality of the maximum value of the deflection and the bending moment in the BEF, and the reference solution, respectively, the plate bending behaviour can be approximated for engineering applications by the BEF model with sufficient

accuracy. Plate theory, finite element modelling and analysis, and ordinary beam bending calculations are used to determine the reference analysis results.

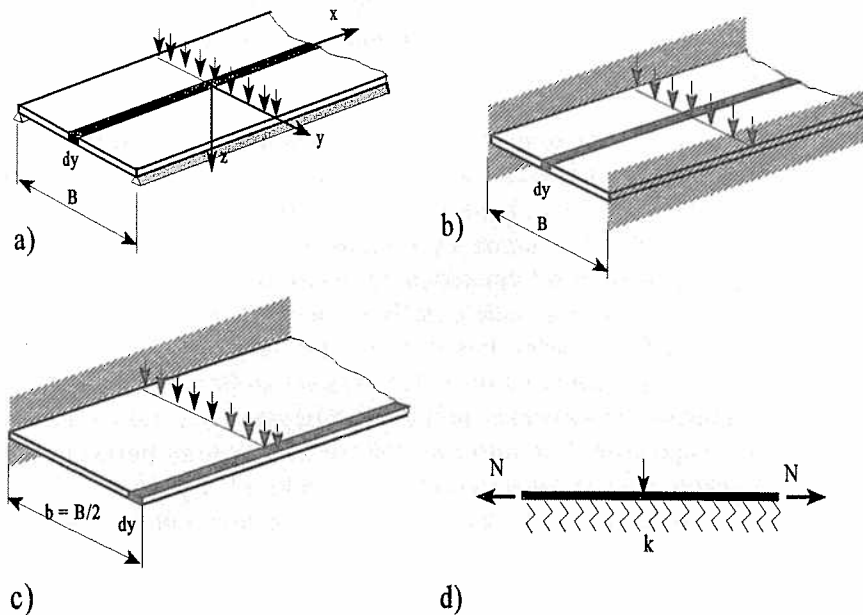


Figure 1.2-1 Longitudinally-supported plate strips under transverse line load: a) simply-supported, b) fixed and c) cantilever plate strip with one free edge, the other being fixed; d) BEF model of the unit width plate strip, dy .

1.3 Contents

In Chapter 2, Lévy's (1899) method is applied to a semi-infinite plate strip that is simply supported at the longitudinal edges, and loaded by transverse harmonic edge line and edge moment loads. In Lévy's method, a two dimensional plate problem is solved, based on a one dimensional differential equation of the fourth order. Deflection and internal force functions are presented.

In Section 3.1 at the beginning of Chapter 3, two types of BEF model, the one parameter Winkler (1867) model, and the two parameter Pasternak (1954) model are presented. Deflection and internal force functions for a semi-infinite two parameter BEF are derived. In Section 3.2, following the principles of finite element formulations, the stiffness matrix of a semi-infinite beam on elastic foundation is determined. By

comparing the differential equations of the simply-supported plate strip of Chapter 2 and the semi-infinite two parameter BEF model, it is shown in Section 3.3 that under harmonic (cosine) loading, the foundation parameters are directly obtainable by setting equal the differential equations of the plate and BEF solutions. Under constant line loads the internal beam forces of the BEF model are compared with the internal plate forces of Levy's method, which are a superimposition of the series expressions of harmonic loads.

In Chapter 4, Section 4.1, the results of a FE analysis linear shell element model of a simply-supported plate under constant edge line loading are compared with the closed-form solutions of Chapter 2. This case is used for verification of the accuracy of FE modelling. In Section 4.2, the same FEA model is used to test the accuracy and correctness of more complicated theoretical formulae of a plate strip fixed to prevent rotation along the longitudinal supporting (stiffener) lines. In Section 4.3, a semi-infinite cantilever plate strip, with one edge free and the other fixed, is analysed by FEA only, since a closed-form reference solution is complicated. In Section 4.4, the effect of in-plane loading is analysed theoretically and verified by geometric non-linear FEA when the plate is simply supported. The effect of Poisson's ratio, ν , on bending behaviour is discussed in Section 4.5. A generalised BEF model of a plate that is supported elastically against rotation along the two support lines is presented in Section 4.6.

The generalised BEF model, based on the results of Chapters 3 and 4 and presented in Section 4.6, is applied in Chapter 5 to the analysis of simply-supported and fixed plates of finite length. Deflection functions and stiffness matrices of a two node, two parameter BEF element are given in Section 5.1. The results of shell element FEA runs are compared with the predictions based on the finite element formulations of a two node two parameter BEF element.

In Chapter 6, the BEF model developed is applied to the stress analysis of an experimental test panel that is longitudinally stiffened and loaded. It contains an offset misalignment resulting from the thickness change superimposed by offset and angular misalignments as a result of manufacturing tolerances. The panel was also analysed by shell element FEA for comparison.

The results of the study are discussed and the final conclusions of the thesis are given in Chapter 7.

Chapter 2

CLASSICAL ANALYSIS OF PLATE STRIPS BASED ON LEVY'S METHOD

The theoretical basis of this study and the formulae that are commonly used in geometric linear plate theory, and which are needed in this study, are introduced at the beginning of the chapter. The biharmonic differential equation of a rectangular plate is presented. By applying Levy's method, deflection and internal force functions are obtained for a semi-infinite plate strip, simply supported along its longitudinal edges and subjected to harmonic lateral line and edge moment loads. These solutions are used in Chapter 3 to obtain the parameters of a uniaxial bending model.

2.1 Differential equation of plate bending

The assumptions of small deflection plate theory (Kirchoff, 1850, 1876) are used throughout this study. A simply-supported plate strip of width, B , and thickness, h , is shown in Figure 2.1-1a) together with the co-ordinate system, and an element $dx dy$ at the location x, y . When subjected to a lateral pressure, p_z , the plate deflects in the out-of-plane z direction by $w(x,y)$, which results in rotations around the x and y axes, as well as in-plane displacements $u(x,y,z)$ and $v(x,y,z)$, Figure 2.1-1b). The positive directions of internal stresses are shown in Figure 2.1-1c).

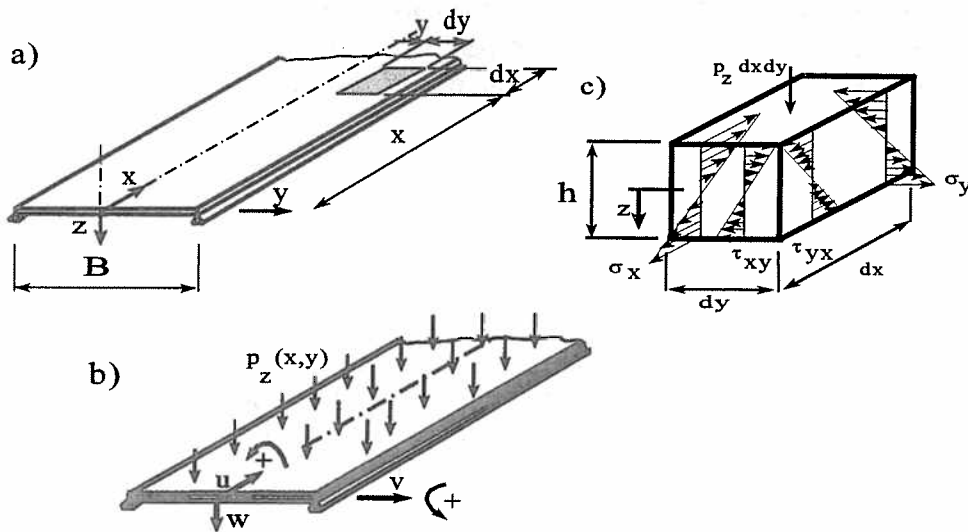


Figure 2.1-1 Laterally-loaded rectangular plate: a) geometry; b) loading and displacement definitions; c) a free body model of a volume of the plate.

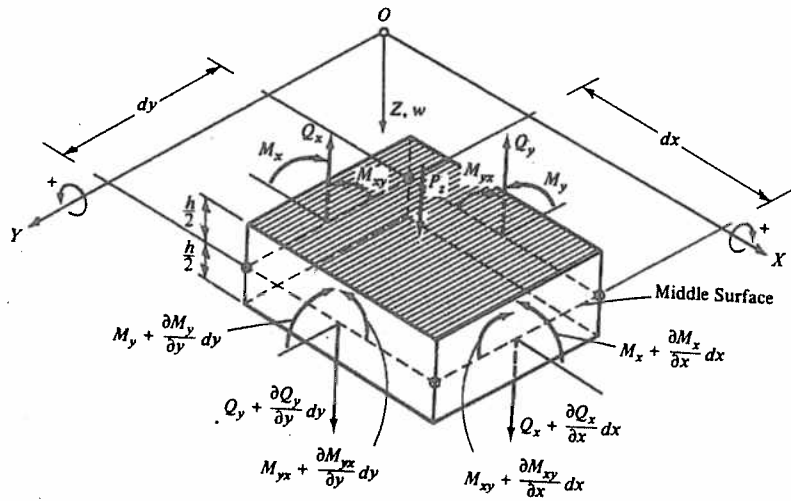


Figure 2.1-2 External and internal forces on a mid-plane element (Szilard, 1974).

The internal forces on a plate element $dx dy$ subjected to lateral pressure, p_z , are shown in Figure 2.1-2. The shear forces, Q_x and Q_y , are obtained by summing the moments about the x and y axes. In this study, all force components in plates are expressed per unit length. The summation of all forces in the z direction yields the third force equilibrium equation. By using these equations, the differential equation governing the lateral force balance of a plate element is given by

$$\frac{\partial^2 M_x}{\partial x^2} + 2 \frac{\partial^2 M_{xy}}{\partial x \partial y} + \frac{\partial^2 M_y}{\partial y^2} = -p_z. \quad (2.1-1)$$

M_x and M_y result in bending stresses parallel and perpendicular, respectively, to the direction of the simple supports, the longitudinal direction. The internal forces are then related to the stresses, which, according to Hooke's law in two dimensions, are related to the strains. Finally, when the strains are functions of the lateral deflection, w , the internal bending moments per unit length, M_x and M_y , can be related to w through

$$M_x = -K \left(\frac{\partial^2 w}{\partial x^2} + \nu \frac{\partial^2 w}{\partial y^2} \right), \quad K = \frac{Eh^3}{12(1 - \nu^2)}. \quad (2.1-2)$$

$$M_y = -K \left(\frac{\partial^2 w}{\partial y^2} + \nu \frac{\partial^2 w}{\partial x^2} \right). \quad (2.1-3)$$

In Eqns (2.1-2) and (2.1-3), ν is Poisson's ratio, E is Young's modulus of elasticity, and h is the plate thickness. K represents the bending or flexural rigidity of the plate. Similarly, the expression for the twisting moment, M_{xy} , in terms of the lateral deflection is

$$M_{xy} = -(1 - \nu)K \frac{\partial^2 w}{\partial x \partial y}. \quad (2.1-4)$$

The edge force per unit length, V_x , is calculated by using

$$V_x = -K \left(\frac{\partial^3 w}{\partial x^3} + (2 - \nu) \frac{\partial^3 w}{\partial x \partial y^2} \right). \quad (2.1-5)$$

When Eqns (2.1-2), (2.1-3) and (2.1-4) are substituted into (2.1-1), the governing differential equation of the plate subjected to a lateral pressure load is obtained:

$$\frac{\partial^4 w}{\partial x^4} + 2 \frac{\partial^4 w}{\partial x^2 \partial y^2} + \frac{\partial^4 w}{\partial y^4} = \frac{p_z}{K}. \quad (2.1-6)$$

When no lateral load exists, $p_z = 0$, and Eqn (2.1-6) becomes a homogeneous biharmonic differential equation:

$$\nabla^2 \nabla^2 w = 0, \quad \nabla^2 = \frac{\partial^2}{\partial x^2} + \frac{\partial^2}{\partial y^2}, \quad (2.1-7)$$

where ∇^2 is the two dimensional Laplacian operator.

2.2 Analysis of plate strips based on single Fourier series (Levy's method)

In Levy's method (Levy, 1899) a two dimensional biharmonic plate problem is solved using the product of two deflection functions $X(x)$ and $Y(y)$ (Szilard, 1974). It is also assumed that the edges $y = \pm B/2$ are simply supported. The deflection function $w(x,y)$ can be expressed by a single trigonometric series:

$$w(x,y) = X(x) Y(y) = \sum_m X_m(x) \cos(\eta_m y) ,$$

$$\eta_m = \frac{m\pi}{B} , \quad m = 1, 3, 5... \quad (2.2-1)$$

When this is substituted into Eqn (2.1-7), the following equation results:

$$K \sum_m \left[X_m''''(x) - 2\eta_m^2 X_m''(x) + \eta_m^4 X_m(x) \right] \cos(\eta_m y) = 0 , \quad (2.2-2)$$

where X_m'''' and X_m'' are the fourth and second differentials of X_m with respect to x , respectively. For a specific value of m

$$X_m''''(x) - 2\eta_m^2 X_m''(x) + \eta_m^4 X_m(x) = 0 . \quad (2.2-3)$$

Eqn (2.2-3) is a linear, homogeneous, differential equation of the fourth order with constant coefficients. The general solution of Eqn (2.2-3) was given by Nádai (1915) in the form of hyperbolic functions. For a semi-infinite plate strip, the solution, $X_m(x)$, that satisfies Eqn (2.2-3) can be represented in a simple form by

$$X_m(x) = A_{1,m} e^{-\eta_m x} + A_{2,m} \eta_m x e^{-\eta_m x} . \quad (2.2-4)$$

The deflection function $w(x,y)$ of Eqn (2.2-1) is

$$w(x,y) = \sum_m (e^{-\eta_m x} [1 , \eta_m x] \begin{Bmatrix} A_{1,m} \\ A_{2,m} \end{Bmatrix} \cos(\eta_m y)) , \quad \{A_m\} = \begin{Bmatrix} A_{1,m} \\ A_{2,m} \end{Bmatrix} . \quad (2.2-5)$$

Eqn (2.2-5) is valid for the analysis of semi-infinite plate strips - the deflection vanishes at $x = \infty$. The vector $\{A_m\}$ of the two unknown deflection amplitudes, shown in Eqn (2.2-5) for each value of m is determined next, followed by determination of the deflection and internal force functions.

2.3 Semi-infinite plate strips under lateral edge loads

2.3.1 Deflection functions

Using matrix notation, the deflection, $w(x,y)$, of Eqn (2.2-5) can be expressed as

$$w(x, y) = \sum_m [H_m(x)] \{A_m\} \cos(\eta_m y),$$

$$[H_m(x)] = \begin{bmatrix} e^{-\eta_m x} & \eta_m x e^{-\eta_m x} \end{bmatrix}. \quad (2.3-1)$$

The coefficients, $A_{1,m}$ and $A_{2,m}$, of the vector $\{A_m\}$ are determined from the boundary conditions at $x = 0$, Fig. 2.3-1, as a function of the displacements, $U_{1,m}$ and $U_{2,m}$, the nodal point displacement (degree of freedom) vector $\{U_m\}$ at $x = 0$ being given by

$$(w_m)_{x=0} = U_{1,m}, \quad \left(\frac{\partial w_m}{\partial x} \right)_{x=0} = -U_{2,m}, \quad \{U_m\} = \begin{Bmatrix} U_{1,m} \\ U_{2,m} \end{Bmatrix}. \quad (2.3-2)$$

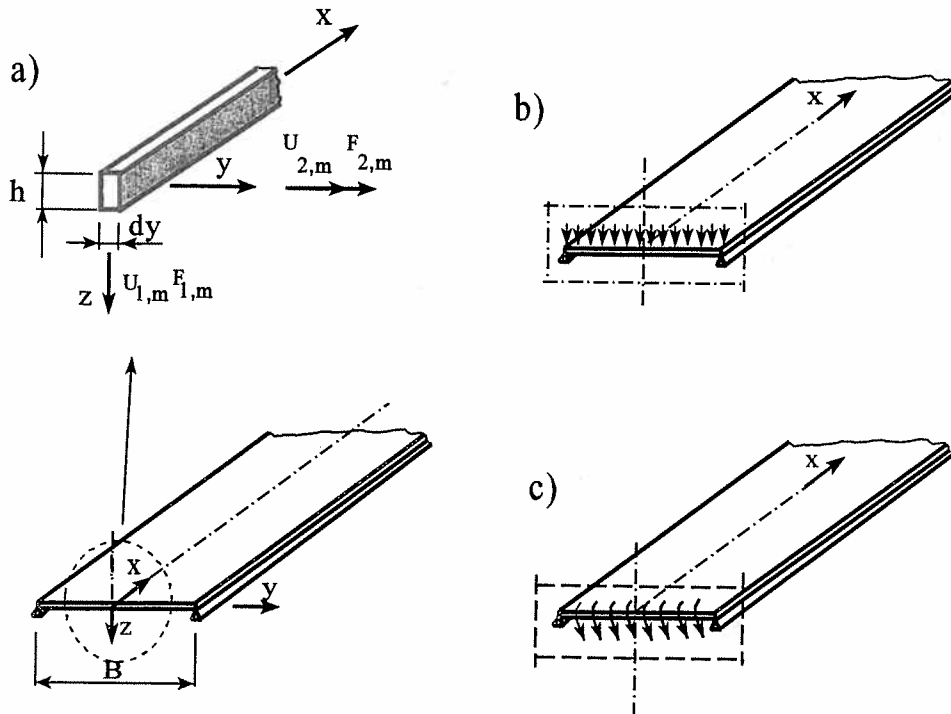


Figure 2.3-1 Simply-supported semi-infinite plate strip: a) degrees of freedom, and internal forces at $x = y = 0$; b) symmetric mode of deflection at $x = 0$ under lateral line loading; and c) antisymmetric mode under edge moment loading.

The slope of deflection, $\partial w_m / \partial x$ at $y = 0$, is determined by differentiating the row matrix $[H_m(x)]$:

$$\frac{\partial}{\partial x} w_m(x, 0) = \frac{\partial}{\partial x} [H_m(x)] A_m, \quad \frac{\partial}{\partial x} [H_m(x)] = [H_m(x)] [D_m],$$

$$[D_m] = \frac{m\pi}{B} \begin{bmatrix} -1 & 1 \\ 0 & -1 \end{bmatrix} = \eta_m [D]. \quad (2.3-3)$$

The coefficient matrix $[D_m]$ on the right hand side of the matrix $[H_m(x)]$ denotes the differentiation operation of $[H_m(x)]$. The boundary conditions of Eqn (2.3-2) can be expressed as

$$\begin{Bmatrix} U_{1,m} \\ U_{2,m} \end{Bmatrix} = \begin{bmatrix} 1 & 0 \\ \eta_m & -\eta_m \end{bmatrix} \begin{Bmatrix} A_{1,m} \\ A_{2,m} \end{Bmatrix} = [E_m] \{A_m\}. \quad (2.3-4)$$

By inverting the matrix $[E_m]$, the coefficient vector $\{A_m\}$ is obtained as the product of the shape function coefficient matrix $[G_m]$, $[G_m] = [E_m]^{-1}$, and the nodal point displacement vector $\{U_m\}$:

$$\{A_m\} = \begin{Bmatrix} A_{1,m} \\ A_{2,m} \end{Bmatrix} = \begin{bmatrix} 1 & 0 \\ 1 & -\frac{1}{\eta_m} \end{bmatrix} \begin{Bmatrix} U_{1,m} \\ U_{2,m} \end{Bmatrix} = [G_m] \{U_m\}. \quad (2.3-5)$$

The deflection component, $w_m(x, 0)$, at the centre-line, $y = 0$, of a semi-infinite plate strip can then be determined, and is expressed as the shape function $[N_m(x)]$ of $\{U_m\}$:

$$w_m(x, 0) = [N_m(x)] \{U_m\}, \quad [N_m(x)] = [H_m(x)] [G_m],$$

$$[N_m(x)] = \begin{bmatrix} e^{-\eta_m x} (1 + \eta_m x), & -x e^{-\eta_m x} \end{bmatrix}. \quad (2.3-6)$$

By substituting $\{A_m\}$ from Eqn (2.3-5) and $[N_m]$ from Eqn (2.3-6) into Eqn (2.3-1), $w(x, y)$ can be written:

$$w(x, y) = \sum_m [H_m(x)] \begin{bmatrix} 1 & 0 \\ 1 & -\frac{1}{\eta_m} \end{bmatrix} \begin{Bmatrix} U_{1,m} \\ U_{2,m} \end{Bmatrix} \cos(\eta_m y),$$

$$w(x, y) = \sum_m \begin{bmatrix} e^{-\eta_m x} (1 + \eta_m x), & -x e^{-\eta_m x} \end{bmatrix} \begin{Bmatrix} U_{1,m} \\ U_{2,m} \end{Bmatrix} \cos(\eta_m y). \quad (2.3-7)$$

By using Eqns (2.3-3) and (2.3-5), $\partial w_m / \partial x$ at $y = 0$ is

$$\frac{\partial w_m}{\partial x} = [H_m(x)][D_m][G_m]\{U_m\} = [H_m(x)] \begin{bmatrix} 0 & -1 \\ -\eta_m & 1 \end{bmatrix} \begin{Bmatrix} U_{1,m} \\ U_{2,m} \end{Bmatrix}, \quad (2.3-8)$$

resulting in the function, $\partial w(x,y)/\partial x$:

$$\begin{aligned} \frac{\partial w}{\partial x}(x,y) &= \sum_m [H_m(x)] \begin{bmatrix} 0 & -1 \\ -\eta_m & 1 \end{bmatrix} \begin{Bmatrix} U_{1,m} \\ U_{2,m} \end{Bmatrix} \cos(\eta_m y) \\ &= \sum_m \left[-\eta_m^2 x e^{-\eta_m x}, -e^{-\eta_m x} (1 - \eta_m x) \right] \begin{Bmatrix} U_{1,m} \\ U_{2,m} \end{Bmatrix} \cos(\eta_m y). \end{aligned} \quad (2.3-9)$$

Similarly, by using Eqn (2.3-7) the slope of deflection in the y -direction, $\partial w(x,y)/\partial y$, is written:

$$\begin{aligned} \frac{\partial w}{\partial y}(x,y) &= -\sum_m \eta_m [H_m(x)] \begin{bmatrix} 1 & 0 \\ 1 & -\frac{1}{\eta_m} \end{bmatrix} \begin{Bmatrix} U_{1,m} \\ U_{2,m} \end{Bmatrix} \sin(\eta_m y) \\ &= \sum_m \left[-\eta_m e^{-\eta_m x} (1 + \eta_m x), \eta_m x e^{-\eta_m x} \right] \begin{Bmatrix} U_{1,m} \\ U_{2,m} \end{Bmatrix} \sin(\eta_m y). \end{aligned} \quad (2.3-10)$$

2.3.2 Internal forces

The bending moments, $M_x(x,y)$ and $M_y(x,y)$, of Eqns (2.1-2) and (2.1-3) are functions that are related to the second differentials of $w(x,y)$, and are obtained by using Eqns (2.3-3) and (2.3-6). The twisting moment $M_{xy}(x,y)$ of Eqn (2.1-4) can also be calculated using Eqn (2.3-7). The sign of these moments is defined as shown in Fig. 2.1-2. In order to determine the edge force, V_x , in Eqn (2.1-5), the third differential of $w(x,y)$ is needed. All these expressions can be obtained by successive differentiation of the shape function $[N_m(x)]$, or the vector $[H_m(x)]$. By using the matrix $[D_m]$ of Eqn (2.3-3), these operations become simpler matrix powers of $[D_m]$, given by

$$[D_m][D_m] = [D_m^2] = \eta_m^2 \begin{bmatrix} 1 & -2 \\ 0 & 1 \end{bmatrix}, \quad [D_m^3] = -\eta_m^3 \begin{bmatrix} 1 & -3 \\ 0 & 1 \end{bmatrix}. \quad (2.3-11)$$

The bending moment parallel to the support lines, $M_x(x,y)$, can be written explicitly as

$$\begin{aligned}
M_x(x,y) &= -K \sum_m [H_m(x)] \left[[D_m^2] - \nu \eta_m^2 [I] \right] [G_m] \{U_m\} \cos(\eta_m y) = \\
&= K \sum_m [H_m(x)] \begin{bmatrix} (1 + \nu) \eta_m^2 & -2 \eta_m \\ -(1 - \nu) \eta_m^2 & (1 - \nu) \eta_m \end{bmatrix} \begin{Bmatrix} U_{1,m} \\ U_{2,m} \end{Bmatrix} \cos(\eta_m y) . \quad (2.3-12)
\end{aligned}$$

Correspondingly, the bending moment transverse to the support lines, $M_y(x,y)$, is

$$\begin{aligned}
M_y(x,y) &= -K \sum_m [H_m(x)] \left[-\eta_m^2 [I] + \nu [D_m^2] \right] [G_m] \{U_m\} \cos(\eta_m y) \\
&= K \sum_m [H_m(x)] \begin{bmatrix} (1 + \nu) \eta_m^2 & -2 \nu \eta_m \\ (1 - \nu) \eta_m^2 & -(1 - \nu) \eta_m \end{bmatrix} \begin{Bmatrix} U_{1,m} \\ U_{2,m} \end{Bmatrix} \cos(\eta_m y) . \quad (2.3-13)
\end{aligned}$$

The twisting moment $M_{xy}(x,y)$ is

$$\begin{aligned}
M_{xy}(x,y) &= (1 - \nu) K \sum_m [H_m(x)] \eta_m [D_m] [G_m] \{U_m\} \sin(\eta_m y) \\
&= (1 - \nu) K \sum_m [H_m(x)] \begin{bmatrix} 0 & -\eta_m \\ -\eta_m^2 & \eta_m \end{bmatrix} \begin{Bmatrix} U_{1,m} \\ U_{2,m} \end{Bmatrix} \sin(\eta_m y) . \quad (2.3-14)
\end{aligned}$$

The edge force, $V_x(x,y)$, (see Fig. 2.1-2) is calculated by using Eqn (2.1-5), resulting in

$$\begin{aligned}
V_x(x,y) &= -K \sum_m [H_m(x)] \left[[D_m^3] - (2 - \nu) \eta_m^2 [D_m] \right] [G_m] \{U_m\} \cos(\eta_m y) = \\
&= K \sum_m [H_m(x)] \begin{bmatrix} -2 \eta_m^3 & (1 + \nu) \eta_m^2 \\ -(1 - \nu) \eta_m^3 & (1 - \nu) \eta_m^2 \end{bmatrix} \begin{Bmatrix} U_{1,m} \\ U_{2,m} \end{Bmatrix} \cos(\eta_m y) . \quad (2.3-15)
\end{aligned}$$

2.3.3 Reaction forces at the line $x = 0$

The components of the reaction force vector, $\{F_m\}$, at the origin, $x = 0$, are $F_{1,m}$ and $F_{2,m}$, (see the positive directions from Fig. 2.3-1a). They consist of the components of the reaction edge force, equal to $-V_{x,m}(0, y)$, and the reaction bending moment, $-M_{x,m}(0, y)$, which can be calculated by using Eqns (2.3-15) and (2.3-12), resulting for each component m in

$$\sum_m \begin{Bmatrix} -V_{x,m}(0,y) \\ -M_{x,m}(0,y) \end{Bmatrix} = \sum_m \begin{Bmatrix} F_{1,m} \\ F_{2,m} \end{Bmatrix},$$

$$\sum_m \begin{Bmatrix} F_{1,m} \\ F_{2,m} \end{Bmatrix} = K \sum_m \begin{bmatrix} 2\eta_m^3 & -(1+\nu)\eta_m^2 \\ -(1+\nu)\eta_m^2 & 2\eta_m \end{bmatrix} \begin{Bmatrix} U_{1,m} \\ U_{2,m} \end{Bmatrix} \cos(\eta_m y). \quad (2.3-16)$$

In Chapter 3 the forces based on Eqn (2.3-16) are compared with those obtained by BEF analysis.

Chapter 3

APPLICATION OF BEF THEORY TO THE ANALYSIS OF PLATE STRIPS

Two types of beam on elastic foundation (BEF) model are presented in Section 3.1. These are known as the Winkler and the Pasternak models. The deflection and internal force functions of a semi-infinite two parameter BEF are obtained in Section 3.2, and presented in finite element method (FEM) formulations. In Section 3.3 the BEF foundation parameters of the semi-infinite plate strip are presented for a specific set of boundary conditions and loading. Under harmonic (cosine) lateral line loading when the semi-infinite plate strip is simply-supported, the parameters are obtained by setting equal the corresponding parameters of the differential equations of the plate theory, presented in Chapter 2, and the BEF theory, presented in Section 3.2. Under constant lateral line loading, slightly different foundation parameters are obtained by equating the maximum deflection and the bending moment of the plate and BEF solutions, respectively. The parameters in the classical analysis of the simply-supported plate strip under constant line loading, being the superimposition of the series expressions of harmonic loads, are determined by using Levy's method. The procedure demonstrated is applied to constant edge moment loading, and further in Chapter 4 to other boundary conditions at the longitudinal edge lines.

3.1 BEF foundation models

Beam on elastic foundation models were originally developed for the analysis of beams on elastic soil. Winkler (1867) was the first to present the governing differential equation and the solution for a beam, which consisted of fourth order and zero order terms. This most common elementary foundation is named the Winkler foundation, after its developer. The differential equation of the Winkler-type BEF is:

$$EI \frac{d^4}{dx^4} w(x) + kw(x) = q(x) . \quad (3.1-1)$$

The sum of the product, EIw'''' , and the lateral reaction pressure of the foundation, $kw(x)$, is in equilibrium with the external line load, $q(x)$. E is the modulus of elasticity, and I the moment of inertia of the beam. When applied to the plate analysis, EI is equal to K , Eqn (2.1-2), for a unit width plate or shell if the effect of Poisson's ratio, ν , is not taken into account, i.e. $\nu = 0$. The term k is the foundation modulus, and $w(x)$ is the deflection of the beam.

Equations similar to (3.1-1) govern the boundary value problems of shells of revolution under axisymmetric loading. The analysis of discontinuity stresses in shells is similar to a semi-infinite beam on elastic foundation problem, to which Eqn (3.1-1) can be applied. The mathematical solution of the Winkler equation is obtained by using

damping harmonic functions. The period of these functions is $2\pi\lambda$, where the inverse of λ is the characteristic length.

If there is no contribution from the Winkler-foundation, the contribution of an axial force, N , to Eqn (3.1-1) is a second-order parameter:

$$EI \frac{d^4}{dx^4} w(x) - N \frac{d^2}{dx^2} w(x) = q(x) , \quad (3.1-2)$$

where tensile forces are defined to be positive. The term Nw'' is the internal lateral reaction resulting from the axial force, N , and/or the second order foundation parameter denoted in general by N . Under compressive axial loading the solutions of the homogenous part of Eqn (3.1-2) are well known in the eigenvalue problems of beam buckling. The interaction of axial loading and beam bending, i.e. beam-column behaviour, takes into account the effect of axial loading as a deflection and moment amplification factor. From a purely mathematical viewpoint, Eqn (3.1-2) is analogous to the differential equation of generalised (warping) torsion, which takes into account the contribution of the fourth order term, the warping torsion rigidity, known as Vlasov's torsion, (1961) together with the second order term, the ordinary St. Venant torsion.

The differential equation of the two parameter Pasternak (1954) BEF model consists of the foundation parameter related to the second order term, N , and the parameter, k , of the ordinary Winkler model of zero order. In Pasternak's model, the second order parameter was originally considered to consist of the stiffness of the shear layer connecting the Winkler springs together. Other two parameter elastic foundations are known by the names Filonenko-Borodich (1940) and Vlasov (1966). In the Filonenko-Borodich model, the second order parameter is the tension value of the beam. In spite of physically different behaviour, mathematically these two models are similar. Vlasov's model is a special two parameter soil model.

Finally, the effect of the elastic foundation, together with the second and fourth order terms define the complete homogeneous differential equation of the fourth order in bending:

$$EI \frac{d^4}{dx^4} w(x) - N \frac{d^2}{dx^2} w(x) + kw(x) = 0 . \quad (3.1-3)$$

Eqn (3.1-3) is used throughout this study. It is valid for both the pure two parameter foundation case, as well as an axially-loaded beam on a two parameter elastic foundation.

Hetényi (Hetényi, 1946) presented solutions for a number of fundamental finite and semi-infinite beam on elastic foundation problems, in which the beam was loaded axially and laterally simultaneously. Starting from the homogeneous fourth order

differential equation of an elastic deflection curve, Eqn (3.1-3), Hetényi solved the four roots of the fourth order characteristic equation. The roots are complex numbers. Hetényi also showed that if one real value solution of the deflection (e.g. for tension) is known, another real value solution (e.g. for compression) can be obtained by using operations of complex mathematics. The two degree of freedom stiffness matrix of a semi-infinite beam element on an elastic foundation, under simultaneous axial loading, can be derived directly from Hetényi's solutions, as shown in the next section. The necessary steps required to determine the deflection function and to formulate the four degree of freedom stiffness matrix of a BEF finite element of finite length, L , are given in Chapter 5.

3.2 Finite element formulations for semi-infinite BEF

The solution of the fourth order governing differential equation (3.1-3), containing the second and zero order terms, is given first. The procedure used is analogous to that presented in Section 2.3. Two types of real value deflection function, and related expressions for internal forces, can be developed: **a)** the product of exponential and trigonometric functions; **b)** the product of exponential and hyperbolic functions. Final functions for deflection, slope of deflection and internal forces for case a) are given in Sections 3.2.1 and 3.2.2.

The fourth order differential equation governing the behaviour of beam-columns and tensioned beams on elastic foundations is given by Eqn (3.1-3). By substituting $w(x) = Ae^{mx}$ into Eqn (3.1-3), a characteristic equation can be obtained:

$$Elm^4 - Nm^2 + k = 0 . \quad (3.2-1)$$

The four roots of Eqn (3.2-1) are

$$m_{1,2,3,4} = \pm \sqrt{\frac{N}{2EI} \pm i \sqrt{\frac{k}{EI} - \left(\frac{N}{2EI}\right)^2}} = \pm m_{1,2} , \quad (3.2-2)$$

and the general solution corresponding to these roots is

$$w(x) = A_1 e^{-m_1 x} + A_2 e^{-m_2 x} + A_3 e^{m_1 x} + A_4 e^{m_2 x} . \quad (3.2-3)$$

In the case of a semi-infinite beam on an elastic foundation, Fig. 3.2-1, all the partial functions of the deflection function, $w(x)$, must vanish at infinity. Therefore, the function of deflection that also satisfies Eqn (3.2-1) can be expressed using the decreasing exponential and trigonometric sine and cosine functions:

$$w(x) = e^{-\alpha x} [A_1 \cos(\beta x) + A_2 \sin(\beta x)] , \quad (3.2-4)$$

where the foundation symbols used are

$$\lambda = \sqrt[4]{\frac{k}{4EI}}, \quad n = \frac{N}{N_w} = \frac{N}{4EI\lambda^2}, \quad N_w = 4EI\lambda^2,$$

$$\alpha = \sqrt{\sqrt{\frac{k}{4EI}} + \frac{N}{4EI}} = \lambda\sqrt{1+n}, \quad \beta = \lambda\sqrt{1-n}. \quad (3.2-5)$$

When Eqns (3.2-2) and (3.2-5) are compared, $m_1 = \alpha + i\beta$ and $m_2 = \alpha - i\beta$.

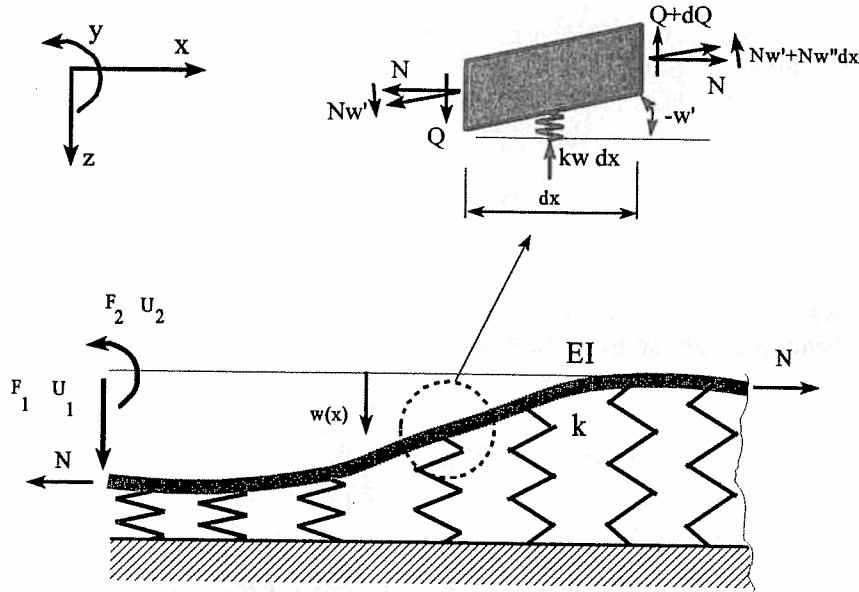


Figure 3.2-1 Co-ordinate system, degrees of freedom, and internal forces in a semi-infinite BEF element, under simultaneous axial loading, N .

Equation (3.2-4) is similar to the deflection function of an ordinary semi-infinite beam on an elastic foundation, without the effect of N (in which case $\alpha = \beta = \lambda$). The normalised second order foundation parameter, n , is the ratio of N to N_w , where N_w is denoted in this study as the critical compression load (without sign) of the one parameter foundation model, the subscript W after Winkler. In the case $N < -N_w$, $w(x)$ of Eqn (3.2-4) and α of Eqn (3.2-5) become complex, corresponding to the loss of stability (if the beam is infinite in length). Thus the variable α is real when the variable $n > -1$.

The solutions related to $-1 < n < 1$ are given next. In the case $N > N_w$, or $n > 1$, β changes through zero to complex. When denoting a new variable, $\beta_1 = \lambda\sqrt{(n-1)}$ then $\beta = i\beta_1$. Since β is complex, the expressions β and $\sin(\beta x)$ are transformed to $i\beta_1$ and

$i \sinh(i\beta x)$, respectively. Similarly, $\cos(\beta x)$ equals $\cosh(\beta x)$. The real value expressions related to $n > 1$ as a function of β_1 and $\beta_1 x$ are obtainable directly from Eqns (3.2-8) to (3.2-17), when $i^2 = -1$ is also substituted in these equations.

3.2.1 Deflection $w(x)$ and slope of deflection $\phi(x)$ functions

The procedure shown in Section 2.3 is applied in this section, also. Now the variable n is within the range $-1 < n < 1$. Using matrix notation, the deflection, $w(x)$, of Eqn (3.2-4) can be expressed as

$$w(x) = [H(x)]\{A\}, \quad [H(x)] = \begin{bmatrix} e^{-\alpha x} \cos(\beta x) & e^{-\alpha x} \sin(\beta x) \end{bmatrix}. \quad (3.2-6)$$

The coefficients A_1 and A_2 of the vector $\{A\}$ are determined from the boundary conditions at $x = 0$, Fig. 3.2-1, as a function of the nodal point displacements, U_1 and U_2 , of the degree of freedom vector, $\{U\}$:

$$w(0) = U_1, \quad -\frac{dw}{dx}(0) = U_2, \quad \{U\} = \begin{Bmatrix} U_1 \\ U_2 \end{Bmatrix}. \quad (3.2-7)$$

By using Eqn (3.2-6) and the boundary conditions of Eqn (3.2-7), the deflection function $w(x)$ is solved and can be expressed as

$$w(x) = [H(x)] \begin{bmatrix} 1 & 0 \\ \frac{\alpha}{\beta} & -\frac{1}{\beta} \end{bmatrix} \begin{Bmatrix} U_1 \\ U_2 \end{Bmatrix}. \quad (3.2-8)$$

The function of the slope of deflection, $\phi(x)$, is determined by differentiating the row vector $[H(x)]$, and is written as

$$\phi(x) = \frac{dw}{dx} = [H(x)] \begin{bmatrix} 0 & -1 \\ -\frac{2\lambda^2}{\beta} & \frac{\alpha}{\beta} \end{bmatrix} \begin{Bmatrix} U_1 \\ U_2 \end{Bmatrix}. \quad (3.2-9)$$

3.2.2 Internal forces in a semi-infinite beam element on elastic foundation

The bending moment, $M(x)$, relative to the second differential of the deflection function, can be written explicitly as

$$M(x) = -EI \frac{d^2 w}{dx^2} = EI[H(x)] \begin{bmatrix} 2\lambda^2 & -2\alpha \\ \frac{-2\lambda^2\alpha}{\beta} & \frac{\alpha^2 - \beta^2}{\beta} \end{bmatrix} \begin{Bmatrix} U_1 \\ U_2 \end{Bmatrix}. \quad (3.2-10)$$

The pure shear force (normal to the deflected axis of the beam), $Q(x)$, is accordingly

$$Q(x) = -EI \frac{d^3 w}{dx^3} = EI[H(x)] \begin{bmatrix} -4\lambda^2\alpha & -\beta^2 + 3\alpha^2 \\ \frac{2\lambda^2}{\beta}(\alpha^2 - \beta^2) & -\frac{\alpha^3}{\beta} + 3\alpha\beta \end{bmatrix} \begin{Bmatrix} U_1 \\ U_2 \end{Bmatrix}. \quad (3.2-11)$$

Under simultaneous axial loading, with a tensile load, N , defined as positive, a part of the external lateral loading (perpendicular to the undeformed axis) will be supported, in the deformed state, by the transverse component, $N\phi(x)$, of the axial force, as shown in Fig. 3.2-1. By using Eqn (3.2-5), N can be expressed as a function of α and λ by

$$N = 4EI(\alpha^2 - \lambda^2) = 4EI\lambda^2 n. \quad (3.2-12)$$

The total transverse shear force, $V(x)$, called the *generalised shear*, is expressed by

$$V(x) = Q(x) + N\phi(x). \quad (3.2-13)$$

After the necessary substitutions, $V(x)$ can be obtained:

$$V(x) = EI[H(x)] \begin{bmatrix} -4\lambda^2\alpha & 2\lambda^2 \\ \frac{-2\lambda^2}{\beta}(\alpha^2 - \beta^2) & 2\lambda^2 \frac{\alpha}{\beta} \end{bmatrix} \begin{Bmatrix} U_1 \\ U_2 \end{Bmatrix}. \quad (3.2-14)$$

3.2.3 Stiffness matrix of a semi-infinite beam element on elastic foundation

The nodal load vector, $\{F\}$, which is related to U_1 and U_2 and the corresponding columns of the element stiffness matrix $[S]$, obtained by using e.g. Eqns (3.2-10) and (3.2-14), can be solved by using the relations

$$\{F\} = [S]\{U\},$$

$$\begin{Bmatrix} F_1 \\ F_2 \end{Bmatrix} = \begin{Bmatrix} -V(0) \\ -M(0) \end{Bmatrix} = \begin{bmatrix} EI \frac{d^3 w(0)}{dx^3} - N \frac{d w(0)}{dx} \\ EI \frac{d^2 w(0)}{dx^2} \end{bmatrix}. \quad (3.2-15)$$

The stiffness matrix [S] (determined according to the unit deflection method) is then written explicitly:

$$[S] = EI \begin{bmatrix} 4\lambda^2\alpha & -2\lambda^2 \\ -2\lambda^2 & 2\alpha \end{bmatrix}. \quad (3.2-16)$$

It can be seen that [S] is valid, independent of the character of the parameter β . If the necessary steps are performed for $n > 1$, it can be shown that Eqn (3.2-16) is valid for $n > 1$ also. Under high axial tension, $n \gg 1$, α is much larger than λ . In this case [S] can be formulated as

$$[S] = 2EI\lambda^2 \begin{bmatrix} \sqrt{\frac{N}{EI}} & -1 \\ -1 & \sqrt{N/k} \end{bmatrix}, \quad \alpha \approx \frac{1}{2} \sqrt{\frac{N}{EI}}, \quad \alpha \gg \lambda. \quad (3.2-17)$$

3.3 Application of BEF theory to the analysis of a simply-supported plate strip

3.3.1 BEF parameters under harmonic loading

By comparing Eqns (2.2-3) and (3.1-3), denoting $K = EI$ when $\nu = 0$, the equality of the differential equations for the centre-line of the plate strip are obtained for each component, m :

$$w_m'''' - \frac{N_m}{K} w_m'' + \frac{k_m}{K} w_m = X_m'''' - 2\eta_m^2 X_m'' + \eta_m^4 X_m, \quad \eta_m = \frac{m\pi}{B}. \quad (3.3-1)$$

By equating the zero order terms, the (Winkler) foundation parameter, k_m , is

$$k_m = K\eta_m^4 = K \frac{m^4 \pi^4}{B^4}, \quad (3.3-2)$$

and correspondingly the second order (Pasternak) parameter, N_m , is

$$N_m = 2K\eta_m^2 = 2K \frac{m^2 \pi^2}{B^2} . \quad (3.3-3)$$

These values, when substituted into Eqn (3.2-5), give

$$\begin{aligned} \frac{1}{\lambda_m} &= \sqrt[4]{\frac{4K}{k_m}} = \frac{\sqrt{2}}{m\pi} B , \quad n_m = \frac{N_m}{4K\lambda_m^2} = 1 , \\ \frac{1}{\alpha_m} &= \frac{1}{\sqrt{2}\lambda_m} = \frac{1}{\eta_m} , \quad \beta_m = 0 , \end{aligned} \quad (3.3-4)$$

and for the lowest value $m = 1$:

$$\frac{1}{\lambda} = \frac{\sqrt{2}}{\pi} B , \quad n = n_{lin} = 1 , \quad \frac{1}{\alpha} = \frac{B}{\pi} , \quad \beta = 0 . \quad (3.3-5)$$

These parameters apply for harmonic loading of the maximum value of 1.0. The contribution of the second order Pasternak foundation in the parameter n is denoted in this study by n_{lin} , when necessary, since N in general also contains the effect of the true axial loading.

Since according to Eqn (3.3-4) β approaches zero when $n_m \rightarrow 1$, then $\cos(\beta x) \rightarrow 1$ and $\sin(\beta x) \rightarrow \beta x \rightarrow 0$ for each harmonic component m . Therefore, when the expressions of deflection and internal forces of Sections 2.3 and 3.2 are compared, the equality of functions based on the plate theory and BEF theory is evident. Firstly, for each harmonic component, m , the matrices $[H(x)]$ of Eqns (2.3-1) and (3.2-6) are equal when $\eta_m = m\pi/B$. It follows that the deflections of Eqns (2.3-7) and (3.2-8) and, respectively, the slope of deflections (2.3-9) and (3.2-9) at the centre-line, $y = 0$, can also be set equal. When Poisson's ratio, ν , is set to zero the bending moment, $M_x(x)$, in Eqn (2.3-12) of the plate theory is equal to M_x in Eqn (3.2-10) of the BEF theory. The edge force, $V_x(x)$, in Eqn (2.3-15) equals the generalized shear force $V(x)$ in Eqn (3.2-14). Therefore, the force balance equations, the semi-infinite stiffness matrices of Eqns (2.3-16) and (3.2-16) are also equal.

3.3.2 BEF parameters under constant lateral line loading

Constant lateral line loading at $x = 0$ of intensity $2V_0$ in the transverse y direction of a plate strip of width B of infinite length is shown in Fig. 1.2-1a). The loading, V_0 , of a semi-infinite plate strip can be presented as a series expression of symmetric harmonic loads with a period of expansion of $2B$ (Girkman, 1946, p. 44):

$$V_m = V_0 \frac{4}{\pi} \frac{1}{m} \sin\left(\frac{m\pi}{2}\right),$$

$$V_x(0, y) = \sum_m V_m \cos(\eta_m y), \quad m = 1, 3, 5, \dots \quad (3.3-6)$$

A lateral load of intensity $V_0 = 1$ is shown in Fig. 4.1-2 for a number of harmonic components. Because of symmetry, under a restrained slope of deflection ($U_2 = 0$), by substituting Eqn (3.3-6) into Eqn (2.3-15), the unknowns, $U_{1,m}$, of the maximum deflection, $w(0,0)$, can be solved. In the plate analysis, by using Eqns (2.3-7) and (3.3-6), the lateral deflection, $w(x,y)$, is a superimposition of the solved $U_{1,m}$ values, represented also in (Girkman, 1946, p. 186) as

$$w(x, y) = 2 V_0 \frac{B^3}{\pi^4 K} \sum_m \frac{1}{m^4} (1 + \eta_m x) e^{-\eta_m x} \cos(\eta_m y), \quad m = 1, 3, 5, \dots \quad (3.3-7)$$

Based on Eqns (2.3-12) and (3.3-6), the bending moment, $M_x(x)$, (see Figs 2.1-1 and 2.1-2) is

$$M_x(x, y) = 2 V_0 \frac{B}{\pi^2} \sum_m \frac{1}{m^2} (1 + \nu - (1-\nu) \eta_m x) e^{-\eta_m x} \cos(\eta_m y), \quad m = 1, 3, 5, \dots \quad (3.3-8)$$

In the BEF model, the maximum deflection, U_1 , is obtained using Eqn (3.2-14) or Eqn (3.2-16) when $U_2 = 0$. The maximum value of the bending moment is calculated using Eqn (3.2-10) (or S_{21} of [S] of Eqn (3.2-16)).

When the plate is simply supported along the longitudinal edges and subjected to constant lateral line loading, the characteristic length, $1/\lambda$, and the parameter, n ($= \eta_{lin}$), of the BEF formulation can be solved by using two conditions at the centre-line, $y = 0$, of the plate strip, with $\nu = 0$:

1. the deflections, w , at $x = 0$ of the plate solution of Eqn (3.3-7) and the BEF solution of Eqn (3.2-16) are set equal; and
2. the curvatures, $\partial^2 w / \partial x^2$, (or bending moments, M_x) at $x = 0$ of the plate solution of Eqn (3.3-8) and the BEF solution of Eqn (3.2-16) are set equal.

Equating K of the plate analysis of Eqn (2.1-2) with EI of the beam bending, these two conditions are given as

$$\begin{aligned}
(i) \quad & \frac{2V_0 B^3}{K\pi^4} \sum_m \frac{\sin(m\pi/2)}{m^4} = \frac{V_0}{4K} \frac{1}{\lambda^3} \frac{1}{\sqrt{1+n}}, \\
(ii) \quad & \frac{2V_0 B}{\pi^2 K} \sum_m \frac{\sin(m\pi/2)}{m^2} = \frac{V_0}{2K} \frac{1}{\lambda} \frac{1}{\sqrt{1+n}},
\end{aligned} \tag{3.3-9}$$

resulting in

$$\frac{1}{\lambda} = \sqrt{2} \frac{B}{\pi} \sqrt{\frac{0.989}{0.916}} = 1.47 \frac{B}{\pi} = 0.468 B, \quad n = 0.588. \tag{3.3-10}$$

The numerator of Eqn (3.3-10), 0.989, is the sum expression of condition (i) of Eqn (3.3-9), and the denominator, 0.916, the sum of condition (ii).

For the first harmonic mode, $m = 1$, alone, the parameters of Eqn (3.3-5) substituted into Eqn (3.3-9) result in the ratio $4/\pi$ of the plate solution vs. 1.0 of the BEF analysis, the theoretical deflection being larger. If the harmonic lateral loading of Eqn (3.3-6) is normalized by the maximum value of $4/\pi V_0$, the deflection and bending moment of lateral loads of maximum value 1.0 are equal.

By comparing the foundation parameters of the first mode of harmonic loading and constant line loading, Eqns (3.3-5) and (3.3-10), the deflection of constant loading is 26% higher than calculated using the parameters of Eqn (3.3-5). Similarly, the bending moment is 17% higher. However, if the total load ratio, $\pi/4$, is taken into account, the deflections are almost equal, $(1.26 \times \pi/4)$, and the bending moment is 91.6% of the true value based on plate or BEF analysis using the parameters of Eqn (3.3-5). It can be seen that the effect of assumptions related to the shape of the transverse line loading has a minor numerical effect on the deflection and bending moment values under equal total loadings. Therefore, the parameters of constant line loading, Eqn (3.3-10), can be applied to other types of transverse line loads when at first the total loading is initially distributed as constant loading over B .

When a simply-supported plate strip of infinite length is subjected to constant transverse lateral line loading of total intensity, $2V_0$, the maximum value of deflection at the centre-line, $w_{\max} = U_1$, can be calculated from Eqn (3.2-16) by using the parameters $1/\lambda$ and n of Eqn (3.3-10). The bending moment, M_{\max} , is calculated from Eqn (3.2-10). These two expressions are

$$w_{\max} = \frac{V_0}{K} \frac{1}{4\lambda^3} \frac{1}{\sqrt{1+n}}, \quad M_{\max} = V_0 \frac{1}{2\lambda} \frac{1+\nu}{\sqrt{1+n}}, \tag{3.3-11}$$

where the effect of the stress biaxiality in a simply-supported plate strip is taken into account in the factor $1 + \nu$ (see Eqn (3.3-8)).

The validity of analysing a simply-supported plate under constant line loading, based on the BEF approach, is further verified and discussed in Chapter 4. The functions $w(x)$ and $M(x)$ for a simply-supported plate are presented in, for example, Figs 4.1-2, 4.2-3 and 4.2-4.

3.3.3 Effect of constant edge moment loading on bending behaviour

A reaction edge moment of constant value, $M_{x,0}$, acting as external loading is studied in this section for a semi-infinite plate strip when $U_{1,m} = 0$ at $x = 0$. Based on a procedure shown in Section 3.3.2 for line loading, the validity of the parameters of Eqn (3.3-10) can be tested. By equating the slope of deflections, U_2 , of the plate theory solution, obtained using Eqn (2.3-12), and the BEF solution using Eqn (3.2-10), the following equations can be written:

$$M_{x,0} \frac{2B}{\pi^2 K} \sum_m \frac{1}{m^2} \sin\left(m \frac{\pi}{2}\right) = M_{x,0} \frac{1}{2K\lambda} \frac{1}{\sqrt{1+n}},$$

$$U_{2,m} = \frac{M_m}{2K\eta_m}, \quad M_m = M_{x,0} \frac{4}{\pi} \frac{1}{m} \sin\left(m \frac{\pi}{2}\right), \quad m = 1, 3, 5, \dots, \quad (3.3-12)$$

where the constant edge moment loading is written as the sum of cosine expressions of M_m (similar to the line loading of Eqn (3.3-6)). The equality is valid when the known values of λ and n in Eqn (3.3-10) are used in the BEF solution on the right-hand side. For the first harmonic mode alone, $m = 1$, by substituting the parameters of Eqn (3.3-5) into Eqn (3.3-12), the ratio $4/\pi$ is again obtained, the theoretical slope of deflection being larger. For equal maximum loading, when the left-hand side of Eqn (3.3-12) is multiplied by $\pi/4$, the slope of deflections are equal.

In the BEF analysis using Eqn (3.2-16), the slope of deflection, ϕ_{\max} , and the generalised shear force, V_{\max} , of Eqn (3.2-14), are given by

$$\phi_{\max} = \frac{M_0}{2K} \frac{1}{\lambda} \frac{1}{\sqrt{1+n}}, \quad V_{\max} = M_0 \lambda \frac{1+v}{\sqrt{1+n}}. \quad (3.3-13)$$

Chapter 4

ON GENERALISATION OF THE BEF MODEL

The accuracy of the finite element analysis (FEA) model that is used to verify the BEF model is tested in Section 4.1. The model represents a semi-infinite plate, simply supported along the longitudinal edges, which is subjected to a uniform lateral line load and uniform edge moment loading. The accuracy of the FEA model results for linear shell elements is compared with, and verified by, the closed-form solutions of Chapter 2. Secondly, in Section 4.2, the same FEA model is modified to verify more complicated theoretical formulae which describe a plate strip that is fixed to prevent rotation about the longitudinal support lines. Thirdly, Section 4.3 shows the FEA of a semi-infinite plate strip, with one free edge, the other being fixed. By equating the deflection and bending moment of the BEF model and plate theory, and/or FEA solutions, the two foundation parameters for the three types of boundary condition analysed are determined. In Section 4.4 the effect of axial and transverse in-plane loading on the parameters of the BEF model is based on an approximate plate theory analysis, which is verified by geometric non-linear FEA runs. The models developed are based on a value of Poisson's ratio, ν , of 0. The effect of Poisson's ratio on bending behaviour is discussed in Section 4.5, where the effect of geometric nonlinearity resulting from in-plane loading is also taken into account. The generalised BEF model is presented in Section 4.6, which takes into account the effect of the variable rotation stiffness of the longitudinal support lines, the effect of Poisson's ratio, the effect of axial in-plane loading, N_x , and transverse in-plane loading, N_y .

4.1 FEA verification of simply-supported semi-infinite plate strip model

FEA model description

The finite element analysis was performed using the Geostar 1.75A module of the Cosmos/M (1996) FEA package. A Young's modulus of 210 GPa and a Poisson's ratio $\nu = 0$ were used for the material constants. (The effect of the true Poisson's ratio for steel, $\nu = 0.3$, is discussed in Section 4.5.) Constant values for the total width, B , of the plate strip (200 mm) and the thickness, h , (2 mm) are used in all the models. Figure 4.1-1 shows the element model, a quarter of the whole geometry, under constant lateral line loading in the deformed shape. Linear shell element types were used. The model consisted of 20 evenly-spaced elements in the half width, $B/2$, (100 mm). In the longitudinal direction, x , 40 elements (spacing ratio 5) were used up to a distance of 500 mm. Boundary conditions of symmetry were applied at the $y = 0$ line. The plate was simply supported along the line $y = B/2 = 100$ mm. Under lateral line loading at $x = 0$, symmetry boundary conditions were applied at the loading line. In the second loading case, under constant edge moment loading along the line $x = 0$, the boundary conditions of the nodes at $x = 0$ line were antimetric.

Unless stated otherwise, the model presented is used as the basis for all FEA verifications of this study.

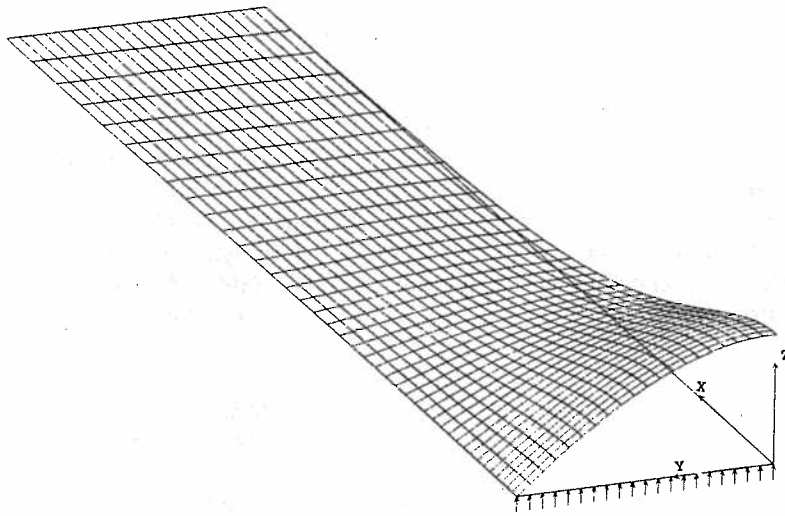


Figure 4.1-1 FE model of a simply-supported plate under transverse lateral line loading in the deformed condition.

Results

With lateral line loading, the maximum deflection predicted by FEA, 1.16 mm, agreed with the theoretical value obtained using Eqn (3.3-9i). FEA gave a bending moment of 36.87 Nmm/mm when the theoretical value of Eqn (3.3-9ii) was 37.04. Based on the FEA results, the foundation parameters $1/\lambda = 1.473B/\pi$ and $n = 0.618$ were determined, whereas the theoretical analysis of Eqn (3.3-9) resulted in $1/\lambda = 1.470B/\pi$ and $n = 0.588$. The normalised values of the lateral deflection, s , and the bending moment in the x direction, m_x , of the FEA results and the BEF model (Eqns (3.3-7) and (3.3-8)) of parameters $1/\lambda = 1.473B/\pi$ and $n = 0.618$ are shown in Figure 4.1-2 as a function of the normalised longitudinal co-ordinate, x/B . The functions are practically identical.

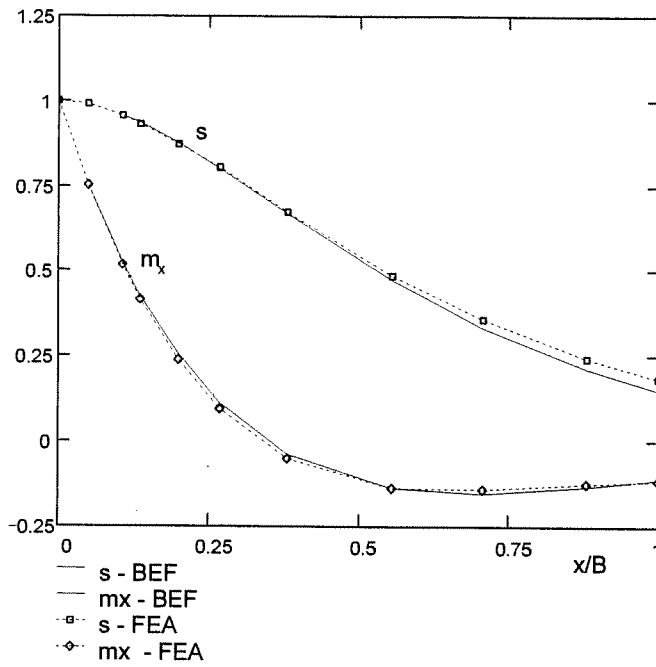


Figure 4.1-2 Normalised deflection, s , and bending moment, m_x , at $y = 0$ as a function of the normalised longitudinal co-ordinate x/B .

4.2 Analysis of a fixed semi-infinite plate strip using classical plate theory, FE analysis and BEF theory

4.2.1 Determination of BEF parameters of a fixed plate under lateral line loading

When the simply-supported longitudinal edges in the x direction are restrained such that they cannot rotate, unknown redundant edge moments are imposed in the transverse y direction. The co-ordinates are shown in Fig. 2.1-1. Either the force or displacement methods can be used for the determination of the unknown edge moment. The finite element method is based on the displacement method. It produces accurate results if the entire structure is composed of small elements. In the force method, which is also known as the slope-deflection method (Szilard, 1974), the redundant force/moment is the unknown to be determined from the compatibility condition of displacements. In this study, the reaction edge moment $M_{y,1} = -M_{y,1}(x, B/2)$ is the unknown, and the slope of deflection, $\partial w / \partial y$, at the support line, $y = B/2$, represents the displacement compatibility equation needed. The deformed shape of the FE mesh of the simply-supported plate strip of Figure 4.1-1 shows clearly that the slope of deflection is not zero at $y = B/2$. Figure 4.2-1 shows the lateral line loading of unit value in the normalised transverse direction, y/B , as the superimposition of a varying number of harmonic components, see Eqn (3.3-6).

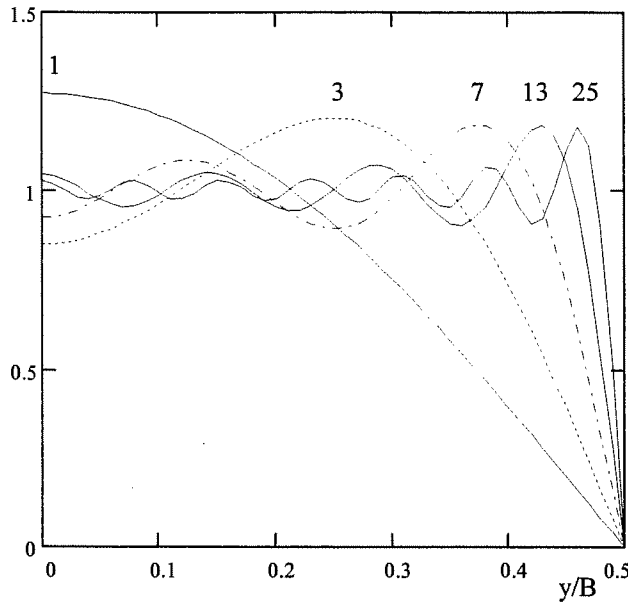


Figure 4.2-1 Lateral line loading, $V_0 = 1$, in the normalised transverse direction y/B as the superimposition of 1, 3, 7, 13 and 25 harmonic components.

The deflection fields of the fixed plate under external unit line loading, V_0 , (subscript $_0$) and unit edge moment loading, $M_{x,0}$, are determined based at $y = B/2$ on the superimposition of the external loading and the redundant edge moment, $M_{y,1}$, (subscript $_1$). These unit loads are applied in a semi-infinite structure. The results are used to determine the foundation parameters, $1/\lambda$ and n , of the BEF analysis. The analysis based on the application of classical plate theory to be shown next is verified by FEA. The determination procedure under external lateral line loading, V_0 , involves determinations described in the following steps.

- i) The slope of deflection caused by V_0 , $\phi_0 = \partial w_0 / \partial y$, at the edge line, $y = B/2$:
 - release the rotation at the line $y = B/2$, i.e analysis of a simply-supported plate;
 - calculate the deflection function, w_0 , which results from the external lateral line loading. Use it to calculate the slope of deflection at $y = B/2$, $\partial w_0 / \partial y(x, B/2) = \phi_0$;
 - represent w_0 and ϕ_0 in the longitudinal direction, x , as a series expression for an arbitrarily chosen length, a ($a \gg B$).
- ii) The unknown edge reaction moment, $M_{y,1}$, at the longitudinal support line, $y = B/2$:
 - represent $M_{y,1}$ as a series expression of length, a ;
 - calculate the slope of deflection, ϕ_1 , resulting from $M_{y,1}$ at $y = B/2$;
 - determine $M_{y,1}$ from the condition $\phi_0 + \phi_1 = 0$ for each component n .
- iii) Internal forces of $M_{y,1}$:
 - determine the deflection, $w_1(x, y)$, the slope of deflections, $\partial w_1 / \partial x$, $\partial w_1 / \partial y$, and the internal forces resulting from $M_{y,1}$.
- iv) Final functions of deflection and internal forces:

- when the plate is considered to be fixed along the longitudinal support lines, superimpose the components of V_0 from i) onto those induced by $M_{y,1}$ from ii).
- v) The two parameters, $1/\lambda$ and n , of the BEF model:
 - equate the deflection, w , and the curvature, $\partial^2 w / \partial x^2$, at the centre-line and at $x = 0$, of the plate and the BEF solutions, and calculate $1/\lambda$ and n ;
 - compare the analysis with the results of shell element FEA.

i) The slope of deflection under constant lateral line loading

Under conditions of restrained, zero slope of deflection, $\partial w_0 / \partial x(0, y) = U_2 = 0$, the deflection and slope of deflection functions, w_0 and $\partial w_0 / \partial y$, are given based on Eqns (3.3-6) and (3.3-7) :

$$\begin{aligned}
 w_0(x, y) &= \sum_m \frac{V_m}{2K\eta_m^3} e^{-\eta_m x} (1 + \eta_m x) \cos(\eta_m y) , \\
 \frac{\partial w_0}{\partial y}(x, y) &= -\sum_m \frac{V_m}{2K\eta_m^2} e^{-\eta_m x} (1 + \eta_m x) \sin(\eta_m y) , \\
 \eta_m &= \frac{m\pi}{B} , \quad m = 1, 3, 5 \dots
 \end{aligned} \tag{4.2-1}$$

When the origin is at the centre-line of a plate of arbitrarily chosen length a , $-a/2 \leq x \leq a/2$, w_0 can be represented in the x direction by a series expression of a symmetric function of period $2a$ by

$$w_0(x, y) = \sum_n A_n \cos(\gamma_n x) , \quad \gamma_n = \frac{n\pi}{a} , \quad n = 1, 3, 5 \dots \tag{4.2-2}$$

The constant, A_n , is determined by integrating the expressions with respect to x up to infinity by

$$\begin{aligned}
 A_{n,i} &= \frac{4}{2a} \int_0^\infty e^{-\eta_m x} \cos(\gamma_n x) dx = \frac{2\eta_m}{a} \frac{1}{(\eta_m^2 + \gamma_n^2)} , \\
 A_{n,ii} &= \frac{4}{2a} \eta_m \int_0^\infty x e^{-\eta_m x} \cos(\gamma_n x) dx = \frac{2\eta_m}{a} \frac{(\eta_m^2 - \gamma_n^2)}{(\eta_m^2 + \gamma_n^2)^2} , \\
 A_n &= 2(A_{n,i} + A_{n,ii}) = \frac{8}{\eta_m a} \frac{1}{\left(1 + \left(\frac{n}{m} \frac{B}{a}\right)^2\right)^2} .
 \end{aligned} \tag{4.2-3}$$

The deflection function, $w_0(x, y)$, of lateral line loading of Eqn (4.2-1) is expressed as a double series expression:

$$w_0(x, y) = \frac{4 B^4}{\pi^4 K a} \sum_m \sum_n \frac{V_m}{m^4} \frac{1}{\left(1 + \left(\frac{n B}{m a}\right)^2\right)^2} \cos(\gamma_n x) \cos(\eta_m y) , \quad (4.2-4)$$

$$m = 1, 3, 5 \dots , \quad n = 1, 3, 5 \dots$$

The slope of deflection of Eqn (4.2-1) at $y = B/2$, $\partial w_0 / \partial y(x, B/2) = \varphi_0$ is

$$\varphi_0 = \frac{-4 B^3}{\pi^3 K a} \sum_m \sum_n \frac{V_m}{m^3} \frac{\sin(m\pi/2)}{\left(1 + \left(\frac{n B}{m a}\right)^2\right)^2} \cos(\gamma_n x) , \quad (4.2-5)$$

$$m = 1, 3, 5 \dots , \quad n = 1, 3, 5 \dots$$

ii) The unknown edge reaction moment $M_{y,1}$ at $y = B/2$

The deflection function, $w_1(x)$, and slope of deflection, $\varphi_1(x)$, of a symmetrically-applied unknown edge moment, $M_{y,1} = -M_{y,1}(x, B/2)$, is now determined. $M_{y,1}$ is a symmetric function defined by

$$M_{y,1} = \sum_n M_{n,1} \sin(n\pi/2) \cos(\gamma_n x) , \quad n = 1, 3, 5 \dots \quad (4.2-6)$$

The boundary conditions for the deflection $w_1(x)$ caused by $M_{y,1}$ are:

$$w_1(\pm a/2, y) = \frac{\partial^2 w_1}{\partial x^2}(\pm a/2, y) = 0 , \quad w_1(x, \pm B/2) = 0 , \quad \frac{\partial w_1}{\partial x}(x, 0) = 0$$

$$M_{y,1} = -M_{y,1}(x, B/2) . \quad (4.2-7)$$

Girkman (1946, p. 205) uses a function

$$w_1 = \frac{1}{\gamma_n^2} [A_n \cosh(\gamma_n y) + \gamma_n y B_n \sinh(\gamma_n y) + C_n \sinh(\gamma_n y) + \gamma_n y D_n \cosh(\gamma_n y)] \cos(\gamma_n x) , \quad (4.2-8)$$

and determines the unknown coefficients A_n , B_n , C_n and D_n , to give

$$w_1 = \frac{-1}{2K} \sum_n \frac{1}{\gamma_n^2} \frac{M_{n,1} \sin(n\pi/2)}{\cosh^2(\gamma_n B/2)} \left[-\frac{\gamma_n B}{2} \sinh(\gamma_n B/2) \cosh(\gamma_n y) - \gamma_n y \cosh(\gamma_n B/2) \sinh(\gamma_n y) \right] \cos(\gamma_n x), \quad n = 1, 3, 5 \dots \quad (4.2-9)$$

when the boundary conditions are applied (Girkman, 1946, p. 221).

By differentiating Eqn (4.2-9), the slope of deflection, $\partial w_1 / \partial y$, is represented by

$$\frac{\partial w_1}{\partial y}(x, y) = \frac{1}{2K} \sum_n \frac{1}{\gamma_n} \frac{M_{n,1} \sin(n\pi/2)}{\cosh^2(\gamma_n B/2)} \left[\gamma_n y \cosh(\gamma_n B/2) \cosh(\gamma_n y) - (\gamma_n B/2 \sinh(\gamma_n B/2) - \cosh(\gamma_n B/2)) \sinh(\gamma_n y) \right] \cos(\gamma_n x). \quad (4.2-10)$$

At the edge line, $y = B/2$, the slope of deflection, $\phi_1 = \partial w_1 / \partial y(x, B/2)$, resulting from the sum of M_n components is

$$\phi_1 = \frac{B}{4K} \sum_n M_{n,1} \sin(n\pi/2) \left[\frac{\tanh(\gamma_n B/2)}{\gamma_n B/2} + \frac{1}{\cosh^2(\gamma_n B/2)} \right] \cos(\gamma_n x) \quad (4.2-11)$$

The boundary condition along the longitudinal edge, $y = B/2$ results in:

$$\phi_0 + \phi_1 = 0. \quad (4.2-12)$$

The component, $M_{n,1}$, of the unknown edge reaction moment, $M_{y,1}$ of Eqn (4.2-6), for each value of n is calculated by superimposing Eqns (4.2-5) and (4.2-11) onto Eqn (4.2-12). This gives

$$M_{n,1} = \frac{\frac{16 B^2}{\pi^3 a} \sin(n\pi/2)}{\frac{\tanh(\gamma_n B/2)}{\gamma_n B/2} + \frac{1}{\cosh^2(\gamma_n B/2)}} \sum_m \frac{\frac{V_m}{m^3} \sin(m\pi/2)}{\left(1 + \left(\frac{nB}{ma} \right)^2 \right)^2}, \quad m = 1, 3, 5 \dots, \quad n = 1, 3, 5 \dots \quad (4.2-13)$$

The edge reaction moment, $M_{y,1}$, normalised by $M_x(0,0)$ of Eqn (3.3-8) of the simply-supported plate is finally written as the sum ratio of $m_{y,1}$

$$m_{y,1} = \sum_n M_{n,1} \frac{1}{2V_0 \frac{B}{\pi^2} \sum_m \frac{1}{m^2} \sin(m\pi/2)} \cos(\gamma_n x) , \quad (4.2-14)$$

$m_{y,1}$ is shown in Figure 4.2-2, for twenty five harmonic components of external loading, V_m of Eqn. (3.3-6), with a varying number of reaction moment $M_{n,1}$ components. The numerical analysis was based on the ratio $a = 5B$.

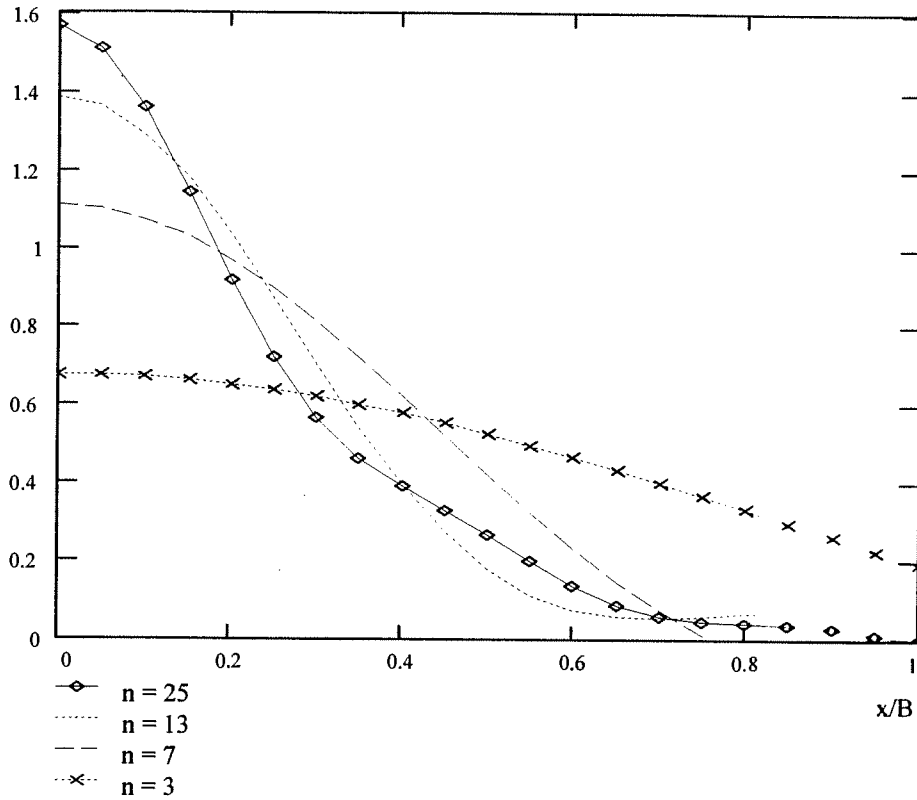


Figure 4.2-2 The normalised edge reaction moment, $m_{y,1}$, as the superimposition of 25, 13, 7 and 3 harmonic components $M_{n,1}$ shown as a function of x/B .

iii) Internal moments of the edge moment, $M_{y,1}$

Based on Eqn (4.2-9), the internal moments resulting from the edge moments $M_{n,1}$ defined in Eqn (4.2-13) can be determined using the equations of Chapter 2, Eqns (2.1-2) to (2.1-4). The bending moment $M_{x,1}(x,y)$ is

$$M_{x,1}(x, y) = \sum_n \frac{-M_{n,1}}{\cosh(\gamma_n B/2)} \frac{\gamma_n B}{4} [((1 - \nu) \tanh(\gamma_n B/2) + \frac{2\nu}{\gamma_n B/2}) \cosh(\gamma_n y) - 2(1 - \nu) \frac{y}{B} \sinh(\gamma_n y)] \sin(n\pi/2) \cosh(\gamma_n x) . \quad (4.2-15)$$

The bending moment $M_{y,1}(x, y)$ is

$$M_{y,1}(x, y) = \sum_n \frac{-M_{n,1}}{\cosh(\gamma_n B/2)} \frac{\gamma_n B}{4} [((1 - \nu) \tanh(\gamma_n B/2) - \frac{4}{\gamma_n B}) \cosh(\gamma_n y) - 2(1 - \nu) \frac{y}{B} \sinh(\gamma_n y)] \sin^2(n\pi/2) \cos(\gamma_n x) . \quad (4.2-16)$$

The twisting moment, $M_{xy,1}(x, y)$, is correspondingly

$$M_{xy,1}(x, y) = (1 - \nu) \sum_n \frac{-M_{n,1}}{\cosh(\gamma_n B/2)} \frac{\gamma_n B}{4} [(\tanh(\gamma_n B/2) - \frac{2}{\gamma_n B}) \sinh(\gamma_n y) - \frac{2y}{B} \cosh(\gamma_n y)] \sin(n\pi/2) \sin(\gamma_n x) . \quad (4.2-17)$$

iv) Final functions of deflection and internal forces

The final functions representing deflections and internal forces are determined by superimposing the functions based on the deflection, w_0 , of V_0 of Eqns (3.3-6) and (4.2-4) onto the functions based on the deflection, w_1 , of $M_{y,1}$ of Eqns (4.2-9) and (4.2-13). At the centre-line of the joint, $x = y = 0$, the final maximum deflection w_{\max} is

$$w_{\max} = w_0(0,0) + w_1(0,0) = \frac{B^3}{2\pi^3 K} \sum_{m=1}^{\infty} \frac{V_m}{m^3} - \frac{B^2}{4\pi K} \sum_{n=1}^{\infty} \frac{M_{n,1} \sin(n\pi/2)}{n} \frac{\tanh(\gamma_n B/2)}{\cosh(\gamma_n B/2)} . \quad (4.2-18)$$

Eqns (3.3-8), (4.2-13) and (4.2-15) are used in order to determine the bending moment, M_x . The maximum value, $M_{x,\max}$, at the joint $x = y = 0$ is

$$M_{x,\max} = M_x(0,0) = M_{x,0}(0,0) + M_{x,1}(0,0) = (1 + \nu) \frac{B}{2\pi} \sum_{m=1}^{\infty} \frac{V_m}{m} - \sum_{n=1}^{\infty} \frac{M_{n,1}}{\cosh(\gamma_n B/2)} [(1 - \nu) \gamma_n \frac{B}{4} \tanh(\gamma_n B/2) + \nu] . \quad (4.2-19)$$

The theoretical model for the determination of the deflection function, w , of a fixed semi-infinite plate strip was verified by the FEA model of Section 4.1 by fixing the rotation around the x axis at the longitudinal support. The normalised deflection functions: $s_{ss} = w_0/w_0(0,0)$, of the simply-supported plate and the superimposed function, $s_{fix} = w/w_0(0,0)$, of the fixed plate are shown in Fig. 4.2-3. The difference $s_{ss} - s_{fix}$ is equal to $-w_1/w_0(0,0)$. Correspondingly, the normalised bending moments are shown in Figure 4.2-4 where $m_{x,fix} = M_x/M_{x,0}(0,0)$ relates to the fixed plate. The functions determined theoretically and verified by FEA correlate well.

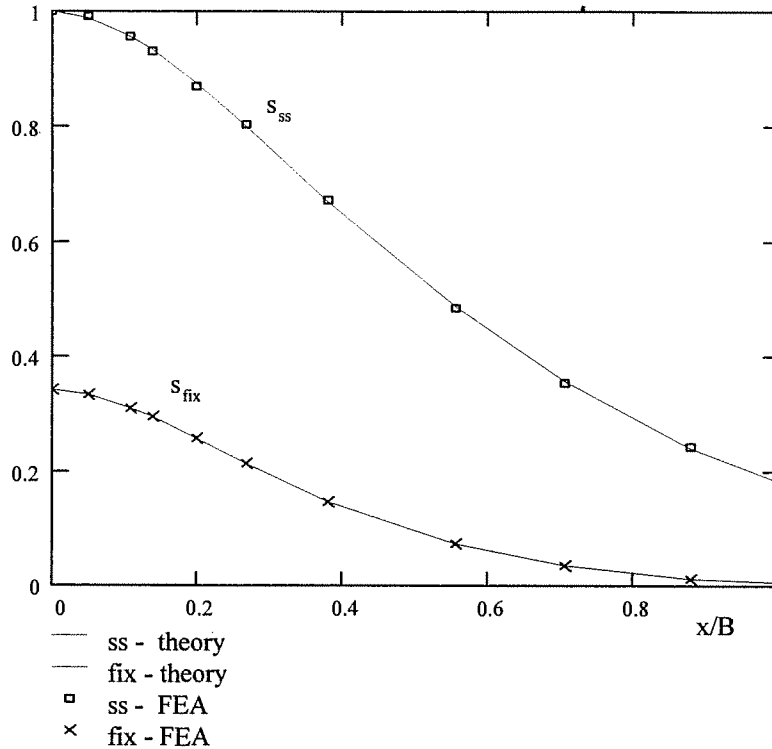
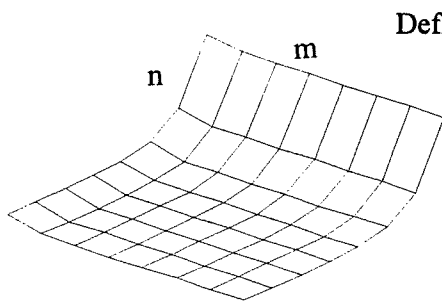


Figure 4.2-3 Normalised deflections, s_{ss} and s_{fix} , of a simply-supported and fixed plate subjected to constant transverse line loading as a function of x/B at the centre-line.

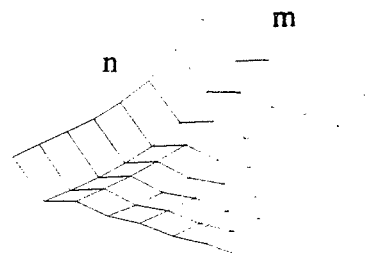
Table 4.2-1 gives the cumulative values of the superimposed maximum deflection and bending moment at $x = y = 0$. They represent the sum expressions of fixed plates, comparable with the sum expressions of Eqn (3.3-9) of the simply-supported plate. The horizontal rows show the effect of the number of harmonic waves (m) that are taken into account in the loading, Eqn (3.3-6). The vertical columns show how the functions stabilize when an increasing number of components (n) of the harmonic reaction moments of Eqn (4.2-13) are taken into account. The deflection and bending moment function surfaces are shown schematically below the table.

Table 4.2-1 Cumulative sum expression values, s_{fix} and $m_{x,\text{fix}}$, for deflection and bending moment, M_x , of a fixed semi-infinite plate subjected to lateral line loading.

		m =							
		1	3	5	7	9	11	13	15
n =	1	$s_{\text{fix}} =$							
	3								
	5								
	7								
	9								
	11								
	13								
	15								
n =	1	$m_{x,\text{fix}} =$							
	3								
	5								
	7								
	9								
	11								
	13								
	15								



Bending moment



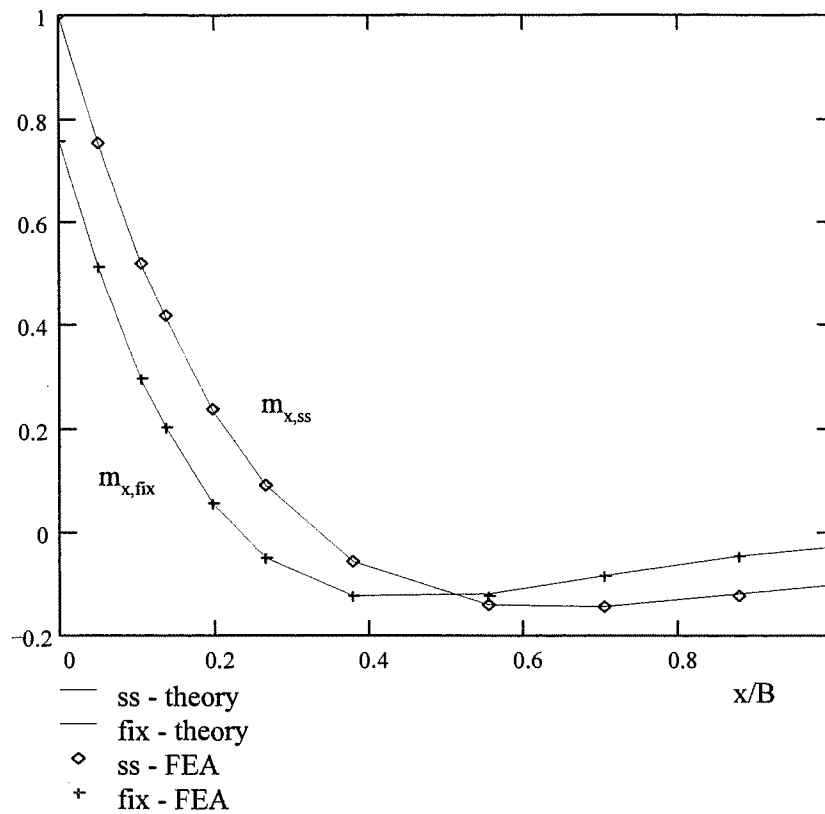


Figure 4.2-4 Normalised bending moments, $m_{x,ss}$ and $m_{x,fix}$, of a simply-supported and fixed plate subjected to constant transverse line loading as a function of x/B at the centre-line $y = 0$.

v) Foundation parameters of the fixed plate

The two foundation parameters, $1/\lambda$ and n , of the fixed plate can be determined based on the equality of the deflection, w , and the curvature, $\partial^2 w / \partial x^2$, at the centre-line of the plate at the line of load application, $x = 0$, of the theoretical plate and BEF analysis. Following the procedure of Section 3.3, w of Eqn (4.2-18) and M_x of Eqn (4.2-19), using $\nu = 0$, are set equal to w and M_x of the BEF theory. By performing the necessary numerical calculations, it can be shown that the deflection of the fixed plate is 34.0% of the deflection of the simply-supported plate. The bending moment ratio is 75.7%. FEA resulted in the ratios 34% and 75.4%. The theoretical analysis resulted in the following equations:

$$\begin{aligned}
 (i) \quad & 0.34 \frac{2V_0 B^3}{K\pi^4} \sum_{m=1}^{\infty} \frac{\sin(m\pi/2)}{m^4} = \frac{V_0}{4K} \frac{1}{\lambda^3} \frac{1}{\sqrt{1+n}}, \\
 (ii) \quad & 0.757 \frac{2V_0 B}{\pi^2 K} \sum_{m=1}^{\infty} \frac{\sin(m\pi/2)}{m^2} = \frac{V_0}{2K} \frac{1}{\lambda} \frac{1}{\sqrt{1+n}},
 \end{aligned} \tag{4.2-20}$$

giving the parameters

$$\frac{1}{\lambda} = 0.985 \frac{B}{\pi} = 0.314 B, \quad n = 0.245. \tag{4.2-21}$$

Values of $1/\lambda = 0.990B/\pi$ and $n = 0.284$ were obtained, based on the results of finite element analysis. The normalised deflection, $s_{\text{fix}} = w/w_0(0,0)$, and the bending moment, $m_{x,\text{fix}} = m_x/m_{x,0}(0,0)$, calculated by BEF and using the FEA are shown in Figure 4.2-5. The BEF curves are based on slightly differing values $1/\lambda = B/\pi$ and $n = 1/\pi$ of a generalized model to be determined in Section 4.6. The bending moment of this model is 0.986 times the theoretical moment. The corresponding deflection ratio is 1.017.

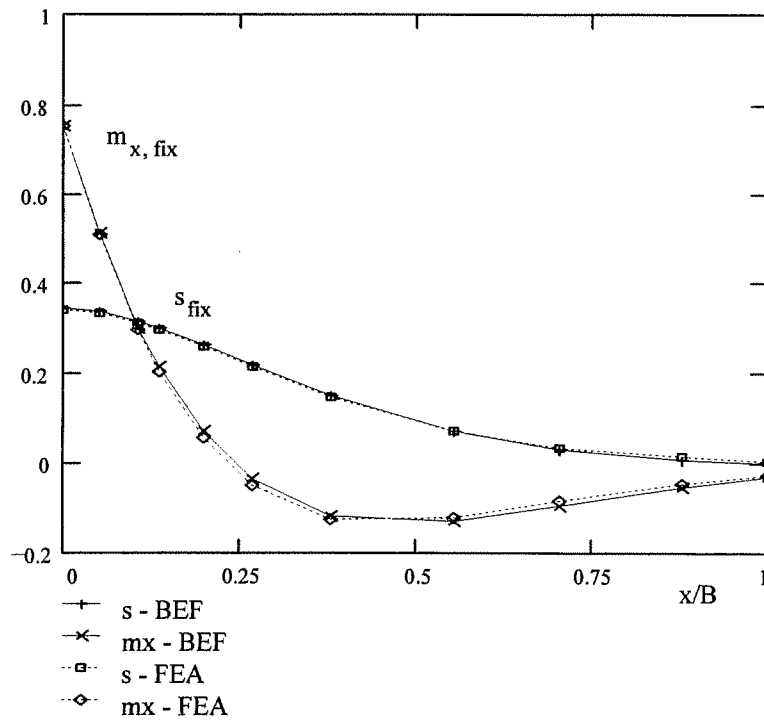


Figure 4.2-5 Normalised deflection, s_{fix} , and bending moment, $m_{x,\text{fix}}$, of a fixed plate subjected to constant transverse line loading as a function of x/B at the centre-line.

4.2.2 Constant edge moment loading

When subjected to external loading in the form of an edge moment of constant value, $M_{x,0} = -M_{x,0}(0,0)$, the deflection function, $w_0(x,y)$, is determined according to similar methods to those described and used in Section 4.2.1. $w_0(x,y)$ is an antimetric function in the x direction from 0 to a , and can be expressed as a double series function of period $2a$

$$w_0(x,y) = \sum_m \sum_n A_n \sin(\gamma_n x) \cos(\eta_m y) , \quad \eta_m = \frac{m\pi}{B} , \quad \gamma_n = \frac{n\pi}{a}$$

$$m = 1, 3, 5, \dots , \quad n = 1, 3, 5, \dots \quad (4.2-22)$$

The edge moment loading, $M_{x,0}$, can be presented in the y direction as an even series expression, similar to the constant lateral line loading of Eqn (3.3-6). The loading and deflection functions are antimetric functions in the x direction. Therefore, at the origin, $x = 0$, the deflection, $w_0(x,y)$, is zero and $\partial w_0 / \partial x(x,y) = U_{2,m}$ is the only degree of freedom in a simply-supported semi-infinite plate strip. The deflection function, $w_0(x,y)$, is determined according to Eqn (2.3-7), ($U_{1,m} = 0$). By using Eqn (2.3-12), each $U_{2,m}$ is related to each component M_m of $M_{x,0}$. The coefficients A_n are obtained by integrating $w_0(x,y)$ of Eqn (2.3-7) in the x direction as a function of $U_{2,m}$ and further of M_m :

$$A_n = 2 U_{2,m} \frac{4}{2a} \int_0^a x e^{-\eta_m x} \sin(\gamma_n x) dx = \frac{4}{a} \frac{2 \eta_m \gamma_n}{(\eta_m^2 + \gamma_n^2)^2} U_{2,m} , \quad (4.2-23)$$

$$U_{2,m} = \frac{M_m}{2K\eta_m} , \quad M_m = M_{x,0} \frac{4}{\pi} \frac{1}{m} \sin(m\pi/2) .$$

In order to determine the edge moment at the fixed longitudinal support line, $y = B/2$, the rotation angle, $\varphi_0 = \partial w_0 / \partial y(x, B/2)$, of the external loading, $M_{x,0}$, must be known. By using w_0 from Eqn (4.2-22) and (4.2-23), φ_0 can be written as

$$\varphi_0 = \frac{4}{\pi^2} \frac{B^3}{Ka^2} \sum_m \sum_n \frac{M_m}{m^3} \frac{n}{\left(1 + \left(\frac{nB}{ma}\right)^2\right)^2} \sin(m\pi/2) \sin(n\pi \frac{x}{a}) . \quad (4.2-24)$$

Each component $M_{n,1}$ of the unknown edge moment, $M_{y,1}$, being also an antimetric function in the x direction, is determined following the procedure shown earlier in Section 4.2.1, and calculated from

$$M_{n,1} = \frac{-\frac{16}{\pi^2} \frac{B^2}{a^2} n}{\frac{\tanh(\gamma_n B/2)}{\gamma_n B/2} + \frac{1}{\cosh^2(\gamma_n B/2)}} \sum_m \frac{M_m}{m^3} \frac{1}{\left(1 + \left(\frac{nB}{ma}\right)^2\right)^2},$$

$m = 1, 3, 5, \dots, n = 1, 3, 5, \dots$

(4.2-25)

In Figure 4.2-6, the normalised bending moment, $m_{x, \text{fix}}$, and the slope of deflection, $r_{\text{fix}} = (\partial w / \partial x) / (\partial w_0 / \partial x)$, for a fixed, continuous plate are shown in the normalised x/B direction at $y = 0$. The slope of deflection results of FEA of the simply-supported case are used for reference. Values of $1/\lambda = B/\pi$ and $n = 1/\pi$, based on the model of Section 4.6, were used in the BEF analysis to calculate the slope of deflection of the continuous plate at $x = y = 0$. This resulted in a r_{fix} -ratio of 76%.

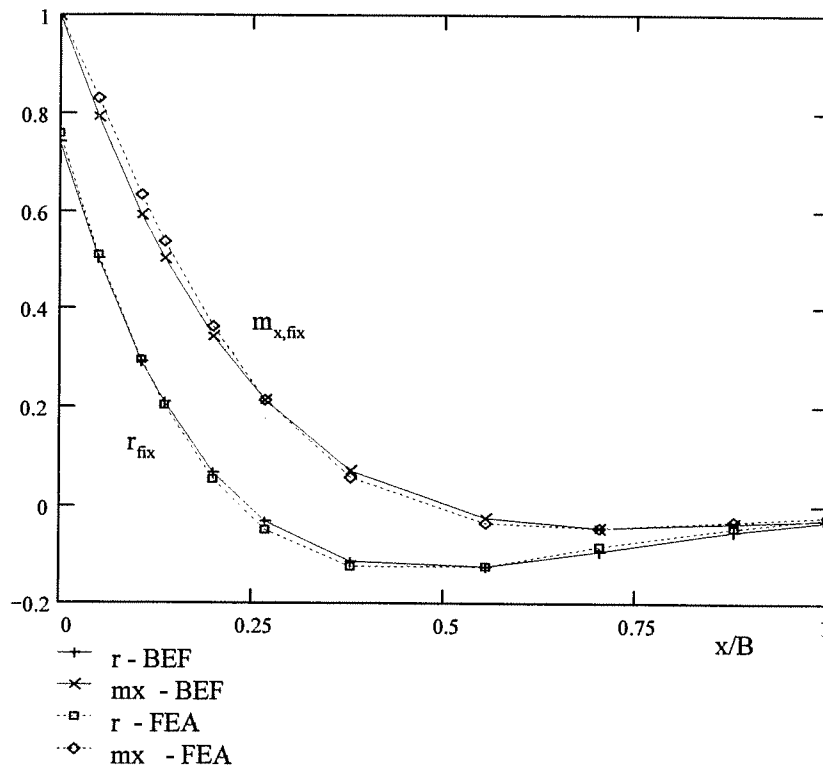


Figure 4.2-6 Fixed continuous plate strip subjected to constant edge moment loading, $M_{x,0}$: normalised slope of deflection, r_{fix} , and bending moment, $m_{x, \text{fix}}$, shown as a function of x/B .

4.3 Application of BEF theory to the analysis of a semi-infinite plate strip with a free edge

The two foundation parameters, $1/\lambda$ and n , of the third type of symmetric plate strip - a strip with one longitudinal free edge and the other fully fixed - are determined by using the results of FEA alone. The model of Section 4.2 is used by releasing the rotation around the longitudinal axis of the nodes at the line $y = B/2$. A detailed analysis of a plate having one edge free and the other, $y = 0$, simply supported, and its verification, are considered to be beyond the scope of this study (the second-order stiffness dominates). As in earlier sections two loading cases, constant line loading and constant edge moment, were studied. Figure 4-3-1 shows the FE model under moment loading in the deformed state.

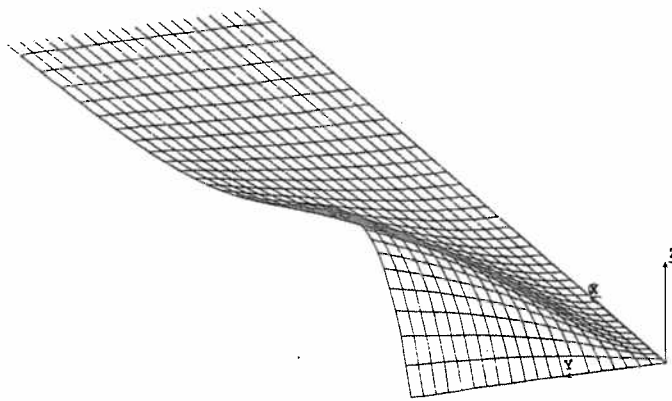


Figure 4.3-1 Deformed shape of a FE model of a semi-infinite cantilevered plate strip subject to an edge moment loading, $-M_{x,0}$ at the line $x = 0$.

Following the procedure used in Sections 4.1 and 4.2, under constant line loading the values of the FEA for w and M_x at $x = 0$, $y = B/2$, using $\nu = 0$, are set equal to w and M_x of the BEF theory. By using the input data of Section 4.1, the FEA resulted in a deflection of 0.768 mm. Thus the deflection of the plate strip of width $B/2$, with one edge free and the other fixed, is 66.2% of the deflection of the simply-supported plate of total width B . The bending stress, 47.9 MPa (bending moment 31.93 Nmm/mm), corresponds to a bending moment ratio of 86.6%. $1/\lambda$ and n are calculated from the equality of: (i) the deflection, w , and (ii) the bending moment, M_x , of the FEA and the BEF solutions, at $x = 0$, giving the equations

$$\begin{aligned}
 (i) \quad 0.768 \text{ mm} &= \frac{1}{4} \frac{V_0}{K} \frac{1}{\lambda^3} \frac{1}{\sqrt{1+n}}, \\
 (ii) \quad 31.93 \frac{\text{Nmm}}{\text{mm}} &= \frac{1}{2} \frac{V_0}{\lambda} \frac{1}{\sqrt{1+n}}, \quad (4.3-1)
 \end{aligned}$$

$$K = 140\,000 \text{ Nmm}, \quad B = 200 \text{ mm}, \quad V_0 = 1 \text{ N/mm}.$$

resulting in

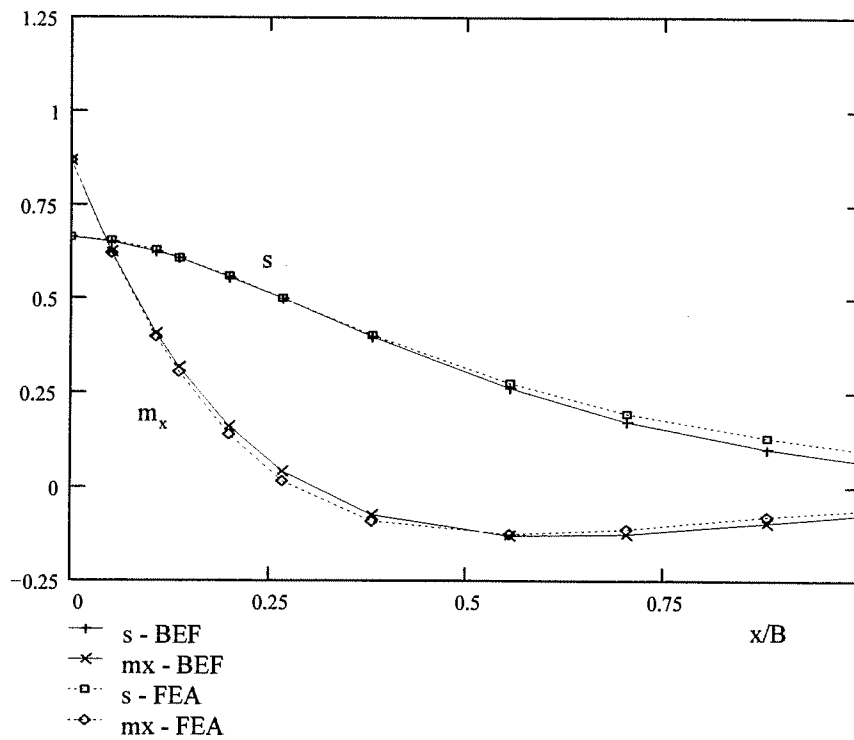
$$\frac{1}{\lambda} = 1.288 \frac{B}{\pi} = 0.82 b, \quad n = 0.65, \quad b = \frac{B}{2}, \quad (4.3-2)$$

where b is the width of the cantilevered plate strip (e.g. 50% of the total width, B , of the flange of a symmetric I-beam flange).

The results of FEA of unit lateral line loading, V_0 , and unit edge moment loading, $-M_{x,0}$, are shown in Table 4.3-1 at the line $y = B/2$ as a function of the coordinate, x , shown in column one. The results of V_0 are given in columns two and three; the axial bending stress in the second and the deflection in the third. The axial bending stress and the slope of deflection, which are the results of $-M_{x,0}$, are given in columns four and five, respectively. The results under line loading, shown in Figure 4.3-2, are compared with the corresponding functions of the BEF theory using the parameters of Eqn (4.3-2) when normalised by the results of the simply-supported plate of width B . The corresponding normalised bending moment, $m_{x,1}$, and slope of deflection, r , functions under moment loading are shown in the x direction in Fig. 4.3-3.

Table 4.3-1 Results of FEA of a plate strip with a free edge.

x [mm]	$\sigma_x(x)$ [MPa]	$\delta(x)$ [mm]	$\sigma_x(x)$ [MPa]	$\phi(x)$ [mrad]
0	47.9	.768	.993	-0.154
10	34.3	.757	.829	-0.110
21.3	22.1	.726	.654	-0.0708
27.2	16.7	.704	.567	-0.0536
39.7	7.60	.648	.404	-0.0245
53.4	.850	.580	.263	-0.0029
76	-5.10	.468	.104	0.0162
111	-7.10	.320	-.005	0.0229
141	-6.20	.224	-.031	0.0197
176	-4.50	.148	-.032	0.0144
200	-3.40	.108	-.027	0.0108

Figure 4.3-2 Plate strip with free edge subjected to constant lateral line loading: normalised deflection, s , and bending moment, m_x , as a function of $x/B = x/(2b)$.

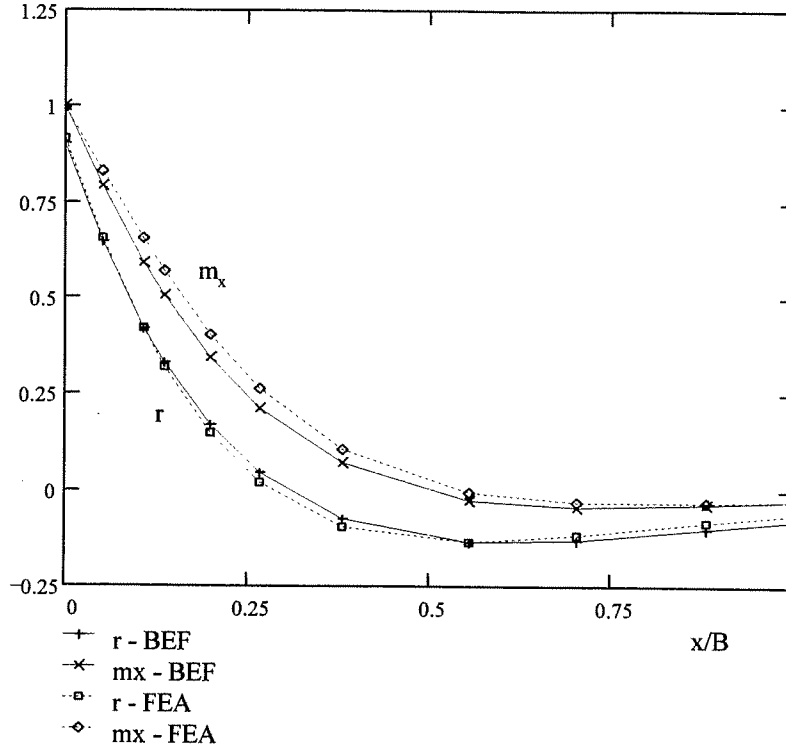


Figure 4.3-3 Plate strip with a free edge under edge moment loading: normalised slope of deflection, r , and bending moment, m_x , as a function of x/B .

4.4 Geometric non-linear effect of in-plane loading on bending behaviour

4.4.1 Geometric non-linear BEF model

As with the case of a BEF under true axial loading, $N = N_x$, the lateral deflection of a plate is influenced by in-plane forces. The effect of membrane forces on the deflection has been expressed as an equivalent fictitious lateral pressure, (Szilard, 1974) resulting in the differential equation:

$$K \frac{\partial^4 w}{\partial x^4} + 2K \frac{\partial^4 w}{\partial x^2 \partial y^2} + K \frac{\partial^4 w}{\partial y^4} = p_z + N_x \frac{\partial^2 w}{\partial x^2} + N_y \frac{\partial^2 w}{\partial y^2} + N_{xy} \frac{\partial^2 w}{\partial x \partial y} \quad (4.4-1)$$

When neither lateral load nor shear in-plane loading exist, $p_z = N_{xy} = 0$, the contribution of N_x and N_y to Eqn (2.2-2) for a simply-supported plate results in

$$\sum_m \left[(K \eta_m^4 + N_y \eta_m^2) X_m(x) - (2K \eta_m^2 + N_x) X_m''(x) + K X_m'''(x) \right] \cos(\eta_m y) = 0. \quad (4.4-2)$$

Proceeding as in Section 3.3.1 under harmonic loading, it can be seen that the zero order Winkler foundation parameter, k_m , and the second-order foundation parameter, N_m , for a simply-supported plate strip are

$$\begin{aligned} k_m &= K \eta_m^4 \left(1 + \frac{N_y}{K \eta_m^2} \right) = K \frac{m^4 \pi^4}{B^4} \left(1 + \frac{N_y B^2}{K m^2 \pi^2} \right), \\ N_m &= 2K \eta_m^2 \left(1 + \frac{N_x}{2K \eta_m^2} \right) = 2K \frac{m^2 \pi^2}{B^2} \left(1 + \frac{N_x B^2}{2K m^2 \pi^2} \right). \end{aligned} \quad (4.4-3)$$

When these values are substituted into Eqn (3.2-5), the following equations are obtained:

$$\begin{aligned} \frac{1}{\lambda_m} &= \sqrt[4]{\frac{4EI}{k_m}} = \frac{\sqrt{2}}{m\pi} B \frac{1}{\sqrt[4]{1 + \frac{N_y B^2}{K m^2 \pi^2}}}, \\ n_m &= \frac{N_m}{4EI \lambda_m^2} = \left(1 + \frac{N_x B^2}{2K m^2 \pi^2} \right) \frac{1}{\sqrt[4]{1 + \frac{N_y B^2}{K m^2 \pi^2}}}, \\ \alpha_m &= \lambda_m \sqrt{1 + n_m}, \quad \beta_m = \lambda_m \sqrt{1 - n_m}. \end{aligned} \quad (4.4-4)$$

For the lowest value, $m = 1$, the following can be obtained (for a simply-supported plate) :

$$\begin{aligned} \frac{1}{\lambda} &= \frac{\sqrt{2}}{\pi} B \frac{1}{\sqrt[4]{1 + \frac{N_y}{N_{Eul}}}}, \quad N_{Eul} = \frac{\pi^2 K}{B^2}, \\ n &= \left(1 + \frac{N_x}{N_W} \right) \frac{1}{\sqrt[4]{1 + \frac{N_y}{N_{Eul}}}}, \quad N_W = 4K \lambda^2 = \frac{2\pi^2 K}{B^2}, \\ \alpha &= \lambda \sqrt{1 + n}, \quad \beta = \lambda \sqrt{1 - n}. \end{aligned} \quad (4.4-5)$$

N_{Eul} is the fundamental Euler buckling load of a prismatic bar of unit width that is simply supported at the ends. In Eqn (4.4-5), N_W is the Winkler buckling load of the one parameter BEF of Eqn (3.2-5), for a simply-supported plate in the case studied.

When no transverse membrane stress exists, $N_y = 0$, the factor $1/\alpha$ required in Eqn (3.2-16) can be represented in general by

$$\frac{1}{\lambda} = \frac{\sqrt{2}}{\pi} B, \quad n = n_x = n_{lin} + \frac{N_x}{N_W},$$

$$\alpha = \lambda \sqrt{1 + n_{lin}} \sqrt{\frac{1 + n}{1 + n_{lin}}} = \lambda \sqrt{1 + n_{lin}} \sqrt{1 + \frac{N_x}{N_W} \frac{1}{1 + n_{lin}}}. \quad (4.4-6)$$

In Eqn (4.4-6), n_{lin} is the value of n of the two parameter foundation when axial in-plane loading is not present, $N_x = 0$. The combined effect of axial loading and n_{lin} is taken into account in n_x . Under a restrained slope of deflection, $U_2 = 0$, the deflection $U_1 = w_{max}$, and the bending moment, M_{max} , are directly proportional to $1/\alpha$. Similarly, under restrained deflection, $U_1 = 0$, the slope of deflection, $U_2 = \phi_{max}$, is directly proportional to $1/\alpha$. Therefore the following equations can be written:

$$\frac{1}{\alpha} = \frac{1}{\alpha_{lin}} K_{gnl},$$

$$\frac{1}{\alpha_{lin}} = \frac{1}{\lambda \sqrt{1 + n_{lin}}}, \quad K_{gnl} = \frac{1}{\sqrt{1 + \frac{N_x}{N_W} \frac{1}{1 + n_{lin}}}}. \quad (4.4-7)$$

K_{gnl} is the factor of geometric non-linearity due to axial in-plane loading, N_x . As an alternative to Eqn (4.4-7), K_{gnl} can be written approximately, and applied in general by using

$$K_{gnl} = \frac{1}{\sqrt{1 + \frac{N_x}{N_{\sigma,x}}}} = \frac{1}{\sqrt{1 + n_x}}, \quad N_{\sigma,x} \approx (1 + n_{lin}) N_W, \quad (4.4-8)$$

where $N_{\sigma,x}$ is the critical buckling load corresponding to the appropriate boundary conditions along the longitudinal support lines. Based on Eqns (4.4-2) to (4.4-8), n_x is the true axial load, N_x , normalised by $N_{\sigma,x}$.

Theoretically, in a fixed plate, $N_{\sigma,x}$ is 1.75 times the value of $N_{\sigma,x}$ for a simply-supported plate, $4\pi^2 K/B^2$, (Timoshenko & Gere, 1936). Based on the BEF model presented, when the parameters $1/\lambda = B/\pi$ and $n_{lin} = 1/\pi$ are used, $N_{\sigma,x}$ in a fixed plate is 1.32 times the value of N_W of Eqn (3.2-5), or 75% of the correct value. For a simply-supported plate,

using $1/\lambda = 1.47B/\pi$ and $n_{lin} = 0.588$, the BEF model predicts $N_{\alpha,x} = 2.94\pi^2 K/B^2$, or 74% of the theoretically correct value. The BEF parameters of the lowest mode $m = 1$, Eqn (3.3-5), predict the correct critical buckling load, $N_{\alpha,x}$, which is equal to $2N_w$ of Eqn (4.4-5), for a simply-supported plate.

The effect of axial loading, N_x , can be taken into account by multiplying the deflection and bending moment values of the linear analysis by the factor K_{gnl} . Since the foundation parameters are series expressions, approximate values of w_{max} and $M_{x,max}$, under a restrained slope of deflection at $x = 0$, and under constant lateral line loading, V_0 , are calculated from

$$w_{max} = \frac{V_0}{K} \frac{1}{4\lambda^3} \frac{1}{\sqrt{1 + n_{lin}}} K_{gnl}, \quad M_{x,max} = V_0 \frac{1}{2\lambda} \frac{1}{\sqrt{1 + n_{lin}}} K_{gnl} K_v. \quad (4.4-9)$$

The factor K_v takes into account the effect of the transverse bending moment, M_y , at the location of $M_{x,max}$. Based on FEA of the fixed plate case, $K_v = 1 + 0.8v$. For the simply-supported plate, $K_v = 1 + 0.8v$. The importance of K_v is discussed further in Sections 4.5 and 4.6.

Similarly, under restrained deflection at $x = 0$, the slope of deflection, ϕ_{max} , under constant edge moment loading, M_0 , is

$$\phi_{max} = \frac{M_0}{K} \frac{1}{2\lambda} \frac{1}{\sqrt{1 + n_{lin}}} K_{gnl}. \quad (4.4-10)$$

Models for FEA verification. The accuracy of Eqns (4.4-9) and (4.4-10) was tested by geometric non-linear FEA under constant axial pre-straining membrane loading, N_x , by using the Cosmos/M program, with lateral line and edge moment loadings of constant value, 1 N/mm and 1 Nmm/mm, respectively, as in the linear elastic model of Section 4.1. Each analysis (which was performed automatically by the program) comprised two steps, or runs. In the first run, pre-tension or pre-compression of constant value in the width direction was analysed to determine the in-plane forces and to form the geometric stiffness matrix. In the second run, single nodal point deflections and internal forces were determined by taking into account the stiffening or softening effect of the in-plane axial loading, N_x . Because of the type of analysis, no redistribution of in-plane stress occurred in the plate. On the tension side, comparative runs were performed, based on membrane stress levels up to twenty times the critical buckling stress. In the figures to be presented, the results are shown for normalised membrane stresses for n_x in the range -1 (equal to the critical buckling load) to four on the tension side.

4.4.2 Geometric non-linearity under constant lateral line loading

Effect of axial in-plane loading in simply-supported plates

Table 4.4-1 shows the maximum deflection and bending moment results normalised by the values of the linear elastic runs. Also shown are two columns of K_{gnl} values calculated by using two values of n_{lin} : 0.618, corresponding to the n of lateral line loading of constant value (see Section 4.1); and 1.0 for harmonic loading (see Section 3.1.1). In the model analysis, $N_x/N_w = 1.0$, corresponding to a tension stress of 34.5 MPa, when $\nu = 0$.

Table 4.4-1 Results of geometric non-linear FEA of constant lateral line loading.

N_x/N_w	$N_x/N_{cr,x}$ $n_{lin} = 1.0$	$\frac{w_{max}(N_x)}{w_{max}(0)}$	$\frac{M_{max}(N_x)}{M_{max}(0)}$	K_{gnl} , $n_{lin} = 0.62$	K_{gnl} , $n_{lin} = 1.0$
-1.80	-0.90	3.20	3.41	3.00i	3.16
-1.50	-0.75	2.00	2.10	3.67	2.00
-1.00	-0.50	1.42	1.45	1.62	1.41
-0.50	-0.25	1.16	1.17	1.20	1.16
0	0	1.00	1.00	1.00	1.00
1.00	0.50	0.817	0.802	0.786	0.817
2.00	1.00	0.702	0.684	0.669	0.707
4.00	2.00	0.565	0.547	0.537	0.577
10.8	5.40	0.358	0.357	0.361	0.395

By using $n_{lin} = 0.618$, accurate values were obtained for the tension side. Physically, in tension, practically no membrane stress redistribution caused by lateral deflection occurs. In compression, $n_{lin} = 1.0$ is less conservative and predicts more correctly the theoretical loss of stability. Based on some true geometric non-linear shell element FE analysis runs for compression, it was found that the membrane stress redistribution in compression is significant when $N_x < -N_w$. Since the true interaction of the lateral deflection and the membrane stress redistribution cannot be neglected, the use of the BEF analysis, (or FEA based on pre-straining), is to be limited to $N_x > -N_w$ in analysis applications.

The effect of the geometric nonlinearity is shown in Figure 4.4-1 as s_{gnl} and $m_{x,gnl}$ as a function of the normalised axial loading, n_x . s_{gnl} is the maximum deflection, w_{max} , normalised by w_{max} of the linear analysis, $N_x = 0$. Correspondingly, $m_{x,gnl}$ is the normalised bending moment. The curve, K_{gnl} , of Eqn (4.4-8) based on $n_{lin} = 1.0$, is

shown as a solid line. In compression it coincides with the deflection curve drawn between the FEA results (dotted line and marked by \square) of FEA. Under high tension loading, the bending moment results (dotted line and \diamond) diverge slightly from the K_{gnl} curve but only marginally from the deflection results of FEA, which can also be seen in Table 4.4-1.

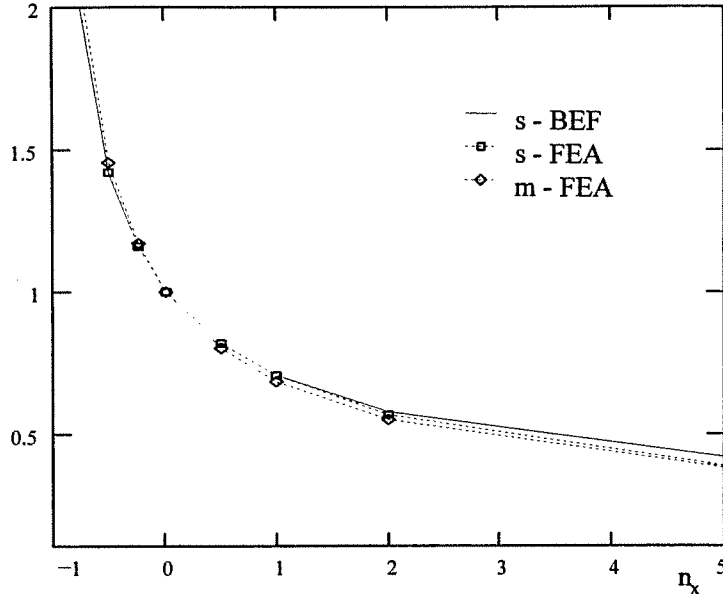


Figure 4.4-1 Simply-supported plate strip, $\nu = 0$, under constant lateral line loading, V_0 ; normalised deflection, s_{gnl} , and bending moment, $m_{x,gnl}$, as a function of n_x .

Effect of transverse in-plane loading

The validity of the geometric non-linearity shown in Eqn (4.4-5) for the plate strip subjected to constant transverse in-plane loading was analysed by FEA for comparison in two cases: simply supported and fixed at the longitudinal stiffener lines. The FEA results corresponding to $\nu = 0$ are shown in Figures 4.4-2 and 4.4-3 by dotted lines. The theoretical curves are indicated by solid lines. The symbol definitions of Figure 4.4-1 apply. The elementary Euler-buckling load for steel, calculated using Eqn (4.4-11) and resulting in a value of 17.3 MPa for a slenderness ratio, B/h of 100, was used to normalise the in-plane loading. A value four times greater is the Euler-buckling load of a plate fixed at the ends. For the calculation of deformations and internal forces in a simply-supported plate, the following parameters, based on a model to be shown in Section 4.6, were used:

$$\frac{1}{\lambda} = \frac{B}{\pi} \frac{1.5}{\sqrt[4]{1+n_y}}, \quad n = \frac{0.71}{\sqrt{1+n_y}}, \quad n_y = \frac{N_y B^2}{\pi^2 K}. \quad (4.4-11)$$

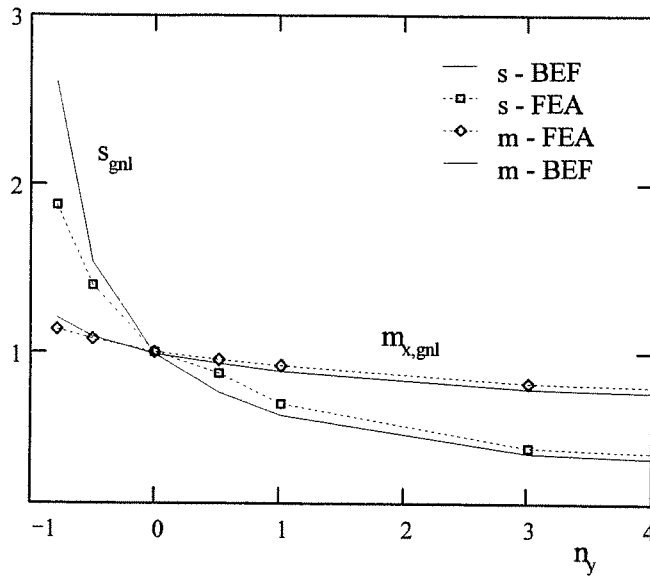


Figure 4.4-2 Simply-supported plate strip, $\nu = 0$, under line loading V_0 : s_{gnl} and $m_{x,gnl}$ against n_y .

Correspondingly, the parameters for the fixed plate are:

$$\frac{1}{\lambda} = \frac{B}{\pi} \frac{1}{\sqrt[4]{1+n_y}}, \quad n_x = \frac{1}{\pi} \frac{1}{\sqrt{1+n_y}}, \quad n_y = \frac{N_y B^2}{4\pi^2 K}. \quad (4.4-12)$$

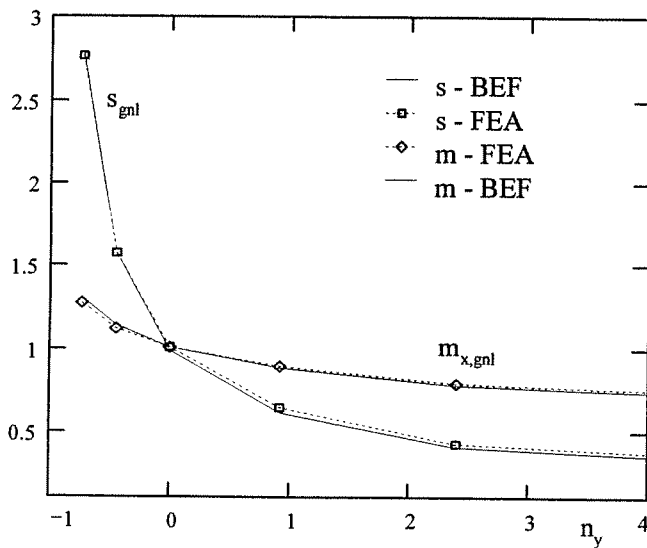


Figure 4.4-3 Fixed plate strip, $\nu = 0$, under V_0 : s_{gnl} and $m_{x,gnl}$ against n_y .

4.5 Effect of biaxial stress state on bending behaviour

The BEF model presented in Chapters 3 and 4 was based on stress uniaxiality by setting Poisson's ratio, ν , equal to zero when determining the foundation parameters, $1/\lambda$ and n . In this section, the use of the BEF model is widened to engineering materials having $\nu > 0$, e.g. for steel for which $\nu = 0.3$. The bending stiffness, K , and the bending moment resulting from lateral deflection, M_x , are influenced by ν : when $\nu = 0.3$, K is $1/(1 - \nu^2) = 1.10$ times the value for K for the uniaxial case; M_x is the sum of M_x and ν times M_y for $\nu = 0$. The validity of the BEF models for $\nu = 0.3$ was tested by the shell element FEA models of Section 4.1 under unit lateral line loading.

4.5.1 Linear analysis

Simply-supported plate strip

The maximum deflection at the centre-line was 91% of the deflection obtained in Section 4.1, i.e. 1.16 mm. The maximum bending moment was exactly 30% higher (48 Nmm/mm compared with 37 Nmm/mm) than the case when $\nu = 0$, since $M_y(0,0) = M_x(0,0)$ in Eqns (2.3-12) and (2.3-13). The results of the plate theory were numerically equal to the results of the FEA and BEF analysis based on Eqn (3.3-11). Therefore the foundation parameters of Chapter 3 are valid for $\nu > 0$.

Fixed plate strip

The two parameters, $1/\lambda$ and n , of the BEF theory of a fixed plate are determined for a material using $\nu = 0.3$. By performing the necessary numerical calculations, it can be shown that the deflection, w , of the fixed plate is 34.0% of the value for a simply-supported plate strip, also for $\nu = 0.3$. When $\nu = 0.3$, based on theoretical calculations, the bending moment, M_x , of the fixed plate is 0.721 times the value 48 Nmm/mm for M_x for a simply-supported plate (compared with 0.757 times the value 37 Nmm/mm, when $\nu = 0$). Based on the theoretical analysis, the bending moment ratio of the fixed plate is 1.24, $K_\nu = 1 + 0.8\nu$ when Poisson's ratios of 0.3 and 0 are compared. Following the theoretical procedure shown in Section 3.3.2, it can be shown that the BEF parameters for $\nu = 0.3$ are $1/\lambda = 0.985B/\pi$ and $n = 0.25$, which are the same as those of $\nu = 0$ determined in Section 4.2.1.

For $\nu = 0.3$, FEA resulted in 70.7% of the bending moment of the simply-supported plate, i.e. 48.3 Nmm/mm (cf. 75.4% for $\nu = 0$). Therefore, when the bending moment of the BEF solution is multiplied by K_ν in the theoretical solution, the two equations based on the FEA results can be written as

$$\begin{aligned}
 (i) \quad & 0.34 \times (1 - 0.3^2) \times 1.16 \text{ mm} = \frac{V_0}{4K} \frac{1}{\lambda^3} \frac{1}{\sqrt{1+n}}, \\
 (ii) \quad & 0.707 \times 48.3 \text{ Nmm/mm} = \frac{V_0}{2} \frac{1}{\lambda} \frac{1.24}{\sqrt{1+n}},
 \end{aligned} \tag{4.5-1}$$

resulting in

$$\frac{1}{\lambda} = 0.992 \frac{B}{\pi}, \quad n = 0.28. \tag{4.5-2}$$

In the earlier results, Section 4.2.1, when $\nu = 0$, n varied between 0.25 and 0.29, and $1/\lambda$ was relatively constant, $0.99B/\pi$. By using $1/\lambda = B/\pi$ and $n = 1/\pi$ of the generalised model, Section 4.6, the accuracy of the maximum deflection and bending moment of the linear elastic BEF model of $\nu = 0.3$ is

$$\begin{aligned}
 \frac{M_{\max, \text{mod}}}{M_{\max, \text{def}}} &= \frac{\sqrt{1+0.25}}{0.985\sqrt{1+1/\pi}} = 0.988, \\
 \frac{w_{\max, \text{mod}}}{w_{\max, \text{def}}} &= \frac{\sqrt{1+0.25}}{0.985^3\sqrt{1+1/\pi}} = 1.02,
 \end{aligned} \tag{4.5-3}$$

when the results of the calculation model (mod) are compared with the results defined theoretically (def). It can be concluded that the parameters n and $1/\lambda$ describing the fixed plate are not affected significantly by the value of Poisson's ratio. Minor modifications to the BEF parameters from the exact values also have little influence. The normalised functions, related to deflection, w , and the bending moment, M_x , calculated by BEF and using FEA, shown in Figures 4.5-1, 4.5-2, 4.5-4, 4.5-5, 4.5-6, are based on the values $1/\lambda = B/\pi$ and $n = 1/\pi$.

4.5.2 Effect of geometric non-linearity caused by axial in-plane loading

Fixed plate under constant lateral line loading

The applicability of Eqn (4.4-1) for predicting the combined effect of axial in-plane membrane loading with a value for Poisson's ratio of 0.3 was studied by varying the axial membrane stress level. In Fig. 4.5-1 the maximum deflection (marked by \square) and bending moment FEA results (dotted line and \diamond) normalised by the results of the linear FE analysis, s_{gnl} and $m_{x, \text{gnl}}$, are shown together with the theoretical curve (solid line), which is equal to K_{gnl} of Eqn (4.4-8). The results are shown as a function of the normalised axial stress, n_x .

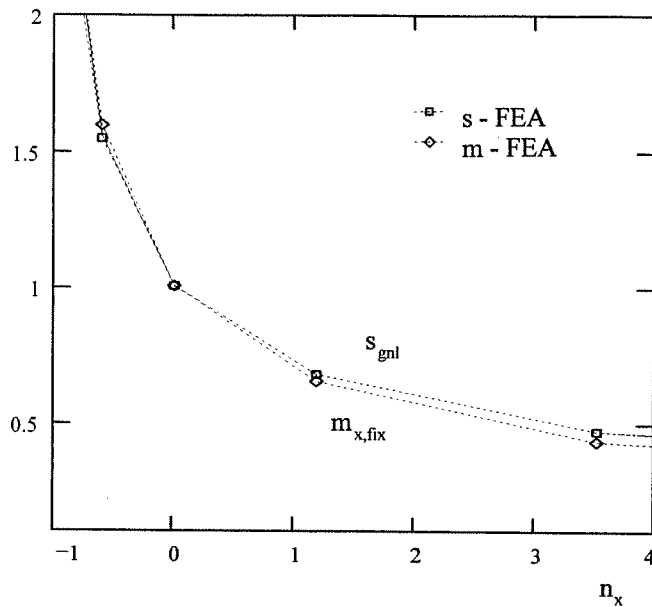


Figure 4.5-1 Fixed plate, $\nu = 0.3$, under constant lateral line loading: s_{gnl} and $m_{x,gnl}$ as a function of n_x .

Fixed plate under constant edge moment loading

The applicability of Eqn (4.4-8) for predicting the combined effect of axial in-plane membrane loading and $\nu = 0.3$ under edge moment loading is illustrated in Figure 4.5-2. The normalised slope of deflection, r_{gnl} , curves (FEA by dotted line and \diamond ; K_{gnl} of BEF by solid line) indicate that the effect of the geometric nonlinearity resulting from axial in-plane loading is predicted well by Eqn (4.4-8).

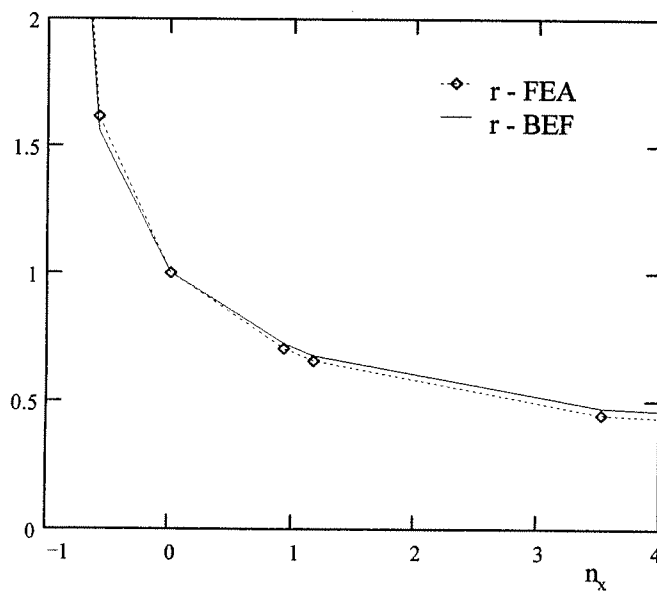


Figure 4.5-2 Fixed plate, $\nu = 0.3$, under constant edge moment loading: normalised slope of deflection r_{gnl} as a function of n_x .

4.5.3 Effect of geometric non-linearity caused by transverse in-plane loading

Simply-supported plate under lateral line loading

The combined effect of variable transverse in-plane loading, N_y , and $\nu = 0.3$ was studied using the model presented, and also by FEA. The results are shown in Figure 4.5-3. FEA results of the maximum deflection are marked by \square , the bending moment by \diamond , and the theoretical curves by solid lines. The effect of the geometric non-linearity on bending behaviour is more important for $\nu = 0.3$ than for $\nu = 0$, when the results of Fig. 4.4-2 are considered. When $\nu = 0.3$, the BEF model based on the parameters of Eqn (4.4-11) is conservative in the case of tension, predicting a significantly higher bending moment than the results of FEA, and vice-versa in compression, whereas when $\nu = 0$, the FEA results and the BEF model correlate well.

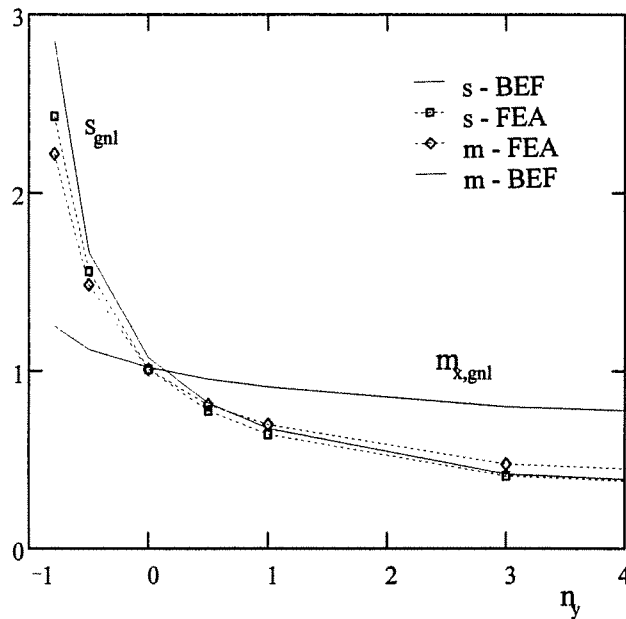


Figure 4.5-3 Simply-supported plate, $\nu = 0.3$, under constant lateral line loading: s_{gnl} and $m_{x,gnl}$ as a function of n_y

Fixed plate strip subject to constant lateral line loading

The results are shown in Fig. 4.5-4. In this case, the bending moment curve of the FEA results agrees well with the prediction of the BEF model. $m_{x,gnl}$ based on $\nu = 0$ is also plotted for comparison (dashed line and \times). Otherwise the notations of Fig. 4.5-3 apply. The results show that the BEF model under the influence of N_y is applicable for a fixed continuous plate under lateral line loading.

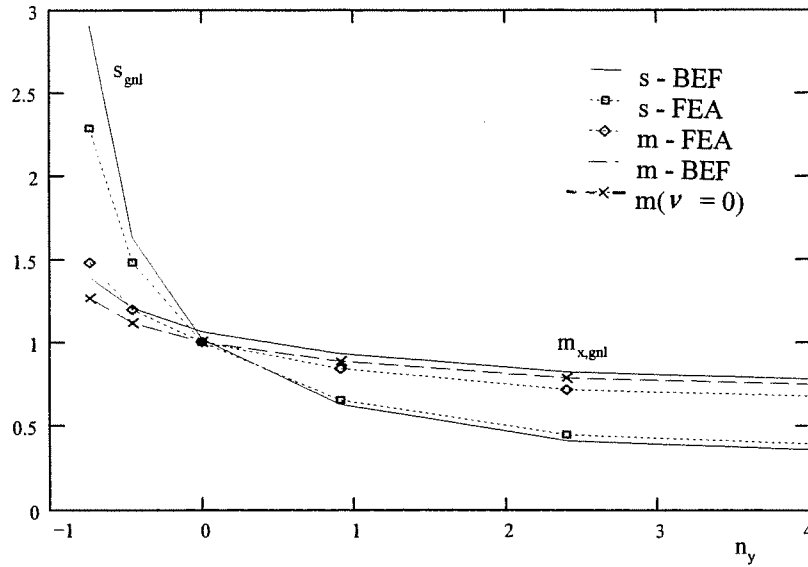
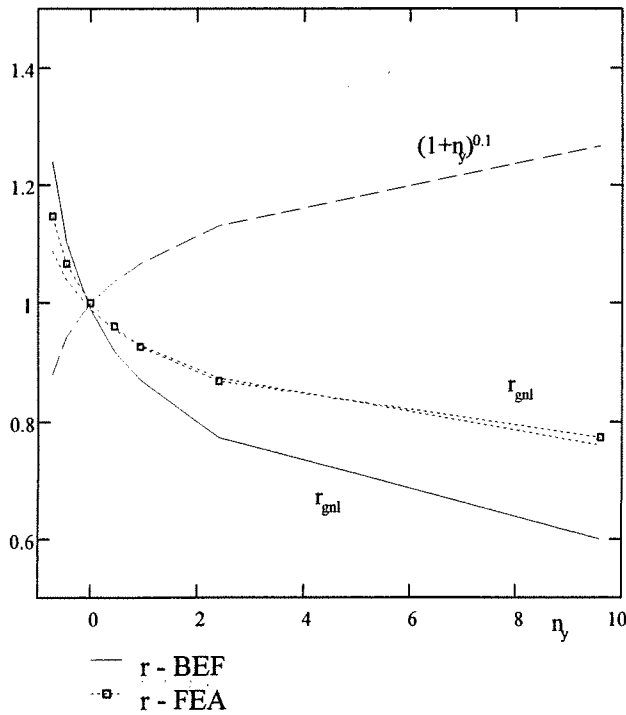


Figure 4.5-4 Fixed plate, $\nu = 0.3$, under constant lateral line loading: s_{gnl} and $m_{x,gnl}$ as a function of n_y .

Fixed plate strip subject to constant edge moment loading



In Fig. 4.5-5 the FEA results of the normalised maximum slope of deflection, r_{gnl} , are marked by a dotted line and \square , and the theoretical curve by solid line.

Figure 4.5-5 Fixed plate, $\nu = 0.3$, under constant edge moment loading: normalised slope of deflection, r_{gnl} , as a function of n_y .

The slope of deflection results shown in Figure 4.5-5 indicate that the effect of the geometric non-linearity on bending behaviour is lower than predicted by using the parameters of Eqn (4.4-12). It was also noticed that a mild empirical correction factor was needed in the BEF model. Therefore, a correction factor chosen by trial and error $(1 + n_y)^{0.1}$, shown as the dashed line in the figure, multiplied by the BEF model slope of deflection (lower solid line), resulted in good convergence with the FEA results, dotted line.

4.5.4 Combined effect of geometric non-linearity caused by axial and transverse in-plane loading on bending behaviour

The combined effect of axial and transverse in-plane loading on bending behaviour was analysed for a fixed plate strip. Only one level of transverse in-plane loading was tested: a compressive load, N_y , equal to 50% of the critical buckling stress ($n_y = -0.5$). The axial membrane stress was varied. The results of $\nu = 0.3$ are shown in Fig. 4.5-6 as a function of normalised axial stress where the FEA results of the maximum deflection are marked by \square , the bending moment by \diamond , and the theoretical curves by a solid line (deflection higher). By applying Eqns (4.4-5) to (4.4-7), the parameters of the BEF model are given by approximative formulae

$$\frac{1}{\lambda} = \frac{B}{\pi^4} \frac{1}{\sqrt{1 + n_y}}, \quad \frac{\alpha}{\lambda} \approx \sqrt{1 + \frac{1}{\pi}} \sqrt{1 + \frac{1.75 n_x}{1 + \frac{0.75}{\sqrt{1 + n_y}}}},$$

$$n_y = \frac{N_y B^2}{4\pi^2 K}, \quad n_x = \frac{1}{1.75} \frac{N_x B^2}{4\pi^2 K}. \quad (4.5-4)$$

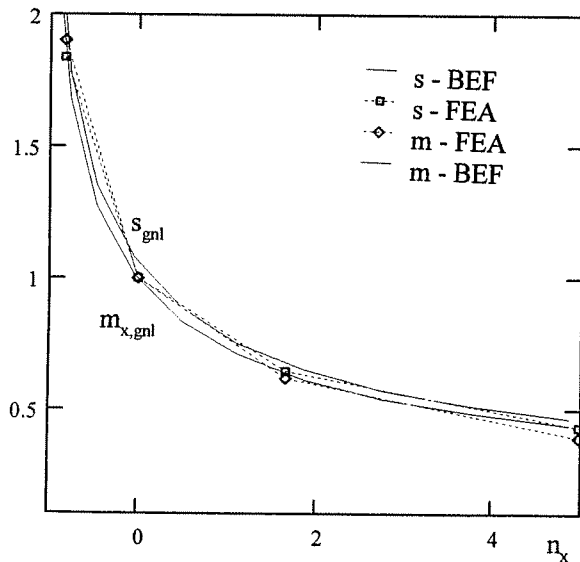


Figure 4.5-6 Fixed plate, $\nu = 0.3$, under constant lateral line loading and normalised transverse compression, $n_y = -0.5$: s_{gnl} and $m_{x,gnl}$ as a function of n_x .

4.6 The generalised BEF model

Two BEF models are developed as the final result of the analysis of semi-infinite plates. The first, in Section 4.6.1, describes the behaviour of the centre-line of a plate strip supported along two edge lines. The second, in Section 4.6.2, describes the free edge line of a cantilever plate. The second order parameter, N , which represents the effect of the torsional stiffness of the BEF model, is determined for the plate supported on two edges. It is used to develop a generalised geometric linear BEF model for the centre-line, taking into account the effect of the rotation stiffness of the longitudinal support lines. The rotation stiffness is shown to be determined using ordinary beam theory. The results of the generalised BEF model are shown to correlate with sufficient accuracy with the linear shell element FEA results, to be used in practical applications. The critical buckling loads, which are required for the determination of the factor of geometric non-linearity, K_{gnl} , are presented, taking into account the effect of rotation stiffness at the support lines. In Section 4.6.2 the same procedure is used, and verified, to determine the BEF model for a cantilever plate.

4.6.1 Model for plate strips supported elastically along longitudinal edge lines

Effect of second order foundation parameter, N

In a simply-supported plate under harmonic cosine loading, the second-order parameter, N , Eqn (3.3-3), which corresponds to the first component, $m = 1$, is

$$N_m = 2K\eta_m^2 = 2K \frac{m^2 \pi^2}{B^2}, \quad N_1 = 19.7 \frac{K}{B^2}. \quad (4.6-1)$$

The parameter N of Eqn (4.6-1) resulted in $n = 1.0$, as shown in Chapter 3.

The superimposed effect of the second order parameter, N , of constant lateral line loading is lower than under the first harmonic component. When theoretically $n = n_{lin} = 0.588$ and $1/\lambda = 1.47B/\pi$, Eqn (3.3-10), the parameter N results in

$$N = 4K\lambda^2 n = 10.7 \frac{K}{B^2}. \quad (4.6-2)$$

In a fixed plate the theoretical values of Eqn (4.2-21), $n_{lin} = 0.245$ and $1/\lambda = 0.985B/\pi$, give

$$N = 4K\lambda^2 n = 9.97 \frac{K}{B^2}. \quad (4.6-3)$$

Based on the parameters of FEA, $n_{lin} = 0.284$ and $1/\lambda = 0.990B/\pi$, N results in the value $11.4K/B^2$. It can be seen that under constant lateral line loading the effect of the torsion stiffness, N , is fairly constant, at least approximately close to 4π (corresponding to $n_{lin} = 1/\pi$ and $1/\lambda = B/\pi$). It is independent of the rotation boundary conditions at the support lines, whether simply supported or fixed. Therefore, it can be deduced and assumed that N is constant for a specific type of loading (in this study constant lateral line or edge moment loading over the width B).

Effect of rotation stiffness at support lines on bending behaviour

The centre-line of a longitudinal plate strip can be considered as the centre-line beam of a series of longitudinal beams resting on a series of transverse beams, on an elastic foundation generated by the transverse bending stiffness of the plate. In this study, constant lateral line loading is applied, since the study concentrates on transverse line loads, harmonic loads, or loads of constant value in the transverse direction. Therefore, the longitudinal beams of the grillage network are supported by the transverse beams. It is assumed that the shape of the support reaction of the transverse beams follows the shape of the external loading, at least close to the load application line. Therefore, the foundation parameter, k , can be determined by calculating the maximum deflection of a beam of length, B , under a specific type of loading. The characteristic length, $1/\lambda$, is determined from Eqn (3.2-5). The determination of k for a simply-supported plate is shown initially: the maximum deflection, w_{max} , of a simply-supported plate strip of unit width under line loading, p , is well known as

$$w_{max} = \frac{5}{384} \frac{p B^4}{K} \quad (4.6-4)$$

It is also generally known that $k = p/w$, and therefore $1/\lambda$ is given, using Eqn (3.2-5), by

$$\frac{1}{\lambda} = \sqrt[4]{\frac{20}{384}} B = 1.50 \frac{B}{\pi} \quad (4.6-5)$$

By comparing Eqn (4.6-5) with Eqn (3.3-10) it can be seen that the expressions for $1/\lambda$, based on the plate theory and the simple beam theory, are practically equal. For the fixed plate, similar determination results in $1/\lambda = B/\pi$.

The effect of the rotation stiffness of the longitudinal support lines caused by joint springs, k_ϕ , is determined by analysing one half of the structure as a beam element model shown in Fig. 4.6-1. The nodal load vector $\{F\}$ consists of equivalent nodal loads $\{F_{eq}\}$ resulting from the constant line loading p .

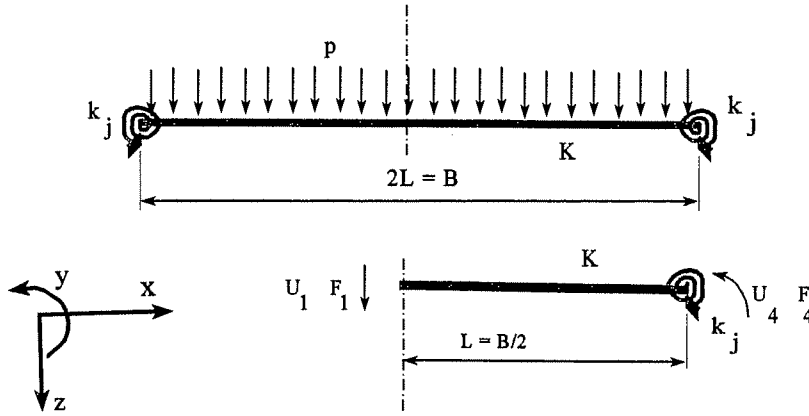


Figure 4.6-1 Beam element FE model consisting of a unit width plate strip and one spring element loaded by equivalent nodal loads resulting from constant line loading.

The determination of $\{F_{eq}\}$ is a standard procedure in the theory of FE analysis. $\{F_{eq}\}$ and the global force balance are given by

$$\{F_{eq}\} = p \begin{Bmatrix} \frac{L}{2} \\ -\frac{L^2}{12} \end{Bmatrix} = \begin{bmatrix} \frac{12K}{L^3} & \frac{6K}{L^2} \\ \frac{6K}{L^2} & \frac{4K}{L}(1+r) \end{bmatrix} \begin{Bmatrix} U_1 \\ U_4 \end{Bmatrix}, \quad L = \frac{B}{2}, \quad (4.6-6)$$

where the parameter r ,

$$r = k_\phi \frac{L}{4K} = k_\phi \frac{B}{8K} \quad (4.6-7)$$

is the non-dimensional rotation stiffness of k_ϕ . By inverting the coefficient matrix, the maximum deflection U_1 (at the centre-line) can be solved, resulting in

$$U_1 = \frac{1}{384} \frac{5+r}{1+r} \frac{pB^4}{K} \quad (4.6-8)$$

Since $k = p/U_1$, the characteristic length of the unit width longitudinal BEF, using Eqn (3.2-5), is:

$$\frac{1}{\lambda} = \frac{B}{\pi} \sqrt{\frac{5+r}{1+r}}. \quad (4.6-9)$$

The characteristic length, $1/\lambda$, of the fixed plate ($r = \infty$) equals B/π , and $1/\lambda$ for the simply-supported plate ($r = 0$) is $1.50B/\pi$.

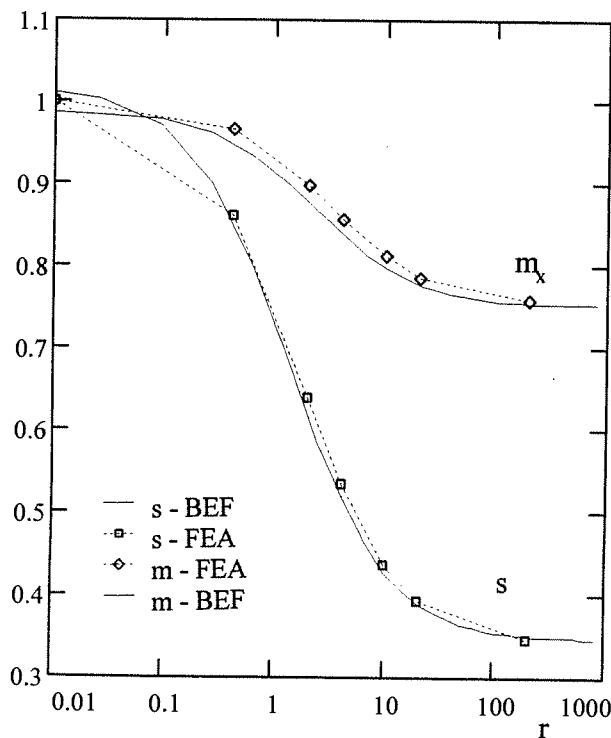
When the value of N of Section 4.6.1:

$$N = \frac{4\pi K}{B^2} \quad (4.6-10)$$

is chosen to describe the torsion stiffness, the parameter n_{lin} of the generalised BEF model, Eqn (3.2-5) is

$$n_{lin} = \frac{1}{\pi} \sqrt{\frac{5+r}{1+r}} \quad (4.6-11)$$

This results in $n_{lin} = 1/\pi$ when the ends are fixed, and in $n_{lin} = 0.711$ when the plate is simply supported. When these parameters are compared with the analysis of a plate of material with $\nu = 0.3$, shown in Section 4.5, the maximum bending moment and the deflection of the BEF model are 95% and 103% of the theoretical values, respectively, in the simply supported case ($r = 0$) and when the plate is fixed at the support lines ($r = \infty$).



Under constant line loading, the functions of the maximum deflection, s , and bending moment, m_x , are shown in Figure 4.6-2, together with the results of the FEA runs, with $\nu = 0.3$. The FEA results of the simply-supported case were used to normalise the results. It can be seen that the correlation is good, except for a minor difference when the normalised rotation stiffness r of Eqn (4.6-7) is zero, corresponding to the simply-supported case.

Figure 4.6-2 Normalised deflection, s , and bending moment, m_x , curves for constant line loading, $\nu = 0$, as a function of the normalised joint rotation stiffness, r .

Effect of Poisson's ratio on bending behaviour

The bending moment, M_x , of a BEF is affected by the bending moment in the transverse direction, M_y , through Poisson's ratio: when the material parameter $\nu = 0.3$ and the plate is simply supported, the multiplication factor, K_ν , is equal to $1 + \nu = 1.3$; for a plate fixed at the ends $K_\nu = 1 + 0.8\nu = 1.24$ (Section 4.5.1). The combined effect of boundary conditions and Poisson's ratio on bending behaviour is small. The reduction caused by the rotation stiffness at the ends can be estimated by the normalised bending moment curve, m_x , e.g. based on Fig. 4.6-2, resulting in the following expression for K_ν :

$$K_\nu \approx 1 + 1.55\nu \frac{1}{\sqrt{\frac{1}{n_{lin}} + 1}}, \quad (4.6-12)$$

where n_{lin} from Eqn (4.6-11) is used. For a fixed plate, Eqn (4.6-12) results in $K_\nu = 1 + 0.76\nu$, and for a simply-supported plate, $K_\nu = 1 + \nu$.

Effect of axial membrane stress

Using Eqns (3.2-5) and (4.6-9), the elementary Winkler buckling load, N_w , of the one parameter foundation model, as a function of r , is

$$N_w = 4K\lambda^2 = \frac{4\pi^2 K}{B^2} \sqrt{\frac{1+r}{5+r}}. \quad (4.6-13)$$

Based on Eqns (4.4-8), (4.6-11) and (4.6-13), $N_{\alpha,x}$ can be calculated. It is $1.31N_w$ when the plate is prevented from rotating, i.e. $r = \infty$, which is 75% of the theoretical buckling load of $1.75N_w$ (Timoshenko & Gere, 1936). Similarly, when the plate is free to rotate, i.e. $r = 0$, $N_{\alpha,x}$ in the generalised BEF model of this study is $1.71N_w$ of Eqn (4.6-13), which is $1.53N_w$ of Eqns (4.4-5) and (4.4-8). $N_{\alpha,x}$ of the model presented is 77% of the true buckling load, which is twice the value of N_w in Eqn (4.4-5). Therefore, an approximation for the true $N_{\alpha,x}$ can be deduced and written in the form

$$N_{\alpha,x} \approx \frac{4\pi^2 K}{B^2} \left(\sqrt{\frac{1+r}{4+r}} + \sqrt{\frac{1+r}{4+2r}} \right). \quad (4.6-14)$$

The effect of the geometric nonlinearity, K_{gri} , is calculated according to Eqns (4.4-8) and (4.6-14) when the axial load is in compression. In tension, the use of K_{gri} calculated according to Eqns (4.4-7) and (4.6-13) is preferable, as shown by the results in Table 4.4-1.

Effect of transverse membrane stress on bending behaviour

The critical buckling load in the transverse direction, under the action of compressive in-plane transverse loading, $N_y < 0$, is determined based on the geometric nonlinear stiffness matrix $[S_c]$: (Cook, 1974)

$$[S_c] = \frac{K}{2 - 2c - \eta L s} \begin{bmatrix} \eta^3 s & S_{21} & S_{31} & S_{41} \\ \eta^2(1 - c) & \eta(s - \eta L c) & S_{32} & S_{42} \\ -S_{11} & -S_{21} & S_{11} & S_{43} \\ S_{21} & \eta(\eta L - s) & -S_{21} & S_{22} \end{bmatrix},$$

$$\eta = \sqrt{\frac{-N_y}{K}}, \quad N_y < 0, \quad s = \sin(\eta L), \quad c = \cos(\eta L). \quad (4.6-15)$$

The global force balance of the beam system shown in Figure 4.6-1 is given by

$$\begin{Bmatrix} F_1 \\ F_4 \end{Bmatrix} = \frac{K}{\Delta} \begin{bmatrix} \eta^3 s & S_{41} \\ \eta^2(1 - c) & \eta(s - \eta L c) + k_\phi \frac{\Delta}{K} \end{bmatrix} \begin{Bmatrix} U_1 \\ U_4 \end{Bmatrix}, \quad \Delta = 2 - 2c - \eta L s. \quad (4.6-16)$$

The critical buckling load, $N_{\alpha,y}$, is found from the condition that the determinant of the global stiffness matrix is zero. Therefore, when $L = B/2$,

$$\frac{k_\phi}{2K\eta} \sin(\eta \frac{B}{2}) + \cos(\eta \frac{B}{2}) = 0, \quad (4.6-17)$$

or $N_{\alpha,y}$ is expressed as

$$N_{\alpha,y} = 4 \frac{K}{B^2} \arctan^2 \left(\frac{-2\pi K}{k_\phi B} \sqrt{\frac{N_{\alpha,y} B^2}{\pi^2 K}} \right). \quad (4.6-18)$$

The effect of transverse membrane loading, N_y , on the foundation parameters and on the geometric nonlinearity, K_{gnl} , is calculated by using Eqns (4.4-11) and (4.4-12). An approximation of the true interaction of N_x and N_y is calculated by using Eqn (4.4-5) when applying $N_{\alpha,y}$ in the expressions for N_{Eul} .

4.6.2 Cantilever plate model

The free edge of a longitudinal plate strip under lateral line loading can be considered as a beam resting on an elastic foundation formed by the transverse bending stiffness of the cantilever plate. Following the methods used in Section 4.6.1, the foundation parameter, k , of the BEF is determined by calculating the maximum deflection, w_{\max} , of a beam of length b ($= B/2$) under constant line loading, p . B is the double width, i.e. the width of the flange of a symmetric I-beam. The maximum deflection, w_{\max} , is

$$w_{\max} = \frac{1}{8} \frac{p b^4}{K} . \quad (4.6-19)$$

The characteristic length, $1/\lambda$, is determined by using Eqn (3.2-5). When $k = p/w_{\max}$, $1/\lambda$ is given by

$$\frac{1}{\lambda} = \sqrt[4]{\frac{1}{2}} b = 0.84 b . \quad (4.6-20)$$

This result from the simple beam theory model in practice equals $1/\lambda = 0.82b$ of Eqn (4.3-2), which was determined by the equality of the FE shell element analysis and the BEF theory results ($\nu = 0$).

When again the value N in Eqn (4.6-10) is chosen to represent the effect of the torsion stiffness, the parameter, n_{lin} , of Eqn (3.2-5) in the generalised BEF model is

$$n_{lin} = 1.74 \frac{1}{\pi} = 0.55 , \quad (4.6-21)$$

whereas Eqn (4.3-2) predicts $n_{lin} = 0.65$. By using the parameters $1/\lambda = 0.82b$ and $n_{lin} = 0.65$ of the FEA the critical axial load parameters are

$$\begin{aligned} N_w &= 4 K \lambda^2 = 5.95 \frac{K}{b^2} , \\ N_{\alpha} &= (1 + n_{lin}) N_w = 9.82 \frac{K}{b^2} . \end{aligned} \quad (4.6-22)$$

N_{α} of Eqn (4.6-22) is 74% of the true critical buckling load of $13.3K/b^2$ (Timoshenko & Gere, 1936), when the plate is restrained against rotation along the support line. By using the parameters $1/\lambda = 0.84b$ and $n_{lin} = 0.55$ of the generalized BEF model determined in this section, $N_w = 5.66K/b^2$, $N_{\alpha} = 8.77K/b^2$, and the ratio 66% are the results comparable with the values of Eqn (4.6-22).

$N_{cr,x}$ of the BEF model based on the BEF parameters of constant line loading, compared with the true buckling load, is about 75% in all three cases analysed: simply supported, fixed and cantilevered.

Under axial compression, K_{gnl} can be calculated for a cantilevered plate from

$$K_{gnl} = \frac{1}{\sqrt{1 + \frac{N_x b^2}{13.3K}}} . \quad (4.6-23)$$

In compression, a symmetric section, similar to the flange of an I-beam, is to be designed against the antisymmetric buckling mode corresponding to the simply-supported boundary condition. In that case the theoretical value $N_{cr,x}$ is $4.5K/b^2$ (Timoshenko & Gere, 1936). When the effect of the zero order term, the bending stiffness, is negligible, applying e.g. Eqn (4.6.22) a critical buckling load based on $n_{lin} = 0.65$ of FEA results is predicted by

$$N_{cr} = (0 + n_{lin})N_W = 3.87 \frac{K}{b^2} , \quad (4.6-24)$$

whereas the BEF model, $n_{lin} = 0.55$, predicts $3.12K/b^2$. These two values are not far from the theoretical value, 87% and 69%, of $4.5K/b^2$, being also close to the general ratio 75% of other cases studied.

Chapter 5

ANALYSIS OF PLATE STRIPS OF FINITE LENGTH BASED ON BEF THEORY

In this chapter it is shown that the BEF theory can be used to determine the axial bending stress at the centre-line of a rectangular plate of finite length. Finite element formulations of a beam of finite length on an elastic foundation are presented in Section 5.1. Previous work is discussed initially. The deflection function of a four degree of freedom beam element is developed, which results in two stiffness matrices: one for compression and moderate tension axial loading; the other for predominant tension (or second order stiffness). Formulations based on the solutions to a single two node BEF element under point loading and point couple loading are presented in Section 5.2. By using the foundation parameters determined in Chapter 4, the BEF model corresponding to the semi-infinite fixed plate is applied to the analysis of a rectangular plate of variable length. In the parametric study the accuracy of the BEF model is verified by ordinary geometric linear shell element FE analysis.

5.1 BEF finite element formulations

5.1.1 Literature review

Stiffness matrix solutions of two node BEF elements, based on polynomial shape functions, were developed in the 1970's by using the energy method. When $\alpha = \beta = \lambda$ in Eqn (3.2-5), FE formulations based on the exact solution of the homogeneous part of Eqn (3.1-1) were first developed independently by Ting and Mockry (1984), and Eisenberger and Yankelevsky (1985). By taking into account the effect of the second order term, N , an exact solution of Eqn (3.1-3), and the stiffness matrix, were developed (Yankelevsky and Eisenberger, 1986), for normalised axial loading, n , in Eqn (3.2-5) in the range $-1 < n < 1$. A solution was presented for a beam element on a two parameter foundation, $0 < n < 1$ (Chiwanga & Valsangkar, 1988). Except for a minor typing error, this solution for the stiffness matrix is equivalent to one presented elsewhere (Yankelevsky & Eisenberger, 1986). Exact analyses for the beam on two parameter foundation problem have been presented (Razaqpur and Shah, 1991), which included two stiffness matrices: one for $n > 1$; and the other for the most common case $0 < n < 1$. (Both k and N were assumed to be positive foundation parameters in these formulations.)

Closed form deflection and internal force functions are generally complicated. The elegant solutions given in the references contain some minor errors, most often typographical. In a number of other publications the deflection functions chosen are not particularly useful. Therefore, in order to present the stiffness matrix of a two node BEF finite element, the development of the deflection and internal force functions are given in detail.

5.1.2 Deflection function $w(x)$, $-1 < n < 1$

Figure 5.1-1 shows the FE-element model and the coordinate system used.

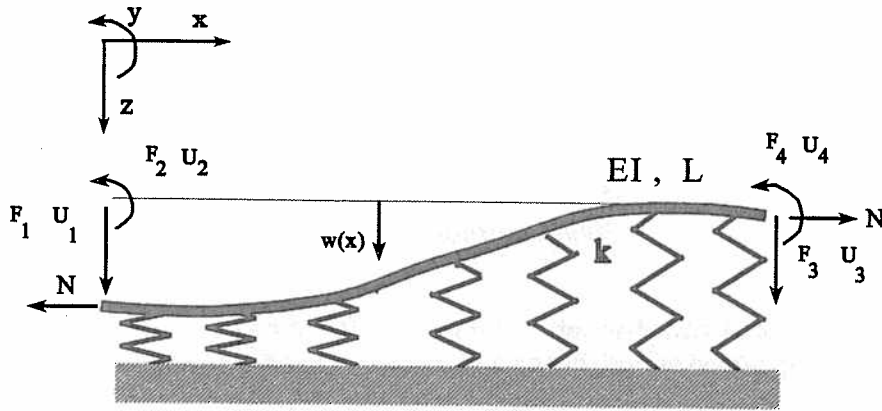


Figure 5.1-1 Coordinate system, degrees of freedom, and internal forces of a beam element of finite length on an elastic foundation subjected to axial loading.

The notation of Eqn (3.2-5), Chapter 3, is used in the formulations shown next. Equation (3.2-1), which is the solution of the governing differential equation, Eqn (3.1-3), is the basis for determining the deflection function and the internal forces of a two node BEF. Two cases relating to the value of n are considered:

- i) $-1 < n < 1$;
- ii) $n > 1$.

In the first case, $-1 < n < 1$, both α and β of Eqn (3.2-5) are real. It is assumed again that $n = n_{lin} + N/N_w$ where N is the true axial loading. A function of deflection $w(x)$ that satisfies the differential equation, Eqn (3.1-3), can be expressed using hyperbolic and trigonometric functions:

$$w(x) = A_1 \cosh(\alpha x) \cos(\beta x) + A_2 \cosh(\alpha x) \sin(\beta x) + A_3 \sinh(\alpha x) \cos(\beta x) + A_4 \sinh(\alpha x) \sin(\beta x) . \quad (5.1-1)$$

When $n > 1$, β in Eqn (3.2-5) changes through zero to complex. In the real value solution, the trigonometric terms cosine and sine in Eqn (5.1-1) are changed to hyperbolic cosine and hyperbolic sine functions of a new variable β_1 times x . If necessary, explicit deflection and internal force functions for $n > 1$ can be obtained from the expressions determined for $-1 < n < 1$, which are shown in detail below. The final result, the stiffness matrix for $n > 1$, is given in Section 5.1.4.

By using matrix notation, the deflection, $w(x)$, of Eqn (5.1-1) is expressed as the product

$$w(x) = [H(x)]\{A\} , \quad (5.1-2)$$

where

$$[H(x)] = \begin{bmatrix} \cosh(\alpha x) \cos(\beta x) \\ \cosh(\alpha x) \sin(\beta x) \\ \sinh(\alpha x) \cos(\beta x) \\ \sinh(\alpha x) \sin(\beta x) \end{bmatrix}^T, \quad \{A\} = \begin{Bmatrix} A_1 \\ A_2 \\ A_3 \\ A_4 \end{Bmatrix}. \quad (5.1-3)$$

By applying boundary conditions at $x = 0$ and $x = L$, the four undetermined coefficients of the vector $\{A\}$ can be solved, based on the nodal degree of freedom vector $\{U\}$:

$$w(0) = U_1, \quad \frac{dw}{dx}(0) = U_2; \quad w(L) = U_3, \quad \frac{dw}{dx}(L) = U_4. \quad (5.1-4)$$

The slope of deflection, $\varphi(x)$, is obtained by differentiating either $w(x)$ in Eqn (5.1-1) or $[H(x)]$ in Eqn (5.1-3). Denoting the differentiation operation by the matrix $[D]$:

$$\frac{d}{dx}[H(x)] = [H(x)] \begin{bmatrix} 0 & \beta & \alpha & 0 \\ -\beta & 0 & 0 & \alpha \\ \alpha & 0 & 0 & \beta \\ 0 & \alpha & -\beta & 0 \end{bmatrix} = [H(x)][D], \quad (5.1-5)$$

$\varphi(x)$ can be written as

$$\varphi(x) = \frac{d}{dx}[H(x)]\{A\} = [H(x)][D]\{A\}. \quad (5.1-6)$$

By using the notation

$$\begin{aligned} CH &= \cosh(\alpha L), & SH &= \sinh(\alpha L), \\ c &= \cos(\beta L), & s &= \sin(\beta L), \end{aligned} \quad (5.1-7)$$

the boundary conditions of Eqn (5.1-4) can be represented by

$$\begin{Bmatrix} U_1 \\ U_2 \\ U_3 \\ U_4 \end{Bmatrix} = \begin{bmatrix} 1 & 0 & 0 & 0 \\ 0 & -\beta & -\alpha & 0 \\ CHc & CHs & SHc & SHs \\ -\psi_1 & -\psi_2 & -\psi_3 & -\psi_4 \end{bmatrix} \begin{Bmatrix} A_1 \\ A_2 \\ A_3 \\ A_4 \end{Bmatrix}, \quad (5.1-8)$$

$$\begin{aligned} \psi_1 &= \alpha SHc - \beta CHs, & \psi_2 &= \alpha SHs + \beta CHc, \\ \psi_3 &= \alpha CHc - \beta SHs, & \psi_4 &= \alpha CHs + \beta SHc, \end{aligned}$$

or

$$\{U\} = [E]\{A\}. \quad (5.1-9)$$

The undetermined coefficient vector $\{A\}$ is solved by inverting the matrix $[E]$:

$$\{A\} = [E]^{-1}\{U\} = [G]\{U\}. \quad (5.1-10)$$

Finally, for the case $(-1 < n < 1)$, the matrix $[G]$ is given explicitly by

$$[G] = \frac{1}{\Delta} \begin{bmatrix} \Delta & 0 & 0 & 0 \\ \frac{\alpha}{\beta}(SHCH + \frac{\alpha}{\beta}sc) & -\frac{SH^2}{\beta} & -\frac{\alpha}{\beta}(SHc + \frac{\alpha}{\beta}CHs) & -\frac{\alpha}{\beta^2}SHs \\ -(SHCH + \frac{\alpha}{\beta}cs) & \frac{\alpha}{\beta^2}s^2 & SHc + \frac{\alpha}{\beta}CHs & \frac{1}{\beta}SHs \\ -\frac{\alpha}{\beta}(SH^2 + s^2) & \frac{SHCH}{\beta} - \frac{\alpha}{\beta^2}sc & (1 + \frac{\alpha^2}{\beta^2})SHs & -\frac{SHc}{\beta} + \frac{\alpha}{\beta^2}CHs \end{bmatrix},$$

$$\Delta = SH^2 - \frac{\alpha^2}{\beta^2}s^2. \quad (5.1-12)$$

The deflection at any point, x , within the length, L , of the beam element is

$$w(x) = [N(x)]\{U\} = [H(x)][G]\{U\}, \quad (5.1-13)$$

where the row vector $[N(x)]$ is the shape function of the deflection. By using Eqns (5.1-3), (5.1-5) and (5.1-12), $\phi(x)$ can be expressed by

$$\phi(x) = \frac{d}{dx}[H(x)][G]\{U\} = [H(x)][D][G]\{U\}. \quad (5.1-14)$$

Since the product expressions are long, only the matrix notations are given.

5.1.3 Internal forces in a two node beam element on an elastic foundation

The unit deflection method, according to the finite element method, is used to derive the stiffness matrix of a four degree of freedom beam-column or tensioned-beam element on an elastic foundation when $-1 < n < 1$.

The bending moment, $M(x)$, and the shear force, $Q(x)$, are functions of successive differentiations of the deflection function, $w(x)$, or the matrix, $[H(x)]$. The differentiations can be rearranged to yield a product of $[H(x)]$ and the corresponding matrix $[D]$: $[D]$ was given in Eqn (5.1-5), $[D^2]$ and $[D^3]$ are given in (5.1-16) and in (5.1-17), respectively:

$$[B(x)] = \frac{d^2}{dx^2}[H(x)] = [H(x)][D][D] = [H(x)][D^2], \quad (5.1-15)$$

where $[D^2]$ is the product $[D][D]$ written by

$$[D^2] = \begin{bmatrix} \alpha^2 - \beta^2 & 0 & 0 & 2\alpha\beta \\ 0 & \alpha^2 - \beta^2 & -2\alpha\beta & 0 \\ 0 & 2\alpha\beta & \alpha^2 - \beta^2 & 0 \\ -2\alpha\beta & 0 & 0 & \alpha^2 - \beta^2 \end{bmatrix}. \quad (5.1-16)$$

Correspondingly, $[D^3]$ is

$$[D^3] = \begin{bmatrix} 0 & \beta(3\alpha^2 - \beta^2) & \alpha(\alpha^2 - 3\beta^2) & 0 \\ \beta(\beta^2 - 3\alpha^2) & 0 & 0 & \alpha(\alpha^2 - 3\beta^2) \\ \alpha(\alpha^2 - 3\beta^2) & 0 & 0 & \beta(3\alpha^2 - \beta^2) \\ 0 & \alpha(\alpha^2 - 3\beta^2) & \beta(\beta^2 - 3\alpha^2) & 0 \end{bmatrix} \quad (5.1-17)$$

All the deflection functions needed for determining the internal forces are now fully defined. The bending moment, $M(x)$, and shear force, $Q(x)$, are directly related to the second and third differentials of $w(x)$. The functions of the bending moment and shear force are given by

$$M(x) = -EI \frac{d^2}{dx^2} w(x) = -EI \frac{d^2}{dx^2} [H(x)][G]\{U\} = -EI[H(x)][D^2][G]\{U\} \quad (5.1-18)$$

$$Q(x) = -EI \frac{d^3}{dx^3} w(x) = -EI \frac{d^3}{dx^3} [H(x)][G]\{U\} = -EI[H(x)][D^3][G]\{U\} \quad (5.1-19)$$

The generalised shear force, $V(x)$, (see Section 3.2.2) is

$$V(x) = Q(x) + N\phi(x) = -EI \frac{d^3 w}{dx^3} + N \frac{dw}{dx} \quad (5.1-20)$$

5.1.4 Element stiffness matrix

The element end force vector $\{F\}$ and the columns of the stiffness matrix, respectively, are obtained from the relations given in Eqn (5.1-21), (see also Section 3.2).

$$\{F\} = \begin{Bmatrix} F_1 \\ F_2 \\ F_3 \\ F_4 \end{Bmatrix} = \begin{Bmatrix} -V(0) \\ -M(0) \\ V(L) \\ M(L) \end{Bmatrix} = \begin{Bmatrix} EI \frac{d^3}{dx^3} w(0) - N \frac{d}{dx} w(0) \\ EI \frac{d^2}{dx^2} w(0) \\ -EI \frac{d^3}{dx^3} w(L) + N \frac{d}{dx} w(L) \\ -EI \frac{d^2}{dx^2} w(L) \end{Bmatrix}, \quad \{F\} = [S]\{U\}. \quad (5.1-21)$$

A convenient way to determine the stiffness matrix, $[S]$, is to use the expressions at $x = 0$, according to the unit deflection method. In Eqn (5.1-22), which defines $[S]$, the parameters V and M are related to the expressions for $V(x)$ and $M(x)$, where the subscript of V_{ij} or M_{ij} is related to a product of two vectors: the subscript parameter $i = 1$ corresponds to the first row of the differentiation matrix of $[H(x)]$ (since $x = 0$); and the second parameter j to the column number of $[G]$. When the sign convention for the rotation angle and reaction moments is taken into account, $[S]$ can be written as

$$[S] = \begin{bmatrix} -V_{11}(0) & V_{12}(0) & -V_{13}(0) & -V_{14}(0) \\ \cdot & M_{12}(0) & M_{13}(0) & M_{14}(0) \\ \text{SYMM.} & \cdot & S_{11} & -M_{11}(0) \\ \cdot & \cdot & \cdot & S_{22} \end{bmatrix}. \quad (5.1-22)$$

i) $-1 < n < 1$

The stiffness matrix of a geometric non-linear four degree of freedom beam element on a linear elastic foundation is written explicitly as

$$[S] = \frac{EI}{\Delta} \begin{bmatrix} 4\lambda^2\alpha(SHCH + \frac{\alpha}{\beta}sc) & S_{21} & S_{31} & S_{41} \\ -2\lambda^2(SH^2 + \frac{\alpha^2}{\beta^2}s^2) & 2\alpha(SHCH - \frac{\alpha}{\beta}sc) & S_{32} & S_{42} \\ -4\lambda^2\alpha(SHc + \frac{\alpha}{\beta}CHs) & -S_{41} & S_{11} & S_{43} \\ -4\lambda^2\frac{\alpha}{\beta}SHs & 2\alpha(SHc - \frac{\alpha}{\beta}CHs) & -S_{21} & S_{22} \end{bmatrix},$$

$$\Delta = SH^2 - \frac{\alpha^2}{\beta^2}s^2,$$

$$\alpha = \lambda\sqrt{1+n}, \quad \beta = \lambda\sqrt{1-n}, \quad n = \frac{N}{4EI\lambda^2},$$

$$SH = \sinh(\alpha L), \quad CH = \cosh(\alpha L), \\ s = \sin(\beta L), \quad c = \cos(\beta L). \quad (5.1-23)$$

In Eqn (5.1-23) it was taken into account that $\alpha^2 + \beta^2 = 2\lambda^2$. The parameters α and β are real when $-1 < n < 1$. Since β (or α) can become imaginary, the $[S]$ given above is preferred as the most general solution for the stiffness matrix of a two node BEF element. If the mathematics can handle complex numbers, $[S]$ of Eqn (5.1-23) can be used, with all terms real for $n > 1$.

Semi-infinite BEF element. When the length of the element, L , is large, αL and βL are large constants, and the effect of the trigonometric and hyperbolic functions of Eqn (5.1-23) on the result is marginal. Therefore, the beam element can be considered to consist of two semi-infinite ends. The expressions S_{11} , S_{21} , and S_{22} of Eqn (5.1-23) result in $[S]$ of Eqn (3.2-16).

ii) $n > 1$

The real value stiffness matrix for the case $n > 1$ is now determined from the known solution of Eqn (5.1-23). In this case, the axial load is clearly tensile (in the mathematical sense), and β is complex. When denoting a new real value variable, β_t , shown in Eqn (5.1-24), and seen that $\beta = i\alpha\beta_t$, it is known in mathematics that $\sin(i\beta) = i\sinh(\beta)$ and $\cos(i\beta) = \cosh(\beta)$. The real value stiffness matrix $[S_t]$ of a tensioned beam element on an elastic foundation is given explicitly by

$$[S_t] = \frac{EI}{\Delta} \begin{bmatrix} 4\lambda^2\alpha(SHCH + \frac{\alpha}{\beta_t}shch) & S_{21} & S_{31} & S_{41} \\ -2\lambda^2(SH^2 + \frac{\alpha^2}{\beta_t^2}sh^2) & 2\alpha(SHCH - \frac{\alpha}{\beta_t}shch) & S_{32} & S_{42} \\ -4\lambda^2\alpha(SHch + \frac{\alpha}{\beta_t}CHsh) & -S_{41} & S_{11} & S_{43} \\ -4\lambda^2\frac{\alpha}{\beta_t}SHsh & 2\alpha(SHch - \frac{\alpha}{\beta_t}CHsh) & -S_{21} & S_{22} \end{bmatrix},$$

$$\Delta = SH^2 - \frac{\alpha^2}{\beta_t^2}sh^2, \quad \alpha = \lambda\sqrt{1+n}, \quad \beta_t = \lambda\sqrt{n-1}, \quad n > 1,$$

$$\begin{aligned} SH &= \sinh(\alpha L), \quad CH = \cosh(\alpha L), \\ sh &= \sinh(\beta_t L), \quad ch = \cosh(\beta_t L). \end{aligned} \quad (5.1-24)$$

In Eqn (5.1-24), $2\lambda^2$ is equal to $\alpha^2 - \beta_t^2$, ($2\lambda^2 = \alpha^2 + i^2\beta_t^2$). The remaining definitions of Eqn (3.2-5) apply. Each term S_{ij} , which is not given explicitly, relates to the corresponding term of $[S_t]$. The real value functions of the deflection of Eqn (5.1-13), and the slope of deflection of Eqn (5.1-14), the bending moment of Eqn (5.1-18), and the shear forces of Eqns (5.1-19) and (5.1-20) can be derived in explicit form, when $[H(x)]$ of Eqn (5.1-3) and $[G]$ of (5.1-12) are applied, taking into account the complex character of $i\alpha\beta_t$ in the expressions of β .

5.2 Application of BEF theory to analysis of a plate strip of finite length

The validity of the BEF approach used in the analysis of plates of finite length, L , was tested by analysing the plate model of Section 4.1, in Chapter 4, when node lines at varying distances $x = L$ were fully restrained. The plate was either simply supported or fully fixed along the longitudinal edge lines, when the unit lateral line load at the end $x = 0$ was applied. The fully-fixed plate was also analysed with unit edge moment line loading. The effect of in-plane loading was not studied.

Both the original element mesh (40 elements in the x -direction) and a finer mesh of 60 elements in the x -direction (and more biased towards the origin) were used. As in Section 4.1, the FE analysis was based on the following input data in all the shell element models: Poisson's ratio of $\nu = 0$, width $B = 200$ mm, thickness $h = 2$ mm, and a value for K of 140 000 Nmm.

In order to test the accuracy of the BEF model, the deflection, or the slope of deflection, the bending moment and the support reaction at $x = 0$, and the bending moment, $x = L$, were calculated, based on Eqn (5.1-23) and compared with the results of the FEA.

Results of BEF model for lateral line loading

Since $n = n_{lin} < 1$ Eqn (5.1-23) is used in the BEF analysis. The deflection at the location of the point load application, $x = 0$, and bending moments at $x = 0$ and at the other end $x = L$, are obtainable from the first column of $[S]$ in Eqn (5.1-23), since $U_2 = U_3 = U_4 = 0$. The deflection, U_1 , at $x = 0$ with a point load, V_0 , at $x = 0$ is the product of two factors: the deflection $U_{1,\infty}$ of a semi-infinite BEF of Eqn (3.2-16), and the finite length factor $u_1(\lambda L)$ of deflection resulting from U_1 , given by

$$U_1 = U_{1,\infty} u_1(\lambda L) , \quad (5.2-1)$$

where

$$U_{1,\infty} = \frac{V_0}{4EI} \frac{1}{\lambda^2 \alpha} , \quad u_1(\lambda L) = \frac{SH^2 - \frac{\alpha^2}{\beta^2} s^2}{SHCH + \frac{\alpha}{\beta} sc} . \quad (5.2-2)$$

Similarly, the reaction bending moment, M_1 , at $x = 0$ is given by

$$M_1 = M_{1,\infty} m_1(\lambda L) , \quad (5.2-3)$$

where

$$M_{1,\infty} = -V_0 \frac{1}{2\alpha} , \quad m_1(\lambda L) = \frac{SH^2 + \frac{\alpha^2}{\beta^2} s^2}{SHCH + \frac{\alpha}{\beta} sc} . \quad (5.2-4)$$

The reaction bending moment, M_2 , at $x = L$ is

$$M_2 = M_{1,\infty} m_{2,1}(\lambda L) , \quad (5.2-5)$$

where

$$m_{2,1}(\lambda L) = 2 \frac{\alpha}{\beta} \frac{SH s}{SH CH + \frac{\alpha}{\beta} s c} \quad (5.2-6)$$

corresponds to the finite length factor of the bending moment at $x = L$, resulting from V_0 of the symmetric line loading at $x = 0$.

Results of BEF model under constant edge moment loading

Under edge moment loading, M_0 , the boundary conditions are $U_1 = U_3 = U_4 = 0$. From the second column of Eqn (5.1-23), the slope of deflection U_2 , $x = 0$, under M_0 is the product of the slope of deflection, $U_{2,\infty}$, of a semi-infinite BEF, Eqn (3.2-16), and the finite length factor of rotation, $r_2(\lambda L)$, resulting from U_2 , given by

$$U_2 = U_{2,\infty} r_2(\lambda L) , \quad (5.2-7)$$

where

$$U_{2,\infty} = \frac{M_0}{2EI} \frac{1}{\alpha} , \quad r_2(\lambda L) = \frac{SH^2 - \frac{\alpha^2}{\beta^2} s^2}{SH CH - \frac{\alpha}{\beta} s c} . \quad (5.2-8)$$

The reaction bending moment, M_2 , at $x = L$, which is the product of the applied loading, M_0 , and the relative factor, $m_{2,2}(\lambda L)$, is given by

$$M_2 = M_0 m_{2,2}(\lambda L) , \quad m_{2,2}(\lambda L) = \frac{\frac{\alpha}{\beta} CH s - SH c}{SH CH - \frac{\alpha}{\beta} s c} . \quad (5.2-9)$$

The reaction force, V_1 , at $x = 0$ is

$$V_1 = V_{1,\infty} v_1(\lambda L) , \quad (5.2-10)$$

where

$$V_{1,\infty} = -M_0 \frac{\lambda^2}{\alpha} , \quad v_1(\lambda L) = \frac{SH^2 + \frac{\alpha^2}{\beta^2} s^2}{SH CH - \frac{\alpha}{\beta} s c} . \quad (5.2-11)$$

Comparison of BEF model and shell element FEA results

Results of the comparison are shown in Figs 5.2-1, 5.2-2, 5.2-3 and 5.3-1; the curves based on the BEF model are shown as solid lines, and the results of the shell element runs are shown by dotted lines and symbols. The functions $u_1(\lambda L)$, $m_1(\lambda L)$ and $m_{2,1}(\lambda L)$ for unit lateral line loading, and $u_2(\lambda L)$, $m_{2,2}(\lambda L)$ and the inverse value of $v_1(\lambda L)$ for unit edge moment loading are shown as a function of the normalised length, λL , of the plate. In the BEF models, the characteristic lengths used were $1.5B/\pi$ for the simply-supported plate, and B/π for the fixed plate. The normalised second order parameters used were $n = 0.71$ and $1/\pi$, respectively.

Figure 5.2-1 shows the results for the fixed plate with unit edge moment loading. The $1/v_1(\lambda L)$ of Eqn (5.2-11). values of the shell FEA are determined manually from the axial and shear stress output data by using Eqn (2.1-5). This is not very accurate, as can be seen from the shape of the curve.

Figure 5.2-2 shows the results of a comparison of the simply-supported plate under unit lateral line loading. For the fixed plate, theoretical curves together with the shell FEA results are constructed in Fig. 5.2-3.

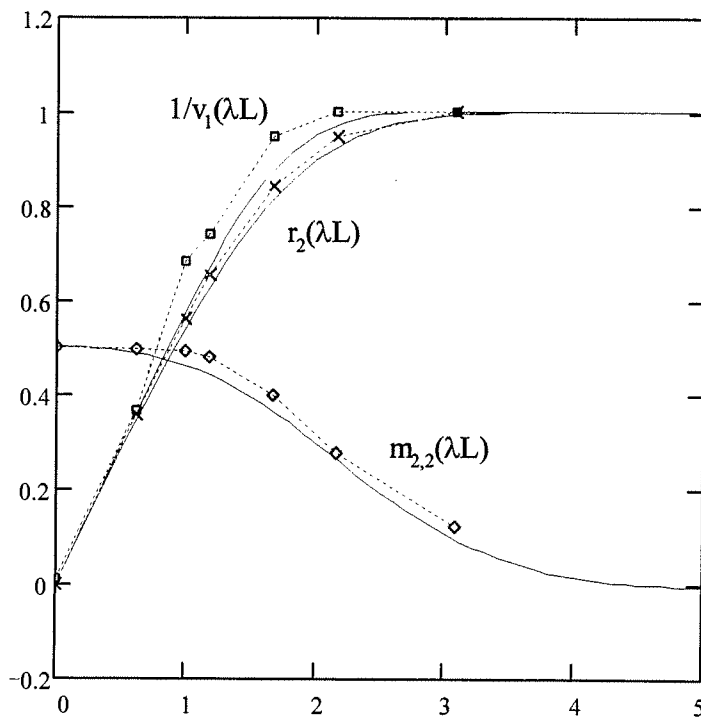


Figure 5.2-1 Fixed plate: finite length factors of the inverse of the reaction force, $1/v_1(\lambda L)$, rotation, $r_2(\lambda L)$, and bending moment at $x = L$, $m_{2,2}(\lambda L)$, under edge moment loading, as a function of λL .

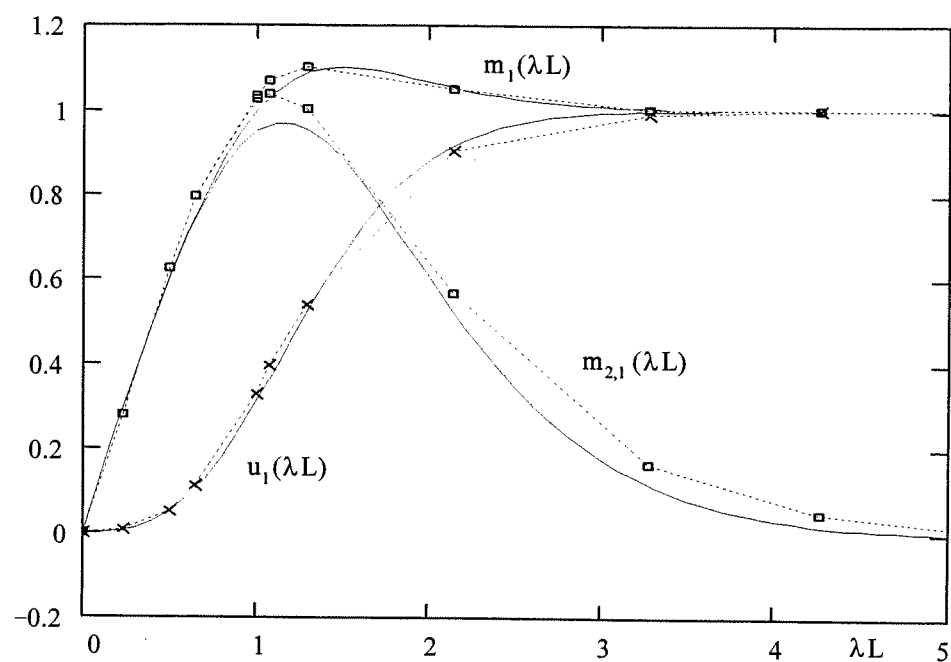


Figure 5.2-2 Simply-supported plate: finite length factors of deflection, $u_1(\lambda L)$, bending moments at $x = 0$, $m_1(\lambda L)$, and $x = L$, $m_{2,1}(\lambda L)$, under lateral line loading, as a function of λL .

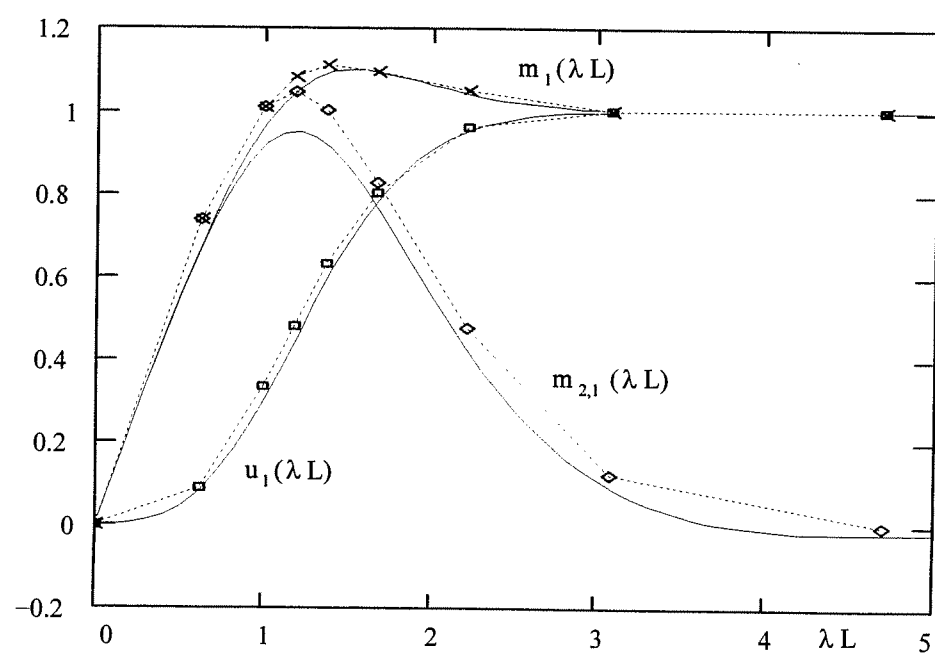


Figure 5.2-3 Fixed plate: finite length factors of deflection, $u_1(\lambda L)$, bending moments at $x = 0$, $m_1(\lambda L)$, and $x = L$, $m_{2,1}(\lambda L)$, under lateral line loading, as a function of λL .

5.3 Discussion

The behaviour of the centre-line section of a rectangular plate fixed at the end $x = L$ was shown to be described by a plate strip model using the BEF theory. The deflection and slope of deflection functions of Figs 5.2-1, 5.2-2 and 5.2-3 show only marginal deviations over the whole range of λL , compared with the FEA results.

It is often essential to know the bending moment at the load application point accurately. In order to test its sensitivity, the results of the shell element FEA and $m_1(\lambda L)$ as a function of λL are plotted in Fig. 5.3-1, see also Figures 5.2.2 and 5.2.3. Three theoretical curves for the tension side are shown as continuous lines: $n_x = 0$, $1/\pi$ (equal to n_{in} of fixed plate) and 1.5 , together with the FEA results, $n_x = n_{in}$, of the simply-support (dotted line and \diamond) and fixed plates (dotted line and $+$) cases. $m_1(\lambda L)$ is fairly insensitive to the type of restraint at the longitudinal edges. The influence of the second order parameter, n_x , in the functions shown is marginal, compared with its significance in the reference semi-infinite case. The effect of λL and transverse in-plane loading was not studied.

The results of Chapter 4 and 5 have shown that the effects of various types of intermediate support in plate structures can be analysed by modelling a one dimensional continuous beam structure composed of BEF elements given by Eqns (5.1-23) and (5.1-24).

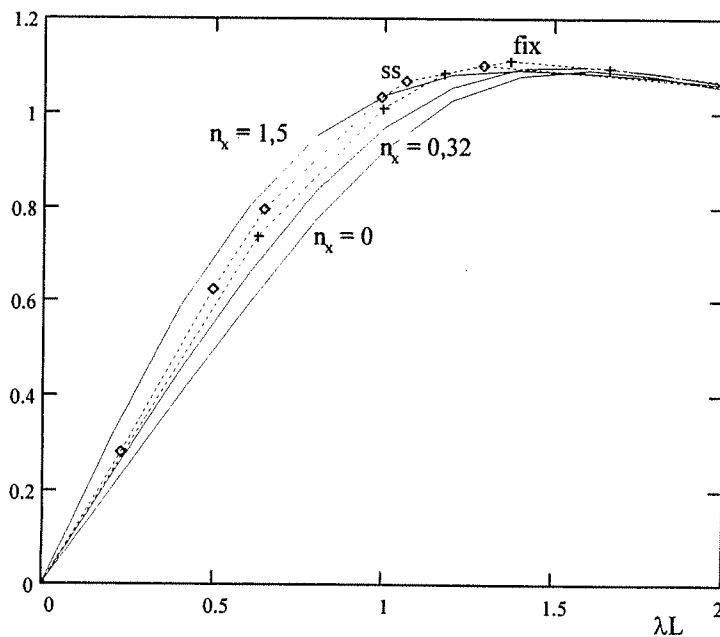


Figure 5.3-1 Comparison of simply-supported and fixed plates: finite length factors of bending moments at $x = 0$, $m_1(\lambda L)$ under lateral line loading, as a function of λL .

Chapter 6

CASE STUDY: EXPERIMENTAL VERIFICATION OF APPLICATION OF BEF THEORY TO ANALYSIS OF STIFFENED PLATE

The BEF models developed in this study are applied to the analysis of a continuous stiffened plate structure containing misalignments, as a demonstration of the method. The experimental test panel was loaded in a test rig, Section 6.2. The panel is also modelled and analysed using shell element FEA, Section 6.3, and the BEF-model of this study, Section 6.4. A summary and a discussion of the data from experimental strain gauge readings, results of FEA, and BEF-models are given in Section 6.5.

6.1 Introduction

An experimental test case study was designed to illustrate the applicability of the BEF method and to verify the accuracy of calculations based on it. A transverse butt joint in a longitudinally-stiffened plate panel was chosen for the case study, containing: i) a natural offset misalignment which resulted from a thickness change; and ii) artificially-introduced angular and offset misalignments. Experimental tests designed to compare measured structural strains with calculated structural stresses were conducted in the Laboratory of Steel Structures of Lappeenranta University of Technology. For comparison, stresses were calculated based on FEA using shell elements and the semi-infinite BEF theory application model of this study.

6.2 Experimental tests

6.2.1 Shape of the panel

The test panel was made of structural steel S355 of nominal yield stress 355 MPa, manufactured by Rautaruukki, Finland. The stiffened plate, length 2 000 mm and width 900 mm, is shown in the 5 MN test rig in Fig. 6.2-1. The panel was strained using a T-shaped groove/shoulder connection at the ends. A drawing of the panel can be found in Appendix 6.2-1. Four longitudinal stiffeners were welded to the top, deck plate, dividing it into three even stiffener spacings of 300 mm: i) longitudinal edge stiffeners of square hollow sections (SHS) 100 x 100 x 3 mm to introduce rotation stiffness at the edge line and thus simulating a part of a continuous plate field; ii) two intermediate flat bar stiffeners of dimensions 10 x 120 mm. The bottom surface of the deck plate, of thicknesses, 5 and 10 mm, was aligned with the upper side of the flat bar stiffeners. The thickness change introduced a natural offset misalignment. The plate

sections were first tack welded together. Subsequently, the stiffeners were welded to the deck plate by intermittent welding. Shrinkage of the butt joint between the plate sections, caused by cooling of the fillet welds, was restrained by the tack welds. Thus a significant angular misalignment was induced in the butt joint of the deck plate.

Prior to testing the shape of the panel was measured by an instrumented movable displacement gauge: i) three longitudinal lines in the outer fields, one in the middle, with the others 20 mm distant from the stiffener surface; and ii) five lines in the centre field, one in the middle, two 65 mm distant from the centre-line, and two 20 mm distant from the stiffener face.

The depth of the natural offset misalignment, 2.5 mm, was 50% of the thickness change, i.e. $(10 - 5)/2$ mm. An additional offset misalignment of 0.3 mm was measured at the centre-line of the panel, which resulted from fabrication tolerances. A short, more localized pit of depth 0.5 mm and length 50 mm could also be observed from the displacement gauge reading. The pit was located on the side of the thicker plate section. An initial deflected shape of 2 mm was measured, caused by weld cooling, equivalent to an average roof top angle of angular misalignment of $2\phi_0 = 4/300$ rad. The depth of the angular misalignment was constant in each of the five measuring lines of the centre field. Fig. 6.2-2 shows the result of the initial shape along the centre-line of the panel measured on the bottom (stiffener) surface of the deck plate.

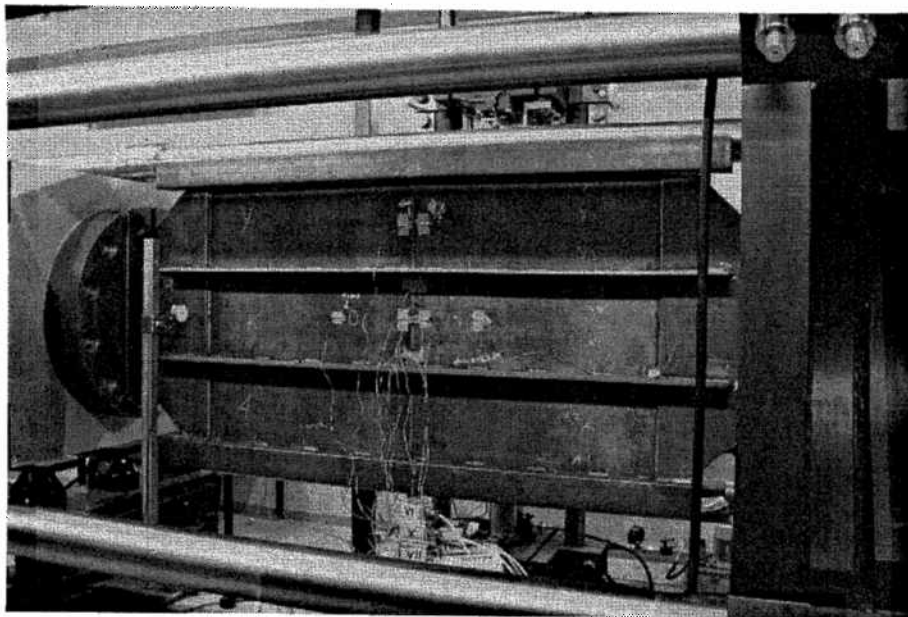


Figure 6.2-1 Test panel in test rig.

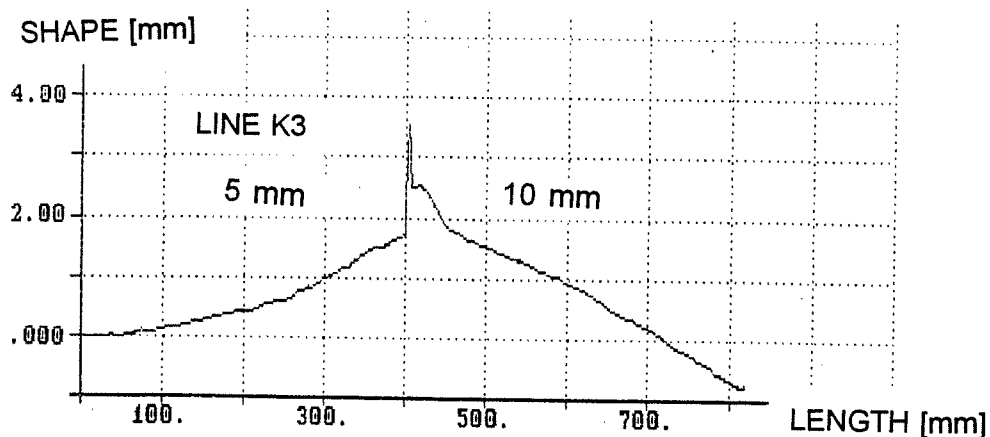


Figure 6.2-2 True shape of the panel bottom surface along the centre-line.

6.2.2 Instrumentation and strain gauge measurements

Strain gauges were attached along the centre-line of the panel, at the stiffener line, and at a distance of 15 mm from the stiffener line. The locations of the strain gauges are shown in Appendix 6.2-2. A rosette gauge was placed on the stiffener line on the outside face, 5 mm from the weld toe. Transverse strains were measured at one location near the stiffener. Two strain gauges at the hot spot locations were placed at distances 3.5 mm and 3.5 + 4 mm from the weld toe. Since the plate thickness, h , is small (5 mm), the strain gauges could not be located close enough to the weld toe, in order to comply with the International Institute of Welding recommendations of $0.4h$ and $1.0h$ (Niemi, 1995). After mounting and welding, the normals to the contacting surfaces of the T shoulders were in line, but not aligned with the plate surface, thus inducing out-of-plane bending moments at the ends of the panel. Therefore, the nominal axial membrane strain was measured using the readings of the gauges outside the joint, gauges 6A and 6C. Uniaxial stress is often assumed in order to transform the measured strains to stresses. This was the case in this example, such that $\sigma = E\epsilon$.

Experimental tests were performed in two stages, since the capacity of the recording PC program was limited to 15 channels. In the first run, the strains at the centre-line of the panel were recorded. The remainder were recorded in the second run. The axial force and displacement of the cylinder actuator were also recorded during the two test runs. Out-of-plane deflections were measured at two locations. The cylinder force was increased stepwise in both runs: 0 → 500 kN → 0 → 1 MN → 0 → 1.5 MN → 0 → 2 MN → 0. During testing, data from each channel were recorded once every second. A

selection of results are presented in Appendix 6.2-3. The maximum applied membrane stress loading, σ_m , was 320 MPa. The maximum structural stress range was 590 MPa when the panel was loaded under pure pulsating tension varying between 0 and 2 MN. The local stress behaviour of the steel S355 was linear elastic.

6.3 FEA models and results

6.3.1 FE models

The test panel presented in Section 6.2, containing misalignments, was modelled using linear shell elements and analysed as geometric linear runs, using the Cosmos/M program (1996). Two types of models were analysed: i) a theoretically straight model; and ii) a model containing angular misalignment based on experimental measurements. The panel modelled in the ideal straight condition was also analysed using solid elements for comparison of FEA techniques. The results of the shell analysis are presented in this study. Accurate results at and very close to the stiffener lines can only be obtained by modelling the local geometry of the joint at the stiffener line by solid element FEA. Detailed stress analysis of the stiffener line is beyond the scope of this study.

Because of symmetry, half of the panel was modelled using approximately 1200 nodes and linear thin shell elements. A value of 210 GPa was used as the Young's modulus for steel and 0.3 for the Poisson's ratio. The edge SHS stiffeners were modelled as beam elements. The fillet welds of the stiffeners were not modelled. The offset misalignment was modelled by a vertical thin shell element of very large flexural rigidity, see Figs. 6.3-1 and 6.3-2. Under far-field pure tension loading of the thinner plate, σ_m , equal to 1.08 MPa the membrane stress in the cross-section of the joint region of the thinner plate varied in the width direction from 1.0 MPa to 1.1 MPa. The membrane stress in the centre-line of the thinner plate at the joint area $x = 0$ of the nominally straight FE model was 1.02 MPa, and 1.0 MPa in the plate containing misalignments, which represented the reference membrane stress, $\sigma_{m,d}$.

6.3.2 Results of shell element FEA

Figure 6.3-1 shows the panel in the deformed condition, together with the co-ordinate system. The undeformed initial shape of the model (neutral axis surface) along the centre-line cross-section, which included the misalignments, is also shown schematically on the left-hand side. Figure 6.3-2 shows three XY-plots of the structural stress extrapolation under $\sigma_m = 1.08$ MPa membrane loading of the initially straight model: i) at the centre-line; ii) at the maximum stress line, $y = 15$ mm from the stiffener line; and iii) at the stiffener line. The plots are shown in the x-axis direction up to distances of 200 mm, 44 mm and 20 mm, respectively.

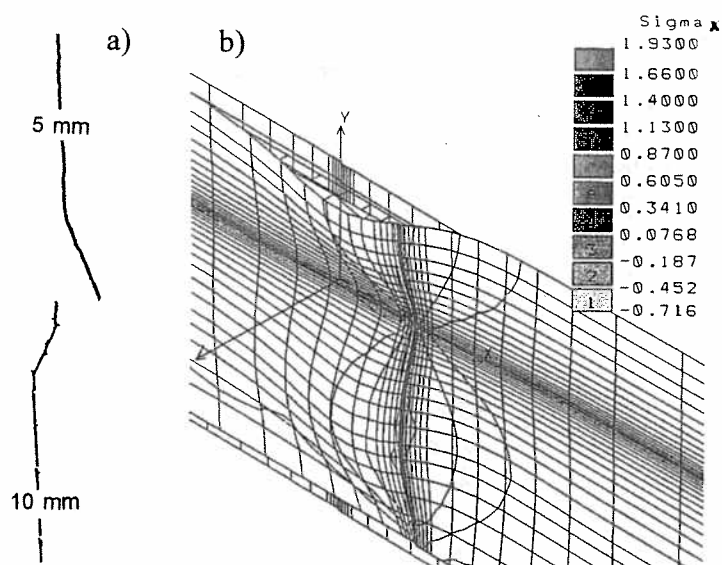


Figure 6.3-1 Thin shell FE model: a) deformed initial shape of the centre-line cross-section ; and b) deformed shape of the FE model under axial loading.

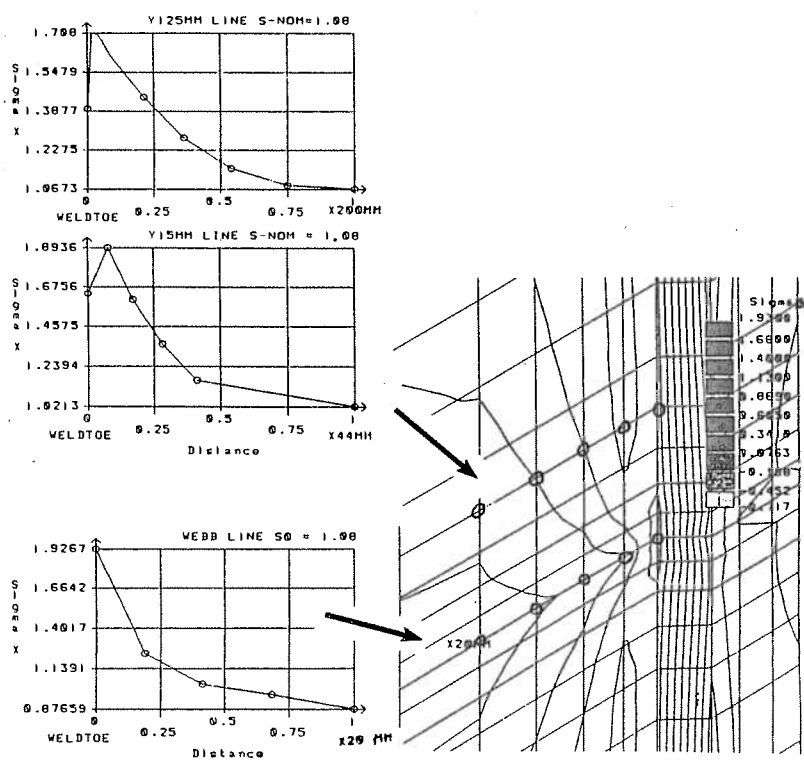


Figure 6.3-2 Surface stress in the 5 mm plate of the initially straight thin shell model.

Table 6.3-1 shows a selection of the results of experimental measurements and FEA based on the element results. Four cases of interest are considered: i) the membrane stress distribution; ii) the centre-line location; iii) the maximum stress line $y = 15$ mm (parallel to the stiffener line but 15 mm distant); and iv) the stiffener line. In cases ii) - iv), extrapolated structural stresses at the weld toe, σ_s , are considered. In addition to the nominal stress, the membrane stress value along the centre-line at the weld toe area, $\sigma_{m,cl}$, is given. The structural stress concentration factor, K_s , is obtained as the ratio of σ_s divided by the nominal membrane stress, σ_m , i.e. $K_s = \sigma_s / \sigma_m$. Since the axial membrane stress in the transverse y direction of the location of interest, y , differs from the far-field nominal value, σ_m , the contribution of the bending stress in the structural stress concentration, $K_b = \sigma_b / \sigma_{m,cl}$, for the centre-line is also shown. In the last row of each block the gradient of the bending stress concentration in the longitudinal direction, $\Delta K_b / \Delta x$, unit [1/mm], is given. The locations of linear extrapolation points are given in the header line of each block, e.g. as the distances of $2h \rightarrow h$. Three columns are shown: a) stress-based results for the nominally straight shape plus additional stresses caused by the real shape containing offset misalignment plus additional stress resulting from angular misalignment; b) two values for the experimental test results (biaxiality correction factor 1.05 included, based on FEA runs - and direct uniaxial strain gauge reading based values comparable with strain-based FEA results); c) strain-based FEA data comparable with the experimental measurements without taking into account the stress-biaxiality.

Table 6.3-1 Summary of linear shell element FEA, $\nu = 0.3$, and test results.

	a) Stress based FEA Straight + misal.	b) Experimental Biaxial - uniaxial	c) Strain based FEA Straight + misal.
i) Membrane			
σ_m	1.08	1.05 - 1.05	1.08
$\sigma_{m,cl}$	1.02 / 1.0	1.00 - 1.00	1.0
ii) Centre-line			
σ_s	1.77 + 0.08 + 0.15	2.04 - 1.92	1.69 + 0.08 + 0.15
K_s	1.64 + 0.08 + 0.14	1.94 - 1.84	1.57 + 0.08 + 0.14
K_b	1.77 + 0.08 + 0.15	2.04 - 1.92	1.69 + 0.08 + 0.15
$\Delta K_b / \Delta x$	0.6/100	1.6/100	-
iii) 15 mm from stiffener	$2h \rightarrow h$	$1.4h \rightarrow 0.7h$	$2h \rightarrow h$
σ_s	2.20	-	2.08
K_s	2.04	1.75 - 1.68	1.94
$\Delta K_b / \Delta x$	8.5/100	4.8/100	7.8/100
iv) Stiffener line	$2h \rightarrow h$		$2h \rightarrow h$
σ_s	1.93	1.3 + 0.25	2.25
K_s	1.79	-	2.10
$\Delta K_b / \Delta x$	16/100	-	12.5/100

According to FEA and the biaxial stress state, the bending stress concentration factor resulting from offset and angular misalignments at the centre-line is 2.00. It correlates well with the experimentally-observed uniaxial value of 1.92 whereas 2.04 is the value with the biaxiality correction included. Without the angular misalignment, the bending stress concentration factor was determined by FEA to be 1.77 ± 0.08 . In the FE model the effect of the extra offset misalignment from the manufacturing tolerances of 0.3 mm resulted in a normalised bending stress of 0.08. Thus, an angular misalignment of 2 mm in the depth produced a change of 0.15 in the stress concentration. In the experimental measurements the stress gradient at the stiffener line was not clear: the value of 1.3 corresponds with the measured value of strain gauge 7A, 0.25 is the extra stress based on the measured gradient. Based on the the stress gradient obtained by thin shell FEA the extra stress is 0.7.

6.4 Two parameter BEF models and results

The test panel shown in Section 6.2 was also modelled and analysed using two parameter, unit width BEF semi-infinite FE elements, described in Section 3.2. Both linear and geometrically non-linear BEF analyses were performed for two extremes of rotation stiffness at the stiffener lines: simply supported (ss) and fixed (fix) to show the sensitivity of the accuracy to assumptions related to the boundary conditions, in general. The test panel, being continuous in the width direction, was very close to a fixed plate resulting in the geometric linear analysis in slightly lower structural stresses than if only a single simply-supported plate section would have been tested. A theoretically straight model resulted in an equivalent point couple of a unit width plate strip resulting from the thickness change. The angular misalignment caused by shrinkage of the transverse butt weld, based on experimental measurements, was modelled as a point load of a unit width plate strip, see Chapter 1.

Based on the model of Section 4.6, Eqn (4.6-9), the characteristic lengths of the thinner plate, 5 mm, and the thicker plate, 10 mm, of width B of 300 mm were shown in this study to be in general equal, having a value of $1/\lambda = 1.5 \times 300/\pi = 143$ mm for the simply-supported case, according to Eqn (4.6-9). Similarly, for the continuous deck plate of the test panel, assuming fixed boundary conditions, the characteristic length is $300/\pi = 95.5$ mm. The second order parameter, n_{in} , according to Eqn (4.6-11), was $1/\pi$ and 0.71 for the fixed and simply-supported cases, respectively. To calculate the factor n under maximum axial membrane loading, the critical buckling stress of the denominator was the elastic buckling stress of the thinner plate. Detailed analysis of the non-linear analysis is shown in Section 6.4.2.

The element stiffness matrices $[S_1]$ and $[S_2]$ of the semi-infinite BEF elements 1 and 2 of thicknesses h and $2h$, respectively, can be derived for the global co-ordinate system from Eqn (3.2-16). The global stiffness matrix $[S_g]$ is therefore obtained by

$$[S_1] = 2EI_1 \begin{bmatrix} 2\lambda^2\alpha_1 & \lambda^2 \\ \lambda^2 & \alpha_1 \end{bmatrix}, \quad [S_2] = 2EI_1 \begin{bmatrix} 16\lambda^2\alpha_2 & -8\lambda^2 \\ -8\lambda^2 & 8\alpha_2 \end{bmatrix}, \quad (6.4-1)$$

$$[S_g] = [S_1] + [S_2].$$

The global equation of the force balance can be written as

$$\{F_g\} = [S_g] \{U\}, \quad (6.4-2)$$

$$\{F_g\} = \begin{Bmatrix} F_0 \\ M_0 \end{Bmatrix} = 2EI_1 \begin{bmatrix} 2\lambda^2\alpha & -7\lambda^2 \\ -7\lambda^2 & \alpha \end{bmatrix} \begin{Bmatrix} U_1 \\ U_2 \end{Bmatrix}, \quad \alpha = \alpha_1 + 2^3\alpha_2.$$

The external load vector $\{F_g\}$ consists of the transverse load, F_0 , and the point couple, M_0 , as the product of the membrane force, $h\sigma_{m,cl}$, and the misalignment. The transverse load, F_0 , resulted from the initial angular misalignment of $2\varphi_0 = 4/300$ rad, and the point couple, M_0 , resulted from the natural offset misalignment of 2.5 mm and 0.3 mm caused by mounting tolerances, see Eqn (6.4-3). The influence of the lateral pressure in F_0 caused by the initial curvature was taken into account approximately by using the averaged apex angle instead of a local one. The load vector is written as

$$\begin{Bmatrix} F_0/\lambda \\ M_0 \end{Bmatrix} = 5\sigma_{m,cl} \begin{Bmatrix} (143 \dots 95) \times 4/300 \\ 2.5 + 0.3 \end{Bmatrix} = \sigma_{m,cl} \begin{Bmatrix} (9.5 \dots 6.3) \\ 12.5 + 1.5 \end{Bmatrix}. \quad (6.4-3)$$

The numbers on the left of F_0/λ , and those used generally in this section, 143 and 9.5, relate to the simply-supported boundary condition. The numbers on the right, 95 and 6.3, refer to the fixed condition.

When inverting the global stiffness matrix, the deflection vector $\{U\}$ is obtained. The internal forces $\{F_i\}$ of the thinner plate (1) are the product of the two-parameter $[S_1]$ and the deflection vector $\{U\}$ solved from Eqn (6.4-2). $\{F_i\}$ can be obtained by

$$\{F_i\} = \begin{Bmatrix} F_1 \\ M_1 \end{Bmatrix} = \begin{bmatrix} 4\lambda^2\alpha_1 & 2\lambda^2 \\ 2\lambda^2 & 2\alpha_1 \end{bmatrix} \frac{1}{4\lambda^2\alpha^2 - 98\lambda^4} \begin{bmatrix} \alpha & 7\lambda^2 \\ 7\lambda^2 & 2\lambda^2\alpha \end{bmatrix} \begin{Bmatrix} F_0 \\ M_0 \end{Bmatrix}. \quad (6.4-4)$$

6.4.1 Geometric linear analysis model and results

Fixed, continuous plate. In the linear elastic case, by using in Eqn (6.4-2), $n_{lin} = 1/\pi$ and $\alpha_1 = \alpha_2 = \alpha_{lin} = \sqrt{(1 + 1/\pi)}\lambda = 1.15\lambda$, the displacements are solved from

$$\begin{Bmatrix} F_0 \\ M_0 \end{Bmatrix} = 2EI_1 \begin{bmatrix} 20.7\lambda^3 & -7\lambda^2 \\ -7\lambda^2 & 10.35\lambda \end{bmatrix} \begin{Bmatrix} U_1 \\ U_2 \end{Bmatrix}, \quad (6.4-5)$$

resulting, using Eqn (6.4-4), in the bending moment, M_1 , of the thinner plate,:

$$M_1 = [0.111K_v, \quad 0.187] \begin{Bmatrix} F_0/\lambda \\ M_0 \end{Bmatrix}. \quad (6.4-6)$$

The effect of stress biaxiality under line loading is taken into account by the factor of stress biaxiality, K_v , as presented in Sections 4.5.1 and 4.6.1, Eqn (4.6-12). The normalised bending stress of the thinner plate, $\sigma_b / \sigma_{m,cl}$, resulting from the shell bending moment, M_1 , gives

$$\frac{\sigma_b}{\sigma_{m,cl}} = 0.24 [0.111K_v, \quad 0.187] \begin{Bmatrix} 6.3 \\ 12.5 + 1.5 \end{Bmatrix}, \quad \sigma_B = M_1 \frac{6}{h_1^2}. \quad (6.4-7)$$

Based on $\nu = 0.3$, resulting in $K_v = 1.24$, the bending stress concentration factors, K_b , at the centre-line of the plate at the joint, are

$$K_b = 1 + \frac{\sigma_b}{\sigma_{m,cl}} = 1 + 0.17K_v + 0.56 + 0.07 : \quad (6.4-8)$$

$$K_b = 1.80, \nu = 0; \quad K_b = 1.84, \nu = 0.3.$$

Simply-supported plate. Based on the parameters: $n_{in} = 0.711$, $\alpha_1 = \alpha_2 = 1.31\lambda$, $K_v = 1.3$ for $\nu = 0.3$, the bending stress concentration factors, K_b , are

$$K_b = 1 + 0.21K_v + 0.50 + 0.06 : \quad (6.4-9)$$

$$K_b = 1.77, \nu = 0; \quad K_b = 1.83, \nu = 0.3.$$

6.4.2 Geometric non-linear analysis results

The effect of the geometric non-linearity of the maximum measured nominal membrane stress in the thinner plate, $\sigma_m = 320$ MPa, caused by the axial loading of 2 MN is considered in this section. For the boundary condition where parallel sides are fixed, the critical buckling stress of the thinner plate, 1, is 370 MPa, and for the thicker plate, 2, is 1500 MPa. For the simply-supported case, the stresses are 210 and 840 MPa, respectively. Based on Eqn (4.5-4) with $N_y = 0$ the factors α_1/λ and α_2/λ for the fixed

case are therefore

$$\frac{\alpha_1}{\lambda} = \sqrt{1 + 1/\pi} \sqrt{1 + \frac{320}{370}} = 1.57, \quad \frac{\alpha_2}{\lambda} = \sqrt{1 + 1/\pi} \sqrt{1 + \frac{1}{4} \frac{320}{370}} = 1.27. \quad (6.4-10)$$

For the simply-supported case when $n_{lin} = 0.71$ the corresponding ratios are: $\alpha_1/\lambda = 2.08$ and $\alpha_2/\lambda = 1.54$. The stress results of the fixed and simply-supported cases are presented below.

Continuous structure, fixed. The normalised bending stress, $\sigma_b/\sigma_{m,cl}$, of the thinner plate, similar to Eqn (6.4-7), is given by

$$\frac{\sigma_b}{\sigma_{m,cl}} = 0.24 [0.10K_v, \quad 0.193] \left\{ \frac{6.3}{12.5 + 1.5} \right\}. \quad (6.4-11)$$

The bending stress concentration factor, K_b , at the centre-line of the joint, taking into account the geometric non-linearity, is

$$\begin{aligned} K_b &= 1 + 0.15K_v + (0.58 + 0.07) : \\ K_b &= 1.80, \quad v = 0; \quad K_b = 1.84, \quad v = 0.3. \end{aligned} \quad (6.4-12)$$

Simply-supported plate. K_b results in

$$\begin{aligned} K_b &= 1 + 0.18K_v + (0.55 + 0.07) : \\ K_b &= 1.80, \quad v = 0; \quad K_b = 1.88, \quad v = 0.3. \end{aligned} \quad (6.4-13)$$

6.5 Summary of results and discussion

Table 6.5-1 shows a summary of the results of Sections 6.3 - 6.4 obtained i) experimentally; ii) using the BEF theory application of this study; and iii) using geometric linear FEA with linear shell elements in Cosmos/M. The bending stress concentration factor, K_b , is used as the value for comparison when true biaxial behaviour, $v = 0.3$, is considered. Two types of calculation model are compared: i) a theoretically straight model; and ii) a model containing angular misalignment based on experimental measurements. The results of both geometric linear and non-linear BEF models are shown (lin/gnl).

Table 6.5-1 Summary of K_b results, $\nu = 0.3$, stress-based comparison.

Method	Centre-line area, lin/gnl	15 mm line from stiffener	Stiffener line
Experimental	2.04/2.04	≈ 1.8	≈ 1.8
BEF model: lin/gnl			
As manufactured, fix	1.84/1.84	-	-
(As manufactured, ss)	(1.83/1.88)	-	-
Ideal straight, fix	1.56/1.58	-	-
Thin shell analysis: lin			
As manufactured	2.00	≈ 2.0	≈ 1.8
Ideal straight	1.75	≈ 2.0	≈ 1.8

6.5.1 Comparison of BEF and FE analysis with experimental measurements

Centre-line section

Based on uniaxial strain, $\nu = 0$ and geometric linear BEF analysis, a comparison of fixed-plate boundary conditions $K_b = 1.80$ in Eqn (6.4-8), shows the two-parameter geometric linear BEF model to be close to the experimentally-observed K_b factor of 1.92, Table 6.3-1. When the stress biaxiality, $\nu = 0.3$, is taken into account, the experimentally-observed K_b factor is 2.04, compared with 1.84 from the BEF model (the effect of biaxiality is based on FEA results being 5% higher than those based on uniaxial strain measurements, Table 6.3-1). Thus the two-parameter geometric linear BEF model in the case studied correlates relatively well with the experimentally-observed behaviour. It can also be seen that offset misalignment dominates in the stress concentration, being ≈ 0.6 compared with ≈ 0.2 for angular misalignment, Table 6.3-1. The angular misalignment is considerably smaller in joints of standard manufacturing quality than that in the test specimen. Therefore, in a joint of good quality but containing a natural offset misalignment, resulting from a thickness change from h to $2h$, the K_b factor is still at least 1.6.

The normalised stress gradient at the centre-line of the panel is very low, about 0.6/100 1/mm. However, the experimentally-observed gradient, based on the strain readings of gauges 3A and 4, was more than twice that based on the FEA and BEF models. If the value of the weld toe line alone is needed, one strain gauge located at a position $0.4h$ gives a satisfactory result. The experimental test showed that the nominal stress level was achieved at a distance of 50 mm from the weld toe, gauges 3A and 4, Appendix 6.2-3. Based on FEA results, 50% of the bending stress should still exist at a distance of 50 mm. According to the BEF model, Figs 4.2-4 and 4.2-5, the bending stress resulting from the angular misalignment is about zero, but 40% of the bending stress caused by offset misalignment still exists. The strain reading of gauge 3B was

slightly higher than the strain of gauge 3A and was not considered in the study.

Maximum stress line and stiffener line

Based on experimental measurements and FEA, the stress concentration results did not change significantly along the weld toe line, Table 6.5-1. In the FE analysis, significant differences were observed at the maximum stress line, 15 mm from the stiffener, depending on the FEA element types and modelling techniques used. The normalised stress gradient at a distance 6 mm from the weld toe lies between 5/100 and 6/100, (in 1/mm), when determined either experimentally or by using FEA. The gradient is ten times larger than at the centre-line. The results of the stress gradient analysis show that the characteristic length of a BEF model for the maximum stress line or the stiffener line is much shorter than for the centre-line.

The stress gradient at the stiffener line was not determined experimentally. According to FEA, Fig. 6.3-2 and Table 6.3-1, the normalised stress gradient is at least 16/100 1/mm, being so large that the more distant strain gauge (gauge 10B: see Appendix 6.2-2) gives unreliable results, if conventional in-line strain gauges are used. At least two strain gauges are therefore required for accurate stress extrapolation at and close to the stiffener line. The rosette strain gauge at the stiffener line showed that no transverse stress existed in the weld line direction. The structural stress, calculated using a stress gradient of 16/100 1/mm, would be around 2.0. Thus, also the experimental results indicated that a fatigue crack could initiate anywhere along the weld toe line in a continuous plate. In a simply-supported plate only the centre-line area is critical.

The BEF model showed that the stress analysis of offset misalignments is not dependent on the characteristic lengths. The (one or two parameter) linear BEF model can be applied to the analysis of the bending stress caused by offset misalignment at the stiffener line and at the maximum stress line. Some FE formulation results for the characteristic lengths $1/\lambda$ are available (Partanen, Tarjauori, Niemi, 1992) particularly for calculating the deep stress gradient close to the stiffener lines. The results of this study, shown in Fig. 6.3-2 and Table 6.3-1, are in agreement with the earlier FE study, indicating that the characteristic length at the stiffener line is less than twice the plate (or flange) thickness.

Effect of strain gauge mounting tolerances

Strain gauge mounting instructions were used to determine the locations of the gauges, Appendix 6.2-2. The principle involved locating the strain gauges A and C at identical distances, measure a , but on opposite sides of the plate. However, the strain gauges were placed at distances of around 4 mm from the weld toe on each side, resulting in deviations in vertical alignment of between 2 - 3 mm in the longitudinal direction when

the locations were inspected afterwards. For the centre-line the stress gradient is so low that the effect of gauge location is not especially significant. The effect of the true locations is taken into account by using correction factors based on FEA when interpreting the experimental measurements.

Geometric non-linearity and behaviour in experimental testing

Under the maximum loading of 2 MN, the BEF models showed that the geometric non-linearity effect was low, marginal for this specific case: based on a uniaxial stress state, the K_b factor was around 1.80 and independent of the boundary conditions, fixed or simply supported. Centre-line K_b results from experimental tests, obtained by Appendix 6.2-3, indicated that the bending behaviour was linear. Under axial loading of the panel from 0 – 1 MN the surface strain range of gauges 3A (or 3B) was 1.42 mm/m, whereas from 1 – 2 MN the surface strain range was 1.39 mm/m, i.e. 98% of the former strain value. However, at the same time, the local membrane strain range (based on gauges 3A and 3C) was higher, ranging from 0.79 mm/m in the load range 0 – 1 MN, and 0.76 mm/m from 1 – 2 MN. Corresponding experimental strain-based values for K_b were 1.80 and 1.83 (1.92 in Table 6.3-1 is based on the maximum value 2 MN). An explanation for this behaviour is the surface at the end of the T shoulders in contact with the T groove of the rig. The location of surfaces in contact changed during the testing, causing a small change in the global bending moment of the panel.

6.5.2 Discussion of present design recommendations

The effect of offset misalignments can be taken into account when modelling the geometry in FEA, as shown in this case study. It is difficult and time-consuming in practical work to model the true shape of a complicated structure containing angular misalignments of assumed shapes. Therefore, design recommendations are needed to determine the structural stress when analysing a model of an ideal shape without misalignments resulting from manufacturing tolerances.

Offset misalignment

The elementary offset misalignment formula, $K_b = 1 + 3e_0/h = 1 + 1.5$, of plates of equal thickness is too conservative to be applied to joints of differing thickness affected by BEF behaviour. Maddox (1985) recommended

$$K_b = 1 + 6 \frac{e_0}{h_1} \left(\frac{1}{1 + (h_2/h_1)^{1.5}} \right), \quad e_0 = \frac{h_2 - h_1}{2} \quad (6.5-1)$$

for the analysis of a joint between plates of differing thickness. This results in $K_b = 1 + 0.78$, which in the case studied is close to the result of the shell element FEA model,

giving $1 + 0.75$, Table 6.3-1. The BEF model produced a factor of 1.56. Thus the formula of Maddox is accurate enough to be applied in future studies.

Angular misalignment in plates or shells affected by a foundation

FEA resulted in a bending stress concentration of 0.15 when the true shape of the model contained an angular misalignment, in the form of a roof topping of apex angle $2\varphi_0$, i.e. $4/300$ rad, equal to $z_0 = 2$ mm in depth (40% of the thickness), see also Fig. 1.1-1. Using the notation (fix) for fixed, and (ss) for simply-supported, pinned ends, the design recommendations (Maddox 1985), give

$$K_{b,fix} = 1 + 3 \frac{z_0}{h} = 1 + 1.2, \quad K_{b,ss} = 1 + 6 \frac{z_0}{h} = 1 + 2.4. \quad (6.5-2)$$

These values, derived from simple beam analysis, are too high compared with the results of the experimental tests, the shell element FEA runs, or BEF analysis of this study. It is clear that it is far too conservative to apply the beam formulae of a free joint to constructions supported by a foundation, e.g. transverse stiffness. The BEF model resulted in a bending stress concentration of 21%, which was 33% higher than that given by the shell element FE analysis. Transverse butt joints in plate structures (as in the test carried out) and rotation symmetric joints in spherical shells and circumferential joints in pipes are the most common examples of BEF behaviour.

According to the BEF model, the geometric non-linearity originating from the angular misalignment was marginal. In addition, the total geometric non-linearity determined experimentally by the load - strain behaviour was marginal. However, in the design recommendations of International Institute of Welding (IIW) edited by Hobbacher (1996) and based on the studies of Maddox (1985), the geometric non-linearity is very strong:

$$K_{b,fix} = 1 + 3 \frac{z_0}{h} \frac{\tanh(\psi/2)}{\psi/2}, \quad K_{b,ss} = 1 + 6 \frac{z_0}{h} \frac{\tanh \psi}{\psi}, \quad \psi = \frac{L}{h} \sqrt{3 \frac{\sigma_m}{E}}. \quad (6.5-3)$$

Eqn (6.5-3) is the result of beam-column analysis, shown e.g. by Timoshenko & Gere (1936). No instructions are given in the IIW recommendations for welded joints affected by BEF behaviour. Equation (6.5-3) is based on the assumption of pinned or fixed ends a distance L apart, and a constant thickness, h . Based on the maximum axial tensile stress of testing, $\sigma_m = 320$ MPa, and the length of the roof topping, $L = 700$ mm, see Fig. 6.2-2, the factor ψ becomes $\psi = 5.5$. By using the true shape of the panel, $z_0 = 2$ mm, approximately equal concentration factors for the fixed and pinned end conditions, $K_b = 1 + 0.43$, are obtained. Based on Eqns (6.5-2) and (6.5-3) the ratio of the bending stresses of the fixed plate ($0.43/1.2 = 0.36$), equal to the factor of geometric non-linearity, is unconservative, compared with experimental observations or BEF calculations.

6.5.6 New model for angular misalignment for plates of differing thickness

BEF model description: The centre-line of a butt joint in a continuous structure of plates of differing thickness containing an apex angle of $2\varphi_0$ is considered. The thickness of the thinner and thicker plates are h_1 and h_2 , respectively. The joint rests on an elastic foundation having parameters $1/\lambda$ and n_{lin} ($1/\lambda = B/\pi$ and $n_{lin} = 1/\pi$ when assumed a fixed plate). It is assumed that the characteristic lengths are equal on both sides of the joint. The factor of stress bi-axiality is K_v , (for a continuous plate $K_v = 1.24$). The ratio of axial membrane stress loading, σ_m , (tension positive) to critical buckling stress is n .

The transverse line load, q , induced by the roof topping is the product of the axial stress, σ_m , and the slope between the plates, $2\varphi_0$, giving $q = 2\sigma_m h_1 \varphi_0$. The bending stress concentration, K_b , resulting from the plate bending stress of the angular misalignment is given by Eqn (6.5-4). It includes a factor for the effect of differing thicknesses, K_h , which can be obtained from the closed form BEF solution of the bending stress caused by a line load q , similar to the numerical analysis of Section 6.4. The effect of the geometric non-linearity, K_{gnl} , Eqn (4.4-8), is most effective when the plates are of equal thickness. For differing plate thickness, K_{gnl} of the thinner plate 1 is slightly higher than the K_{gnl} of plates of equal thickness. K_b can be written:

$$K_b = 1 + \varphi_0 \frac{3}{\lambda h_1} \frac{1}{\sqrt{1 + n_{lin}}} K_v K_{gnl} K_h, \quad (6.5-4)$$

$$K_{gnl} = \frac{1}{\sqrt{1 + n}}, \quad K_h = \frac{8r}{1 + 6r + r^2}, \quad r = \frac{l_2}{l_1} = \frac{h_2^3}{h_1^3}.$$

By using the data of the continuous test panel, $2\varphi_0 = 4/300$, $h_2 = 2h_1$, $\lambda h_1 = 0.057$, $n = 320/370$, resulting in $K_h = 0.57$, $K_{gnl} = 0.73$, $K_b = 1 + 0.30 \times 0.57 \times 1.24 \times 0.73 = 1.16$. If the effect of the geometric non-linearity is neglected, then $K_b = 1 + 0.22$.

It was observed from experiment, BEF analysis, geometric non-linear BEF analysis, and FEA that the stress concentration caused by the angular misalignment is around 0.2. The present recommendations resulted for the fixed plate in $K_{gnl} = 0.36$ and $K_b = 1 + 1.2 \times 0.36 = 1.43$. Since the basis of these recommendations is not correct for joints supported by a foundation Eqn (6.5-4) is more preferable. Especially for the design of joints under alternating compression loading Eqn (6.5-3) cannot be used.

Chapter 7

DISCUSSION AND CONCLUSIONS

7.1 Summary and conclusions

The aim of this thesis was to show that plate strips can be analysed by using the beam on elastic foundation (BEF) approach. It was shown by various methods that the BEF theory can be used to describe the centre-line section of a semi-infinite plate supported along two parallel edges, as well as the free edge of a cantilever plate strip. The transverse bending stiffness of the plate strip forms the foundation. When considering the fourth order governing differential equation of the BEF model, the foundation modulus is shown, mathematically and physically, to be the zero order term, whereas the torsion rigidity of the plate functions as pre-tension in the second order term of the equation.

BEF parameters based on uniaxial stress field

By comparing the differential equations of Lévy's plate analysis and the BEF method, a correspondence regarding harmonic line loading was obtained directly (Chapters 2 and 3). By equating the second and zero order parameters, the two characteristic parameters for a simply-supported plate of width B were obtained for the semi-infinite BEF model for each harmonic component, m : the characteristic length, $1/\lambda$, and the normalized stiffening effect of the torsion stiffness, n_{lin} . The equality resulted in $1/\lambda = \sqrt{2B}/\pi$ and $n_{lin} = 1$ for the lowest mode, $m = 1$.

Under constant line loading, which is represented by the superimposition of harmonic components, slightly different foundation parameters were obtained when the maximum deflection and bending moment values of the plate and BEF solutions were equated: $1/\lambda = 1.47B/\pi$ and $n_{lin} = 0.59$.

The deflection function of a fixed semi-infinite plate strip subjected to line loading was determined, based on classical plate theory to demonstrate the work required, Section 4.2. The theoretical plate analysis results were in good agreement with shell element FEA calculations. The foundation parameters of the BEF model were determined from the equality of the maximum deflection and the bending moment in the axial direction, resulting in $1/\lambda = 0.99B/\pi$ and $n_{lin} = 0.25$. For practical applications such as the analysis of continuous plate fields, $1/\lambda = B/\pi$ and $n_{lin} = 1/\pi$ are easily remembered, whilst still giving accurate results.

The BEF parameters of a plate strip with one edge free the other fixed were determined by using the results of FEA alone, Section 4.3. The BEF parameters were: $1/\lambda = 1.29B/\pi$ and $n_{lin} = 0.65$, where B is the double width of the cantilever plate strip.

In a number of figures it was shown that deflection and bending moment functions of the plate solutions and BEF analysis, respectively, correlated well in the longitudinal direction.

Generalized BEF model

The effect of geometric nonlinearity, caused by in-plane bi-axial loading, on bending behaviour was studied theoretically by comparing the differential equations of Lévy's method and the BEF approach. It was shown that when Poisson's ratio was not taken into account ($\nu = 0$), the correlation between the maximum deflection and bending moment, defined by geometric non-linear FEA and the BEF model, is good when the plate is under the influence of axial or transverse in-plane pre-stress loading. A factor for the geometric nonlinearity, K_{gnl} , was obtained from the comparison, Section 4.4.

The effect of true stress biaxiality ($\nu > 0$) on bending behaviour did not affect the values of the BEF parameters significantly, as shown in Section 4.5. In particular, the flexural rigidity is 10% greater compared with $\nu = 0$, and the product of Poisson's ratio and the transverse bending stress must be superimposed on the bending stress of the axial bending moment. Under axial in-plane loading, the geometric nonlinearity was predicted well by the BEF model, but the biaxiality effect under transverse in-plane loading was not so clear compared with the case $\nu = 0$, Section 4.5.3. It was also found, based on geometric nonlinear shell element FEA, that when the axial load is increased gradually, the membrane stress redistribution became significant when the axial compressive loading exceeded 50% of the buckling load.

Finally, the generalized BEF model was developed in Section 4.6, to describe a centre-line of a plate strip that is supported uniformly and elastically against rotation along the longitudinal edges. The torsional stiffness of the plate between the centre-line and support line was taken into account in the model developed. First, it was shown that the effect of torsion stiffness, N , was fairly constant and independent of the rotation stiffness of the edge support lines. Secondly, it was found that the characteristic lengths, $1/\lambda$, of a simply-supported plate and a fixed plate could also be determined by using elementary deflection formulae. The maximum deflection and bending moment of the BEF model were shown to correlate well with the results of a parametric thin shell FEA when the rotation stiffness at the support line was varied, Fig. 4.6-2. Finally, components of the generalized BEF model that take into account the effect of Poisson's ratio, axial and transverse in-plane loading on bending behaviour were presented.

Effect of finite length on bending behaviour

In Chapter 5 it was shown that the BEF parameters of the semi-infinite model are valid in the geometric linear analysis of a plate of finite length. When the non-dimensional

length of the plate, λL , is about one, the bending moment of the BEF model at the far end is at most 10% lower than that determined by shell element FEA. Otherwise, the correlation is very accurate. It was also found that the boundary conditions, simply-supported or fixed, did not affect the deflection or bending moment functions relative to the normalised finite length of the plate strip.

Engineering understanding

Fast computers and efficient FEA programs are now available to structural engineers. The cross-sectional properties of structures can be varied easily such that the maximum stress level is acceptable for a given load case or load combination. Critical engineering assessment is needed to ensure that the structure will meet all the strength requirements of the total life cycle. If the behaviour of the structure can be understood and approximated in advance with reasonable accuracy, the FEA result can be accepted with more confidence as being numerically accurate, rather than just relying on the numerical data of the computer calculations.

Many structural engineering scenarios can be analysed as a one dimensional problem - this is a general aim in practical work. This study has shown that under constant lateral line and edge moment loadings, the application of BEF theory is a simple tool for the analysis of semi-infinite and finite plate bending problems. The model was successfully applied in the stress analysis of a full-scale test panel, Chapter 6. The use of present fatigue design recommendations for calculating bending stresses caused by misalignments was tested. It was found that stress concentrations resulting from angular misalignments in joints affected by an elastic foundation are not predicted correctly using present formula. A new formula taking into account the stress biaxiality and geometric nonlinearity was presented for a continuous plate.

The damping behaviour of deflections is often noticeable when structural details are analysed. In spite of this, some engineers are not very familiar with the use of BEF theory. Based on the findings of this study, one or two parameter BEF models can be applied to new practical applications to explain bending behaviour in a simple way, with sufficient accuracy. Therefore, the combination of the BEF approach and finite element methods based on shell or solid element analysis can be recommended as a starting point for more theoretical analysis of complicated structural phenomena.

7.2 Future research

Improvement of the BEF model

The BEF model presented can be further developed to take into account the effect of out-of-plane shear deformation.

Finite elements for the analysis of truss or torsion structures on an elastic foundation can be developed. Based on these, and BEF elements, the interaction can be taken into account when analysing elastically-supported plane frame and/or plane grid structures.

The BEF model can be modified to be applied to the analysis of warping behaviour in open sections under the influence of a rotation foundation.

Applications

The plate strip BEF model can be applied to the behaviour of various types of structure, and to develop more accurate parametric design equations for the analysis of plates containing misalignments, e.g. those shown in Figure 1.1-1.

The semi-infinite plate strip BEF model can be applied to the analysis of angled beam joints in plane frames and plane grids.

A model that takes into account the effect of membrane stress redistribution can be developed, based on the interaction of the semi-infinite behaviour of a truss on an elastic foundation and BEF elements.

The semi-infinite BEF model can be applied to the analysis of out-of-plane discontinuity stresses, caused by in-plane shear deformation of the web plate of beam profiles such as I beams and rectangular hollow sections.

Characteristic lengths at stiffener lines can be determined. The BEF model for the centre-line section can be widened to cover the entire width between the stiffeners.

Finally, the most important application of a more accurate stress analysis is in the fatigue assessment of dynamically-loaded structural joints, most notably welded joints.

REFERENCES

Cook, R. 1974. *Concepts and applications of finite element analysis*, 2nd Edition. John Wiley & Sons, Inc. 1981. 537 p.

Chiwanga, M. and Valsangkar, A. 1988. Generalized beam element on two-parameter elastic foundation. *ASCE Journal of Structural Engineering*, Vol. 114, No.6, June 1988, pp. 1414-1427.

Cosmos/M 1996. *Geostar 1.75 User manual*. Structural Research and Analysis Corporation.

Eisenberger, M. and Yankelevsky, D. 1985. Exact stiffness matrix for beams on elastic foundation. *Computers & Structures* Vol. 21, No. 6, pp. 1355-1359.

Filonenko-Borodich, M. 1940. Some approximate theories of the elastic foundation. *Uch. Zap. Mosk. Gos. Univ. Mekh* 46, pp. 3 -18. (in Russian).

Girkmann, K. 1946. *Flächentragwerke*, Einführung in die Elastostatik der Scheiben, Platten, Schalen und Faltwerke. Springer-Verlag, Wien, 6. Auflage 1966. 632 s. (in German).

Hétenyi, M. 1946. *Beams on elastic foundation*. (renewed 10th printing 1974). 10th Printing 1976, The University of Michigan Press, (also John Wiley & Sons, Rexdale Canada). 245 p.

Hobbacher A. 1996. (Chairman of IIW JWG XIII-XV.). Recommendations on fatigue design of welded joints and components. *International Institute of Welding, Doc. XIII-1539-96 / XV-845-96*. International Institute of Welding, October 1996, Woodhead Publishing Ltd., Abington Hall, Abington, Cambridge. 127 p.

Kirchhoff, G. 1850. *J. Math. (Crelle)* 40, 51. (in German).

Kirchhoff, G. 1876. *Vorlesungen über mathematische Physik*, Vol. 1 B.G. Teubner, Leipzig. (in German).

Lévy, M. 1899. Sur l'équilibre élastique d'une plaque rectangulaire. *C. R. Acad. Sci.*, 129(1899), pp. 535 - 539. (in French).

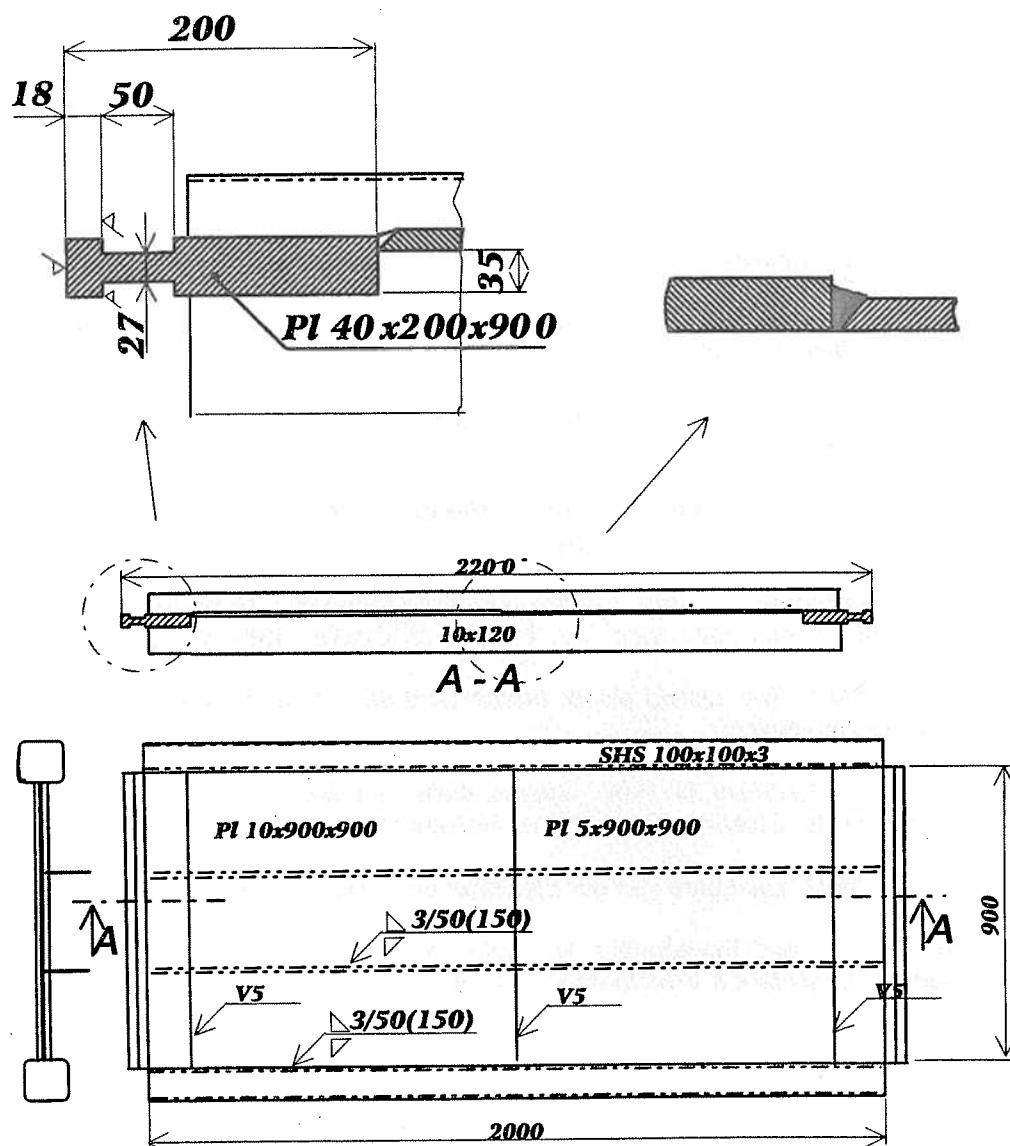
Maddox, S. 1985. Fitness-for-purpose assessment of misalignment in transverse butt welds subjected to fatigue loading. *International Institute of Welding, Doc. XIII-1180-85*. 13 p.

Nádaj, A. 1915. Die Formänderungen und die Spannungen von rechteckigen elastische Platten. *Forsh. A.d. Gebiete d. Ingenieurwesens, (Berlin)* Nos. 170 and 171 (1915). (in German).

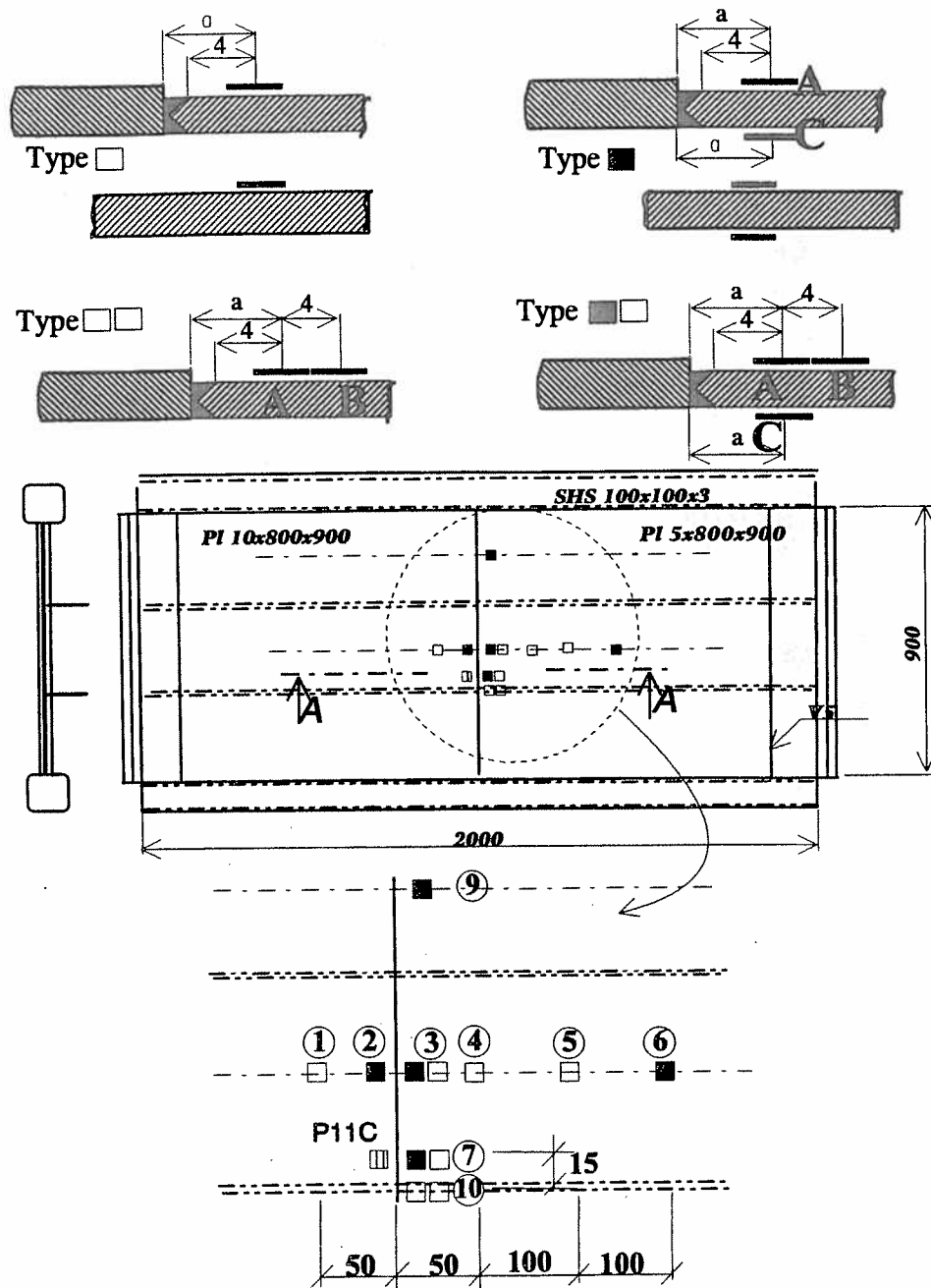
Niemi, E. (Ed.), The International Institute of Welding, 1995, *Stress Determination for*

- Fatigue Analysis of Welded Components*, IIS/IIW-1221-93, (ex doc IIW Document XIII-1458-92, XV-797-92), Abington Publishing, Cambridge, England.
- Partanen, T., Tarjauuri, P. and Niemi, E. 1992. Definition of the hot spot stress gradient in stiffened plate structures based on the beam on elastic foundation theory. *International Institute of Welding, Doc. XIII-1478-92, XV-811-92*. 25 p.
- Partanen, T. 1992. Factors affecting the fatigue behaviour of misaligned transverse butt joints in stiffened plate structures. In: *Engineering Design in Welded Constructions, International Institute of Welding (Ed. M. Bramat), Pergamon Press, Oxford 1992*, pp. 65 - 72.
- Pasternak, P. 1954. On a new method of analysis of an elastic foundation by means of two foundation constants. Gos. Izd. Lit. Po Strait I Akh, Moscow, (in Russian).
- Razqpur, A. and Shah, K. 1991. Exact analysis of beams on two-parameter elastic foundations. *International Journal of Solids Structures, Vol.27, No.4*, pp. 435 - 454.
- Szilar, R. 1974. *Theory and analysis of plates*. Prentice-Hall, Inc. Englewoods Cliffs, New Jersey. 723 p.
- Timoshenko, S. and Gere, J. 1936. *Theory of elastics stability*. McGraw-Hill Kogakusha, Ltd., 2nd Ed. (1961). 541 p.
- Ting, B. and Mockry, E. 1984. Beam on elastic foundation finite element. *ASCE Journal of Structural Engineering, Vol. 110, No.10, October 1984*, pp. 2324 - 2339.
- Vlasov, V. 1961. *Thin-walled elastic beams*. (2nd ed.). Israel Program for Scientific Translations, Jerusalem.
- Vlasov, V., and Leontiev, U. 1966. *Beams, plates and shells on elastic foundations*. Israel Program for Scientific Translations, Jerusalem.
- Winkler, E. 1867. *Die Lehre von der Elastizität und Festigkeit*, Prag. (in German).
- Yankelevsky, D. and Eisenberger, M. 1986. Analysis of beam column on elastic foundation. *Computers & Structures Vol. 23, No. 3*, pp. 351-356.

APPENDIX 6.2-1 STIFFENED PLATE TEST PANEL



APPENDIX 6.2-2 STRAIN GAUGE LOCATIONS IN TEST PANEL



APPENDIX 6.2-3 EXPERIMENTAL TEST RESULTS, RUN 1 AND 2

TP panel 1 test 1/2 14.12.1995

Date: 12-14-1995 Time: 15:48:01

1 V = 500 kN Channel 0;		1 V = 20 mm Channel 1;		1 V = 2 mm Channels 13, 14;		1 V = 0,5 [mm/m] All strain gauge readings				
0: force	1: displac.	2: gauge 1a	3: gauge 2a	4: gauge 3a	5: gauge 3b	6: gauge 4a	7: gauge 5a	8: gauge 6a	9: gauge 6c	10: gauge 3c
0.005	0.000	0.000	0.000	0.000	0.000	0.000	0.000	0.000	0.000	1.450
1.021	0.079	0.120	-0.103	1.514	1.518	0.933	0.889	0.890	0.826	0.171
2.007	0.123	0.253	-0.176	2.852	2.846	1.719	1.699	1.640	1.539	0.313
3.027	0.157	0.415	-0.249	4.282	4.272	2.525	2.446	2.446	2.295	0.449
4.014	0.186	0.566	-0.308	5.610	5.649	3.233	-	3.154	2.979	0.581

11: gauge 2c	12: gauge 2d	13: clock 1	14: clock 2
0.000	0.293	0.000	0.000
1.006	0.957	1.006	1.021
1.845	1.743	1.475	1.485
2.744	2.588	1.914	1.963
3.550	3.374	2.315	2.373

TP-panel 1 Test 2/2

Date: 12-15-1995 Time: 14:18:05

1 V = 500 kN Channel 0;		1 V = 20 mm Channel 1;		1 V = 0,5 [mm/m] All strain gauge readings						
0: force	1: displac.	2: gauge 7a	3: gauge 7b	4: gauge p13c	5: gauge 7c	6: gauge 7d	7: gauge 9a	8: gauge 9c	9: gauge 6c	10: g. r10a1
0.000	0.005	0.000	0.005	-0.005	0.000	-0.010	0.010	0.000	0.000	0.000
1.001	0.146	1.196	1.030	0.269	0.327	0.513	1.396	0.225	0.791	0.376
2.002	0.186	2.295	1.992	0.459	0.654	1.021	2.656	0.396	1.533	0.703
3.003	0.234	3.423	2.969	0.640	0.996	1.533	3.921	0.532	2.275	1.045
4.009	0.283	4.541	3.950	0.796	1.318	2.041	5.156	0.684	2.979	1.387

11: g. r10a2	12: g. r10a3	13: g. p11c	14: clock 1	15: clock 2
0.010	0.000	0.005	0.010	0.005
1.030	0.322	-0.010	0.938	-0.215
2.012	0.640	-0.024	1.421	-0.352
2.998	0.977	-0.059	1.865	-0.498
3.975	1.313	-0.107	2.236	-0.591

43. Third International Seminar on Horizontal Steam Generators October 18-20, 1994, Lappeenranta, Finland. 1995. 413 s.
44. AHOLA, JYRKI. Yrityksen strategiaprosessi: näkökohtia strategisen johtamisen kehittämiseksi konserniorganisaatiossa. 1995. 235 s., liitt. Väitösk.
45. RANTANEN, HANNU. The effects of productivity on profitability: a case study at firm level using an activity-based costing approach. 1995. 169 s., liitt. Diss.
46. Optics in Engineering: First Finnish-Japanese meeting Lappeenranta, 12-14th, June 1995 / ed. by P. Silfsten. 1995. 102 s.
47. HAAPALEHTO, TIMO. Validation studies of thermal-hydraulic code for safety analysis of nuclear power plants. 1995. U.s. Diss.
48. KYLÄHEIKO, KALEVI. Coping with technology: a study on economic methodology and strategic management of technology. 1995. 263 s. Diss.
49. HYVÄRINEN, LIISA. Essays on innovativeness and its evaluation in small and medium-sized enterprises. 1995. U.s. Diss.
50. TOIVANEN, PEKKA. New distance transforms for gray-level image compression. 1996. U.s. Diss.
51. EHSANI, NEDA. A study on fractionation and ultrafiltration of proteins with characterized modified and unmodified membranes. 1996. U.s. Diss.
52. SOININEN, RAIMO. Fracture behaviour and assessment of design requirements against fracture in welded steel structures made of cold formed rectangular hollow sections. 1996. 238 s. Diss.
53. OJA, MARJA. Pressure filtration of mineral slurries: modelling and particle shape characterization. 1996. 148 s. Diss.
54. MARTTILA, ESA. Ilmanvaihdon lämmönsiirtimien teknillinen ja taloudellinen mitoitus. 1996. 57 s. Väitösk.
55. TALONPOIKA, TIMO. Dynamic model of small once-through boiler. 1996. 86 s. Diss.
56. BACKMAN, JARI. On the reversed Brayton cycle with high speed machinery. 1996. 103 s. Diss.
57. ILME, JARNO. Estimating plate efficiencies in simulation of industrial scale distillation columns. 1997. U.s. Diss.
58. NUORTILA-JOKINEN, JUTTA. Choice of optimal membrane processes for economical treatment of paper machine clear filtrate. 1997. U.s. Diss.
59. KUHMONEN, MIKA. The effect of operational disturbances on reliability and operation time distribution of NC-machine tools in FMS. 1997. 133 s., liitt. Diss.
60. HALME, JARKKO. Utilization of genetic algorithm in online tuning of fluid power servos. 1997. 91 s. Diss.
61. MIKKOLA, AKI. Studies on fatigue damage in a hydraulically driven boom system using virtual prototype simulations. 1997. 80 s., liitt. Diss.
62. TUUNILA, RITVA. Ultrafine grinding of FGD and phosphogypsum with an attrition bead mill and a jet mill: optimisation and modelling of grinding and mill comparison. 1997. 122 s. Diss.
63. PIRTILÄ, ANNELI. Competitor information and competitive knowledge management in a large, industrial organization. 1997. 175 s., liitt. Diss.
64. MEURONEN, VESA. Ash particle erosion on steam boiler convective section. 1997. 149 s. Diss.

65. MALINEN, HEIKKI. Forecasting energy demand and CO₂-emissions from energy production in the forest industry. 1997. 86 s. Diss.
66. SALMINEN, RISTO T. Role of references in international industrial marketing - a theory-building case study about supplier's processes of utilizing references. 1997. 375 s. Diss.
67. Fourth International Seminar on Horizontal Steam Generators 11-13 March 1997, Lappeenranta, Finland. 1997. 285 s.
68. KAIKKO, JUHA. Performance prediction of gas turbines by solving a system of non-linear equations. 1998. 91 s. Diss.
69. LEHMUSVAARA, ANTTI. Improving the potentials of logistics processes: identification and solutions. 1998. U.s. Diss.
70. PIHLAJAMÄKI, ARTO. Electrochemical characterisation of filter media properties and their exploitation in enhanced filtration. 1998. U.s. Diss.
71. VIROLAINEN, VELI-MATTI. Motives, circumstances, and success factors in partnership sourcing. 1998. 232 s. Diss.
72. PORRAS, JARI. Developing a distributed simulation environment on a cluster of workstations. 1998. U.s. Diss.
73. LAURONEN, JARI. Spare part management of an electricity distribution network. 1998. 130 s. Diss.
74. PYRHÖNEN, OLLI. Analysis and control of excitation, field weakening and stability in direct torque controlled electrically excited synchronous motor drives. 1998. 109 s. Diss.

Sarjan uusi nimi: ACTA UNIVERSITATIS LAPPEENRANTAENSIS

75. SAARNIO, ANTTI. Choice of strategic technology investment - case of pulp production technology. 1999. 225 s. Diss.
76. MATTILA, HEIKKI. Merchandising strategies and retail performance for seasonal fashion products. 1999. 219 s. Diss.
77. KAUKONEN, JUKKA. Salient pole synchronous machine modelling in an industrial direct torque controlled drive application. 1999. 138 s. Diss.
78. MÄNTTÄRI, MIKA. Fouling management and retention in nanofiltration of integrated paper mill effluents. 1999. U.s. Diss.
79. NIEMELÄ, MARKKU. Position sensorless electrically excited synchronous motor drive for industrial use based on direct flux linkage and torque control. 1999. 142 s. Diss.
80. LEPPÄJÄRVI, SEPPO. Image segmentation and analysis for automatic color correction. 1999. U.s. Diss.
81. HAUTA-KASARI, MARKKU. Computational techniques for spectral image analysis. 1999. U.s. Diss.
82. FRYDRYCH, MICHAEL. Color vision system based on bacteriorhodopsin. 1999. 87 s. Diss.
83. MAKKONEN, MATTI. Size effect and notch size effect in metal fatigue. 1999. 93 s., liitt. Diss.
84. 7th NOLAMP Conference. 7th Nordic Conference in Laser Processing of Materials. Ed. by Veli Kujanpää and John Ion. Vol. I-II. 1999. 559 s.
85. Welding Conference LUT JOIN'99. International Conference on Efficient Welding in Industrial Applications (ICEWIA). Ed. by Jukka Martikainen and Harri Eskelinen. 1999. 418 s.